Chair of Ferrous Metallurgy

Doctoral Thesis

Reduction of hematite using hydrogen plasma smelting reduction

Masab Naseri Seftejani

July 2020

AFFIDAVIT

I declare on oath that I wrote this thesis independently, did not use other than the specified sources and aids, and did not otherwise use any unauthorized aids.

I declare that I have read, understood, and complied with the guidelines of the senate of the Montanuniversität Leoben for "Good Scientific Practice".

Furthermore, I declare that the electronic and printed version of the submitted thesis are identical, both, formally and with regard to content.

Date 29.06.2020

Signature Author
Masab, Naseri Seftejani

Abstract

Hydrogen plasma smelting reduction (HPSR) of iron ore, which is an alternative to conventional iron- and steel-making processes and reduces the emission of greenhouse gases, was introduced at the Montanuniversitaet Leoben in 1992. In HPSR, hydrogen is activated in the plasma arc zone and becomes partially atomized and ionized. Activated hydrogen particles are strong reducing agents for iron oxides. HPSR offers advantages in terms of thermodynamics and kinetics over the conventional carbo-thermic reduction of iron ores. The work for this thesis has been carried out in the framework of the SuSteel project to obtain data and knowledge by the means of laboratory-scale facilities for the development of a testing HPSR plant at voestalpine Stahl Donawitz GmbH.

This thesis provides an overview of generating hydrogen plasma in an arc plasma reactor by collisional processes and discusses the reduction ability of hydrogen species in terms of kinetics and thermodynamics. Furthermore, thermodynamics calculations have been carried out to study the reduction of iron oxide using hydrogen. The reduction behavior of iron oxides was assessed by carrying out a series of experiments. Therefore, the main parameters of reduction namely degree of reduction, degree of hydrogen utilization, reduction rate, and produced amount of metallic iron, and slag were studied.

The thermodynamic aspect of the hematite reduction was considered, and the pertinent calculations were carried out using FactSage™ 7.2. All reduction parameters were calculated using the off-gas chemical composition measured by mass spectrometry. Carbon from the hollow graphite electrode, steel crucible, and ignition pin was introduced to the melt and contributed to the reduction process of iron oxides. Hence, the amount of CO and CO_2 were the components of off-gas. The degree of reduction of hematite, regarding H_2O, CO, and CO_2

as the gaseous reduction products, was determined. The results showed that at the beginning of the experiments, the degree of reduction and hydrogen utilization was high, and then decreased over the operation time because the concentration of iron oxide was gradually decreased. Conducting experiments with CaO caused a decrease in the phosphorus concentration in the produced iron.

The slag formation during the reduction process and the reduction behavior of iron oxides were investigated. Furthermore, the reduction behavior of iron ore during continuous feeding was assessed. For this purpose, the fines of iron oxide and calcined lime were mixed to achieve a basicity of 0, 0.8, 1.6, 2.3, and 2.9, and then the mixtures were charged, melted, and reduced in the hydrogen plasma reactor. The results showed that in the batch process, the degree of hydrogen utilization and reduction rate was gradually decreased during the reduction process. In contrast, during the continuous-feeding experiment, the degree of hydrogen utilization could be kept approximately constant. The highest degrees of reduction and hydrogen utilization were obtained upon the application of slag with a basicity of 2.3. As a main result, the continuous feeding of iron oxides could apply the best conditions for the reduction of iron oxide using hydrogen thermal plasma.

The temperature of the hydrogen plasma arc was measured using the spectroscopic method. A fiber of optical spectrometer was installed on the side of the plasma reactor to monitor the arc, capture the light from the arc, and send it to the optical spectrometer. Then, the arc temperature was calculated using the intensity of two main lines of hydrogen in the spectrum. The results showed that the maximum temperature of the arc was 13,435 K.

Kurzfassung

Die Wasserstoff-Plasma-Schmelzreduktion (HPSR) von Eisenerz, die eine Alternative zu herkömmlichen Eisen- und Stahlerzeugungsverfahren darstellt und den Ausstoß von Treibhausgasen reduziert, wurde 1992 an der Montanuniversität Leoben eingeführt. Bei der HPSR wird Wasserstoff in der Plasmalichtbogenzone angeregt und teilweise zerstäubt sowie ionisiert. Angeregte Wasserstoffpartikel sind starke Reduktionsmittel für Eisenoxide. HPSR bietet Vorteile im Bezug auf Thermodynamik und Kinetik gegenüber der konventionellen kohlenstoffthermischen Reduktion von Eisenerzen. Die Arbeiten zu dieser Dissertation wurde im Rahmen des SuSteel-Projekts durchgeführt mit dem Ziel, Daten und Erkenntnisse mit Hilfe von Anlagen im Labormaßstab für die Entwicklung einer HPSR-Versuchsanlage in größerem Maßstab bei der voestalpine Stahl Donawitz GmbH zu gewinnen.

Diese Dissertation gibt einen Überblick über die Erzeugung von Wasserstoffplasma in einem Lichtbogenplasmareaktor durch Kollisionsprozesse und diskutiert das Reduktionsvermögen von unterschiedlichen Wasserstoffspezien in Bezug auf Kinetik und Thermodynamik. Weiter wurden thermodynamische Berechnungen durchgeführt, um die Reduktion von Eisenoxid mit Wasserstoff zu untersuchen.

Das Reduktionsverhalten von Eisenoxiden wurde durch die Durchführung einer Reihe von Experimenten beurteilt. Dazu wurden die Hauptparameter der Reduktion, nämlich Reduktionsgrad, Wasserstoffausnutzungsgrad, Reduktionsrate, die Menge an erzeugten metallischen Eisen und Schlacke untersucht. Der thermodynamische Aspekt der Hämatitreduktion wurde berücksichtigt, und die entsprechenden Berechnungen wurden mit FactSage™ 7.2 durchgeführt. Der Grad der Wasserstoffausnutzung und der Reduktionsgrad wurden anhand der chemischen Zusammensetzung des Abgases berechnet. Der Kohlenstoff aus der Hohlgraphitelektrode, dem Stahltiegel und dem Zündstift wurde in die Schmelze

eingebracht und trug zum Reduktionsprozess der Eisenoxide bei. Somit waren die Menge an CO und CO_2 die Bestandteile des Abgases. Es wurde der Reduktionsgrad von Hämatit unter Berücksichtigung von H_2O, CO und CO_2 als gasförmige Reduktionsprodukte bestimmt. Die Ergebnisse zeigten, dass zu Beginn der Experimente der Reduktions- und Wasserstoffnutzungsgrad hoch war und dann über die Betriebszeit abnahm. Denn die Konzentration von Eisenoxid wurde allmählich verringert. Die Durchführung von Experimenten mit CaO verursachte eine Abnahme der Phosphorkonzentration im erzeugten Eisen.

Die Schlackenbildung während des Reduktionsprozesses und das Reduktionsverhalten von Eisenoxiden wurden untersucht. Weiterhin wurde das Reduktionsverhalten von Eisenerz bei kontinuierlicher Beschickung bewertet. Zu diesem Zweck wurden die Feinanteile von Eisenoxid und kalziniertem Kalk gemischt, um eine Basizität von 0, 0,8, 1,6, 2,3 und 2,9 zu erreichen, und dann wurden die Mischungen chargiert, geschmolzen und im Wasserstoffplasmareaktor reduziert. Die Ergebnisse zeigten, dass im Chargenprozess der Grad der Wasserstoffausnutzung und die Reduktionsrate während des Reduktionsprozesses allmählich verringert wurde. Im Gegensatz dazu konnte der Wasserstoffnutzungsgrad während des Experiments mit kontinuierlicher Beschickung annähernd konstant gehalten werden. Die höchsten Reduktions- und Wasserstoffausnutzungsgrade wurden bei der Verwendung einer Schlacke mit einer Basizität von 2,3 erreicht. Das Experiment zeigte, dass bei kontinuierlicher Beschickung mit Eisenerz die besten Bedingungen für den Reduktionsprozess mit Wasserstoff angewendet werden konnten.

Die Temperatur des Wasserstoffplasmabogens wurde mit einer spektroskopischen Methode gemessen. Die Faser eines optischen Spektrometers wurde an der Seite des Plasmareaktors installiert, um den Lichtbogen zu überwachen, das Licht des Lichtbogens einzufangen und zum optischen Spektrometer zu senden. Dann wurde die Bogentemperatur unter Verwendung der Intensität von zwei Hauptlinien des Wasserstoffs im Spektrum berechnet. Die Ergebnisse zeigten, dass die maximale Temperatur des Lichtbogens 13,435°K betrug.

Acknowledgement

First, I would like to express my sincere gratitude to my primary Ph.D. supervisor and mentor Univ.-Prof. Dipl.-Ing. Dr.techn Johannes Schenk for his continuous support and assistance throughout my research work. Moreover, his guidance and valuable suggestions helped to achieve the desired results in scientific work and to develop professionally.

It gives me great pleasure in acknowledging the support and help of Ao.Univ.-Prof.Dipl.-Ing.Dr.techn. Christian Weiß for my research work and for introducing me to the flow patterns in the hydrogen plasma reactor.

This work was carried out in the framework of the SuSteel project, which was funded by the Austrian Research Promotion Agency (FFG). Montanuniversitaet Leoben, K1–Met GmbH, voestalpine Stahl Donawitz GmbH, and voestalpine Stahl Linz GmbH were the partners of the SuSteel project, and I wish to thank all my colleagues working in this project.

I would like to thank Dipl.-Ing. Daniel Spreitzer and Dipl.-Ing. Michael Andereas Zarl for their support during my research work. I am thankful to my colleagues Mr. Lukas Demmerer for laboratory technical support.

I am extremely grateful to my wife and my daughters for their love, understanding and continuing support to complete this research work. I am very much thankful to my parents for their love, caring and sacrifices for educating and preparing me for my future.

This thesis is dedicated to my wife and daughter who have always stood by me and dealt with all my absence from many family occasions with a smile.

Table of Contents

Nomenclature

Latin Letters

A_{pr}	Transition probabilities from the energy level of p to r
c	Speed of light in vacuum
C_n	Cycle n
C_p	Heat capacity
e	Elementary charge
E_i	Ionization energy from the i orbital layer
g_e	Statistical weight of the electron
g_p	Statistical weights on the level p
g_q	Statistical weights on the level q
G_r	Partition functions in the r state
h	Planck constant
i_{pr}	Intensity of a spectra line from the energy level of p to r
$k[H_2]$	Apparent rate constant of hydrogen
k	Boltzmann constant
L	Length
M_D	Degree of metallization
m_e	Rest mass of the electron
m_{O,H_2O}	Mass of oxygen in H_2O
m_p	Mass of proton

N	Particle number densities of neutral
N_e	Electron density
N_H	Density of neutral hydrogen atoms
N_i	Density of particles i
N_p	Particle number densities on the energy levels of p
N_q	Particle number densities on the energy levels of q
N_r	Particle number densities on the energy levels of r
$n*$	Quantum number in the excited state
n	Principal quantum number
n_H	Number of hydrogen moles
n_p	Energy level p
P	Collision probability
p	Outer orbit
p_H	Partial pressure of hydrogen
q	Lower orbit
r	Specific reduction rate
r_1	Radius of the first Bohr orbit
R_D	Degree of reduction
R_H	Rydberg constant for hydrogen
R_∞	Rydberg constant for heavy atoms (R_∞)
S_e	Source rate'
t	Time
$\bar{t}$	Mean residence time
t_O	Operation time
t_H	Time of introducing hydrogen into the plasma reactor
V_e	Velocity of electron

$\vec{V}_{He}$	Relative velocity of the hydrogen particle H and electron e
$\dot{V}_A$	Average of the inlet and outlet gas flow rate
S_e	Source rate'
V	Volume of the plasma reactor
V_H	Volume of hydrogen
z	Atomic number
Z_a	Partition function

Greek Letters

δE_i	Refinement of the ionization energy of element i
ΔG	Gibbs free energy changes
ε_0	Permittivity of free space
η_H	Degree of hydrogen utilization
λ	Wavelength
λ_D	Debye length
λ_m,	Mean free path
ν	Collision frequency
υ_{pr}	Frequencies of radiations from the energy level of p to r
σ	Collision cross-section
τ	Meantime of collisions
τ_H	Residence time of hydrogen particles inside the plasma reactor
φ	Collision rate
ψ_i	Density of hydrogen active particles
ω	Mean velocity

Abbreviations

BF	Blast Furnace
BOF	Basic Oxygen Furnace
Ex. 1	Experiment No. 1
EAF	Electric arc furnace
DRI	Direct reduced iron
HGE	Hollow graphite electrode
H-α / Ba-α	Hydrogen-alpha or Balmer-alpha
H-β / Ba-β	Hydrogen-beta or Balmer-beta
H-γ / Ba-γ	Hydrogen- Gamma or Balmer- Gamma
H-δ / Ba-δ	Hydrogen-delta or Balmer-delta
H-ε / Ba-ε	Hydrogen-epsilon or Balmer- epsilon
H-ζ / Ba-ζ	Hydrogen-zeta or Balmer-zeta
H-η / Ba-η	Hydrogen- eta or Balmer- eta
LTE	local thermodynamic equilibrium
n*	Quantum number in the excited state
RTD	Residence time distribution

List of Figures

List of Tables

1 Introduction

This work, which is a cumulative Ph.D. thesis, is structured in peer-reviewed journal papers and the present primary work. The relevant journal papers are attached to this work with the permission of the publishers.

1.1 Background

The Hydrogen plasma smelting reduction (HPSR) process generates plasma by passing an electric current through a gas [1–3]. Then, the collision of electrons and hydrogen molecules leads to exciting those. In this process, argon is used to conduct the current in the plasma arc and hydrogen as a reductant. Therefore, hydrogen and argon mixture is injected into the plasma reactor.

The main reason for the development of the Hydrogen plasma smelting reduction (HPSR) process is to minimize CO_2 emissions in the iron- and steel-making processes. Carbon in conventional iron-making processes reduces iron oxides to produce metallic iron which causes the production of CO_2 [4]. The steel industry produces approximately 5% of anthropogenic CO_2 emissions and approximately 27% of CO_2 emissions from the manufacturing sector in the world [5]. The intensity of CO_2 emissions in the steel industry depends on the production route and varies between 1080 and 2150 t CO_2/t crude steel [6]. The integrated BF-BOF process and the paired HYL 3-EAF produces 2120 kg and 1125 kg of CO_2 per ton of liquid steel respectively [7]. For the recycling of 100% scrap by EAF, 466 kg CO_2/t liquid steel is produced [8]. Several studies have been carried out to reduce CO_2-emissions in the steel industry [9,10]. Potential

sources of carbon for the generation of CO_2 in EAF are graphite electrode, scraps, and charged material. Graphite electrode consumption in EAF is in a range of 2 and 3 kg/t of liquid steel [11]. In an industrial scale of HPSR, carbon only can be introduced into the melt from the hollow graphite electrode. Therefore, it is expected that the direct CO_2 emission will be in the same range as an EAF. Please note that HPSR process consumes more energy to produce liquid iron than that of re-melting charged material in an EAF, hence, the indirect CO_2-emissions, which is the total CO_2 emitted in previous processes namely hydrogen production, will be higher.

By using hydrogen, not only CO_2 emission could be reduced but also the supply of coke would be unnecessary [3,12,13]. Numerous investigations have been carried out to produce iron from ores by hydrogen plasma [3,12,14–20]. The reduction of iron oxides using hydrogen thermal plasma has been studied by some researchers at Montanuniversitaet Leoben [3,21–24]. They studied the main parameters influencing the reduction behavior of different iron ores in the HPSR process. In the HPSR process, using hydrogen as a reducing agent at high temperatures leads to improve reducing conditions. Therefore, this facilitates the production of liquid iron in a one-stage process and decreases the CO_2-emissions, which in turn makes the production process smaller [25]. In the case of constructing a large industrial scale of HPSR, hydrogen plasma reactors could potentially substitute coke ovens, agglomeration plants, blast furnaces, and oxygen steelmaking operations in the next iron making generation [21].

1.2 Objectives

The SuSteel project aims to obtain enough knowledge from a testing plant and recommend parameters to design an HPSR industrial plant. Therefore, the first step was the design and the construction of a testing plant, and the second step was to acquire the technology of the HPSR process to produce steel using the HPSR testing plant. For this purpose, a small hydrogen plasma reactor was installed at the laboratory of the Chair of Ferrous Metallurgy in Montanuniversitaet Leoben to study the characteristics of the HPSR technology. The next step is to employ a testing plant, which generates not only precise mass and energy balance data, but also a better estimation of the production parameters such as the degree of reduction and hydrogen utilization, the reduction rate of iron oxides and produced amount of metallic iron and slag.

The first aim of this work is to study the reduction of hematite using hydrogen thermal plasma by the means of laboratory-scale facilities. For this purpose, first, the generation of hydrogen

plasma in an arc plasma reactor by collisional processes should be studied, and then theoretically, the reduction ability of hydrogen species in terms of kinetics and thermodynamics should be evaluated. To study the reduction behavior of iron oxide, a series of experiments should be conducted and the main parameters of the reduction behavior, namely the degree of hydrogen utilization, degree of reduction, and the reduction rate should be investigated. Furthermore, the mechanism of hydrogen reaction with slag and molten iron oxide should be understood. Therefore, the slag formation with different basicities during the reduction process and the reduction behavior of iron oxides should be studied. Moreover, the study of the reduction behavior during the continuous charging of iron oxide is essential to be investigated.

The second aim of this work is to determine the temperature of the plasma arc of the laboratory plasma reactor. In the HPSR process, hydrogen in the plasma arc zone at high temperatures is activated and partially ionized. Ionized particles of hydrogen are strong reducing agents for iron oxide. The degree of hydrogen atomization and ionization depends on temperature. Therefore, to increase the degree of hydrogen ionization and, consequently, to increase the reduction rate of hematite, the reduction reactions should take place in the area of thermal plasma arc at high temperatures. Hence, the temperature of the plasma arc should be measured to determine the degree of hydrogen ionization.

2 Literature review and theoretical framework

In the first section, the literature review and the theoretical background of the iron oxide reduction using hydrogen are presented. In the following, the flow pattern in a chemical process reactor like the hydrogen plasma reactor is discussed. Finally, the current statement of HPSR technology and the requirements for the industrialization of this process are assessed.

2.1 Thermodynamics of hydrogen thermal plasma

In this section, the thermodynamics of hydrogen at high temperature was studied, and then the reduction behavior of iron oxide using hydrogen in terms of thermodynamics and kinetics are presented.

2.1.1 Ionization of hydrogen

In plasma, there are several basic species: photons, free electrons, atoms, ions, and molecules. Plasma state comprises light electrons and heavy ions; N_e and N_i are the density of the electrons and ions, respectively. The collision of two particles in plasma can cause various phenomena. Particles can change their energy or momentum; wherein neutral particles can become ionized and vice versa. In an elastic collision, the internal energy of particles is constant, and the total kinetic energy is conserved; on the other hand, kinetic energy between the particles is exchanged. In this kind of collision, the mass of the particles defines the amount of transferred energy. When the total kinetic energy of the particles

changes, it is known as an inelastic collision [26,27]. In general, inelastic collision involves ionization, excitation, recombination, charge transfer, and dissociation [26].

In HPSR, the collisional process is the dominant ionization process. Therefore, the collision between particles leads to the atomization and ionization of hydrogen and argon particles in the plasma arc zone [26]. Excitation is a transition of a ground-state electron of an atom or a molecule to a higher level of energy with the absorption of sufficient energy; these states are known as n*. The excited-state lifetimes are limited between 10^{-8} and 10^{-6} s. Ionization occurs when an atom or a molecule acquires sufficient energy to gain or lose an electron to form ions. The ionization energy of a hydrogen atom is 13.6 eV; however, an already excited particle needs less energy given by Bohr's theory. To ionize a hydrogen atom, which already has been excited from the second orbital layer (Ballmer series) with a wavelength of 410 nm, 3.4 eV energy is required.

$$\delta \mathrm{E_i} = \Delta \mathrm{E_i}\left(1 - \frac{1}{\mathrm{n^{*2}}}\right) \rightarrow \Delta \mathrm{E_i} - \delta \mathrm{E_i} = 3.4\ \mathrm{eV} \quad (1)$$

where $\mathrm{E_i}$ is the ionization energy from the i orbital layer, δE_i is the energy that the excited particles have already gained, $\Delta E_i - \delta E_i$ is a refinement of the ionization energy of the excited particles, and n* is the quantum number in the excited state [27,28].

In plasma, not only the number of negative and positive particles but also the rate of ionization and recombination are balanced [29]. In HPSR, hydrogen is used as a reducing agent to reduce iron oxides and the main ionization, atomization, excitation and recombination processes of hydrogen are listed in **Table 2-1**.

Table 2-1: Atomization, excitation, ionization and recombination processes of hydrogen [30]

Components	Reaction	Process
Electron - neutral	$e[-] + H_2 \rightarrow 2H + e[-]$	Collisional atomization
Electron - neutral	$e[-] + H \rightarrow H^+ + 2e[-]$	Collisional ionization
Electron - neutral	$e[-] + H_2 \rightarrow H_2^+ + 2e[-]$	Collisional ionization
Ion - neutral	$H^+ + 2H_2 \rightarrow H_3^+ + H_2$	Collisional ionization
Electron - neutral	$e[-] + H_2 \rightarrow H_2^* + e[-]$	Collisional excitation
Photon - neutral	$hv + H \rightarrow H^+ + e[-]$	Photoionization
Ion - electron	$H^+ + 2e[-] \rightarrow H + e[-]$	Three-body recombination
Ion - electron	$H^+ + e[-] \rightarrow H$	Two-body recombination
Ion - neutral	$H^+ + wall \rightarrow 1/2H_2 + e[-]$	Wall recombination
Neutral - neutral	$H + wall \rightarrow 1/2\,H_2$	Wall recombination

In the HPSR process, the dominant ionization process is collisional ionization by energetic electrons, which are emitted from the graphite electrode. A collision between an electron and molecular or atomized hydrogen could lead to atomize, ionize, or excite the hydrogen particles. Furthermore, photons, emitted from the recombination process, could excite, or ionize the neutrals called photoionization. On the other hand, the penetration of ionized hydrogen particles to the wall of the reactor (refractory lining) or drift to the anode and volume recombination are the dominant recombination processes. [29–32]

At high pressures or temperatures, the collision frequency generates a uniform energy distribution among all the particles. In thermal plasma, also called hot plasma, the temperature of electrons and ions are equal and chemical equilibrium exists. However, in HPSR, a cold flow of the H_2/Ar mixture is injected into the center of the arc zone through the hollow graphite electrode. Consequently, the stream of the cold-flow gas interacts with the plasma arc. Therefore, because of an imbalance of kinetic energy and the temperature difference among the particles, the plasma arc is not in complete thermodynamic equilibrium. Hence, for the simplicity, it is assumed to be at local thermodynamic equilibrium (LTE) and the temperature of the particles are in the same range.

In the case of cold-plasma or non-thermal plasma, it cannot meet all conditions of LTE. Therefore, the electron temperatures are significantly higher than those of heavy particles or ions [33,34].

2.1.2 Hydrogen wavelengths

Rydberg constant for heavy atoms (R_∞) is a physical constant used in Rydberg formula to obtain the hydrogen spectral series given by

$$R_\infty = \frac{m_e e^4}{8\varepsilon_0^2 h^3 c} \tag{2}$$

where $m_e, e, \varepsilon_0, h\ and\ c$ is the rest mass of the electron, the elementary charge, the permittivity of free space, the Planck constant, and the speed of light in vacuum respectively. The Rydberg constant for hydrogen (R_H) is calculated from the reduced mass of the electron by

$$R_H = \frac{R_\infty}{1+m_e/m_p} \sim 1.09 \times 10^7 m^{-1} \tag{3}$$

where m_e and m_p are the mass of the electron and proton, respectively. Rydberg Formula is used to obtain the wavelengths of the emitted photons with consideration of the different energy levels.

There are many hydrogen spectral series emitted by transitions of the electron from an outer orbit to a lower orbit of quantum number. The Lyman series lies in the ultraviolet region, The Balmer series is in the visible region and the Paschen, Brackett, Pfund, and Humphreys series lie in the infrared range. The transition of the electron from an outer layer of a hydrogen atom to the first quantum number emitted the lines in the ultraviolet band in a wavelength range of between 90 and 125 nm called Lyman series. The Balmer series are emitted by the transitions from an outer orbit to the orbital layer 2.

In the present study, Balmer series is used to calculate the temperature of the arc. Therefore, the method of the calculation of the wavelengths of this series is explained. Equation 4 is considered to describe the visible Ballmer series from the hydrogen atom for the fixed value of 2 for the lower energy level (q)

$$\frac{1}{\lambda} = R_H Z^2 \left(\frac{1}{2^2} - \frac{1}{n_p^2}\right) \tag{4}$$

Where n_p is the upper energy level, Z is the atomic number (Z=1). With consideration of the upper energy levels of the hydrogen atom, Balmer series of the hydrogen atom is shown in **Table 2-2**.

Table 2-2: Some wavelengths of the Balmer Series [35]

Transition $p \rightarrow q$	$3 \rightarrow 2$	$4 \rightarrow 2$	$5 \rightarrow 2$	$6 \rightarrow 2$	$7 \rightarrow 2$	$8 \rightarrow 2$	$9 \rightarrow 2$
Symbol	H-α / Ba-α	H-β / Ba-β	H-γ / Ba-γ	H-δ / Ba-δ	H-ε / Ba-ε	H-ζ / Ba-ζ	H-η / Ba-η
$\Delta E_i - \delta E_i$ [eV]	1.89	2.55	2.86	3.03	3.13	3.19	3.23
λ [nm]	656.3	486.1	434.0	410.2	397.0	388.9	383.5

For the current study, H-α and H-β with a wavelength of 656.3 and 486.1 nm are important lines used to calculate the plasma arc temperature.

2.1.3 Collision frequencies

The reduction reaction rate of iron oxide depends on the ionization degree of hydrogen particles. Therefore, the ionization degree of hydrogen plays an important role in this process. Different parameters are used to define the ionization degree namely the cross-section, the mean free path, and the collision rate.

Because atoms and ions do not have an exact size, to define the size, the collision cross-section as an effective blocking area is used. Bohr introduced a theory to use a radius for atoms to define the cross-section area of an atom

$$r = \frac{n^2 r_1}{z} \tag{5}$$

where n is the principal quantum number, r_1 is the radius of the first Bohr orbit which is $5.29 \times 10^{-8}\, m$ for the hydrogen atom and z is the atomic number. Based on Bohr's equation, the cross-section for atomic hydrogen is [27]

$$\sigma = 4\pi r_i^2 = 4 \times \pi \times (5.29 \times 10^{-8})^2 = 3.53 \times 10^{-14} m^2 \tag{6}$$

The collision probability is the probability of occurring a collision for a particle in a certain time

$$\mathrm{P} = \exp(-\varphi \mathrm{t}) \tag{7}$$

φ is the collision rate and t is time [36].

Considering the hydrogen atom, the mean free path λ_m, which is the average distance that an emitted electron travels without collision, is given by

$$\lambda_{\mathrm{m}} = 1/(N_H \sigma) \tag{8}$$

where $\mathrm{N_H}$ is the density of neutral hydrogen atoms. The mean time of collisions (τ) for electrons, with the velocity of V_e is [37]

$$\tau = \frac{\lambda_{\mathrm{m}}}{V_e} \tag{9}$$

Therefore, the collision frequency ν is the collision probability per mean time

$$\nu = \frac{1}{\tau} \tag{10}$$

Thus, in HPSR, to increase the collision frequency, the flow rate of hydrogen injection should be increased. However, the role of the velocity of the particles is more important which depends mainly on temperature.

Regarding the Maxwell-Boltzmann distribution function, the mean velocity (ω) of the particles is given by the temperature [36].

$$\omega = \sqrt{\frac{8.k.T}{\pi.m}} \tag{11}$$

where m is the mass kinetic energy of plasma and k is the Boltzmann constant ($1.38054 \times 10^{-23}\ \mathrm{JK^{-1}}$). Inside the arc plasma, hydrogen molecules or atoms are activated. The density of hydrogen active particles ψ_i on an electrically insulated surface is given by

$$\psi_i = \frac{N_i \omega_i}{4} \tag{12}$$

where N_i is the density of particles i, and combining equations 11 and 12 give the following formula, which is used for the calculation of activated particles:

$$\psi_i = 1.48 \times 10^{-12} N_i \left(\frac{T_i}{m_i}\right)^{1/2} [\mathrm{m^{-2}s^{-1}}] \tag{13}$$

Therefore, to increase the density of the active hydrogen particles, temperature and the number density of hydrogen particles should be increased.

2.1.4 Rate of hydrogen ionization

In the collision process, electrons collide with atoms, which, in turn, atoms are ionized. In the HPSR process, electrons collide with hydrogen atoms. To calculate the rate of hydrogen ionization, imagine an ionization reaction of hydrogen

$$H + e \leftrightarrow H^+ + 2e \tag{14}$$

If $\vec{V}_{He}$ is the relative velocity of a hydrogen particle H and an electron e, and the relevant cross-section is σ_{He}, the collision rate is

$$dw = N_H . \sigma_{He}(\vec{V}_{He}) . \vec{V}_{He} . dt \tag{15}$$

Besides, the probability of total collisions is

$$\frac{\mathrm{dw}}{\mathrm{dt}} = \mathrm{N_H . N_e . \sigma_{He} . (\vec{V}_{He}) . \vec{V}_{He}} = \mathrm{N_H . N_e . \varphi_{He}} \tag{16}$$

where N_e is the density of electrons and φ_{He} is the collision rate or reaction rate [27,31].

If the velocity of the electron is significantly greater than that of hydrogen neutrals, to calculate the rate of production of new electrons per unit volume, the ionization collision frequency ($N_H . \sigma_{ion} . V_e$) multiplied by the electron density N_e which is called the 'source rate' S_e of electrons

$$S_e = N_e . N_H . \sigma_{ion} . V_e \tag{17}$$

Where N_e and N_H are the electron and hydrogen neutral atom density respectively. σ_{ion} is the cross-section for the electron-impact ionization and V_e is the electron velocities. In contrast, the sink rate is a conception to produce natural atoms by the recombination process, which is equal but the inverse of S_e.

The ionization rate ($\sigma_{ion} . V_e$) of hydrogen atoms by the Maxwellian distribution of electrons temperature T_e(eV) is calculated by

$$\sigma_{ion} . V_e = \frac{2\times10^{-13}}{6+T_e/13.6}\left(\frac{T_e}{13.6}\right)^2 e^{(13.6/T_e)} \tag{18}$$

The equation is a good approximation to the ionization rate. **Figure 2-1** shows the graph of the equation 18.

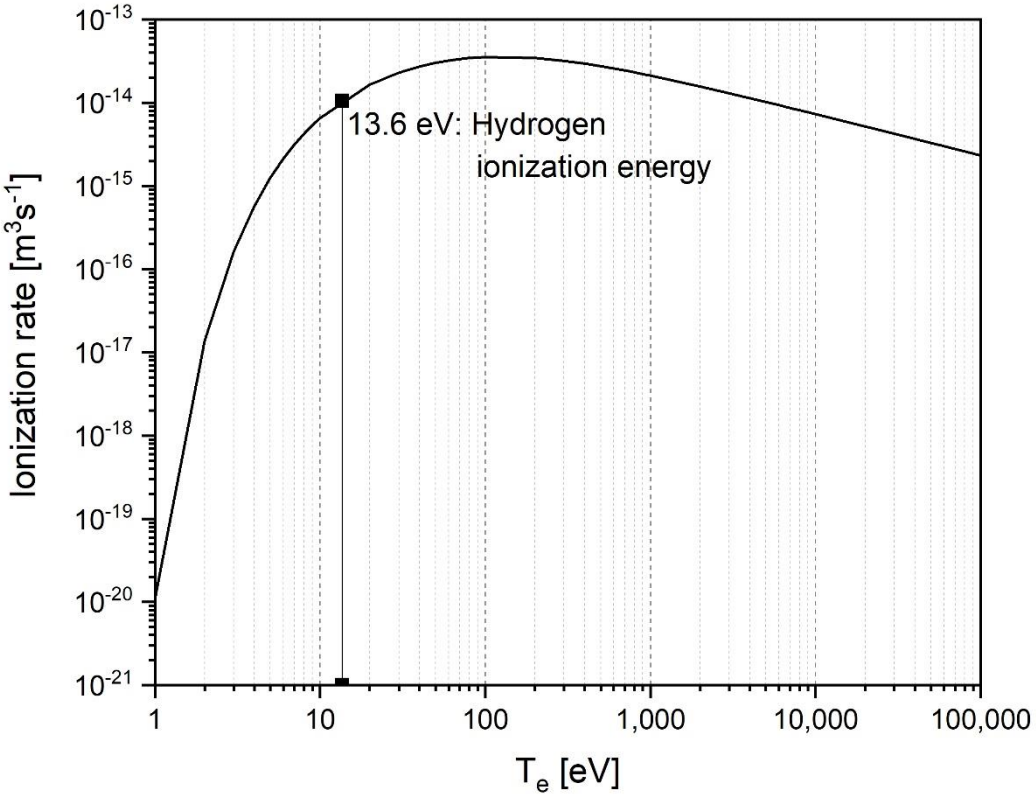

Figure 2-1: Ionization rate of hydrogen atoms over electrons temperature T_e [37].

The figure shows that even at temperatures below 13.6 eV, hydrogen is significantly ionized. The reason is that there are energetic electrons at low temperatures which could ionize hydrogen atoms [37]. The equation shows that at partial ionization of hydrogen, the temperature is the main influencing parameter.

2.1.5 Degree of hydrogen ionization at high temperatures

To calculate the degree of hydrogen ionization at high temperatures, Saha's equation can be used

$$\frac{N_{r+1}N_e}{N_r} = \frac{G_{r+1}g_e}{G_r}\frac{(2\pi m_e kT)^{3/2}}{h^3}e^{-E_r/kT} \tag{19}$$

Where N_r and N_{r+1} are the number densities of atoms in the corresponding state. G_r and G_{r+1} are the partition functions, N_e is the electron number density, $g_e = 2$ is the statistical weight of the electron, m_e is the mass of the electron, E_r is ionization potential of state r (to

reach state $r+1$), T is temperature, h is the Plank's constant, and k is the Boltzmann constant. To determine the degree of hydrogen ionization, the statistical weight of the hydrogen electron was considered two, whereas one for the ionized hydrogen [31]. With consideration of the degree of ionization $x = N_{r+1}/N_r$, that becomes

$$\frac{x^2}{1-x} = \frac{1}{d}\left(\frac{2\pi m_e kT}{h^2}\right)^{3/2} e^{-13.6eV/kT} \tag{20}$$

The graphical representation of the degree of pure hydrogen ionization for the HPSR process is shown in **Figure 2-2**.

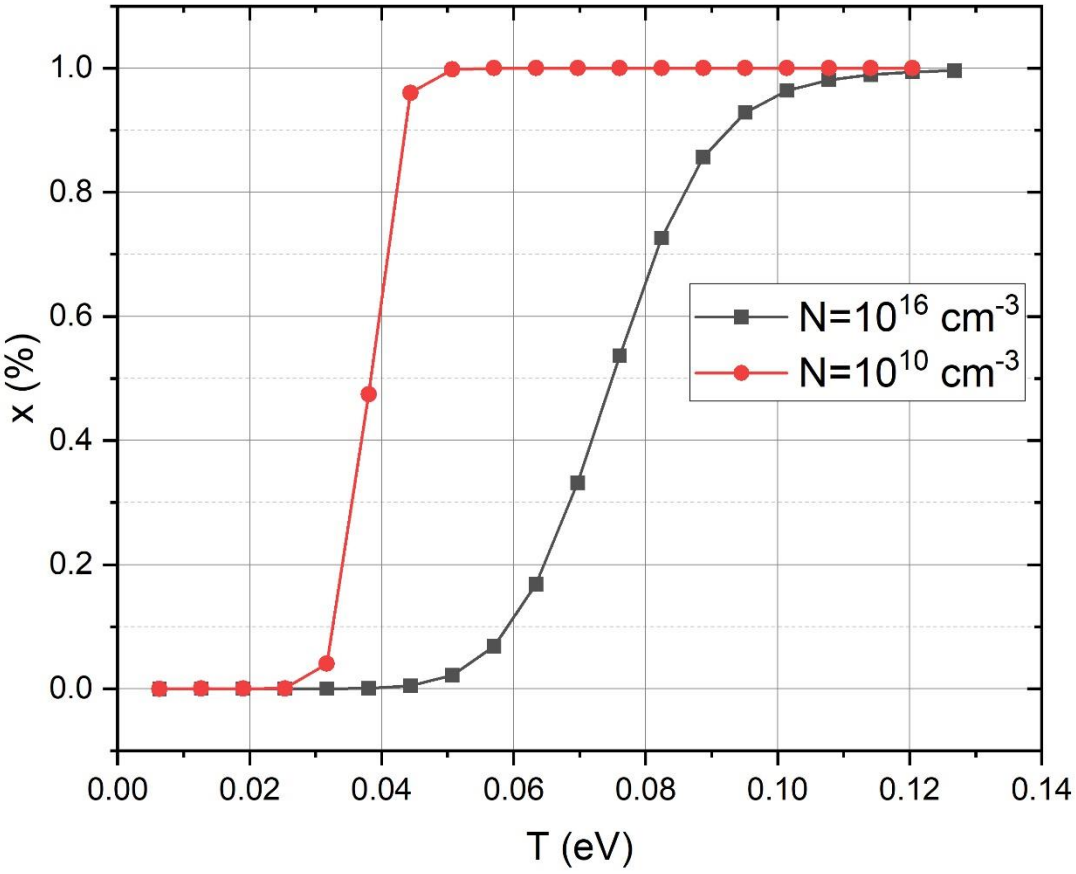

Figure 2-2: The degree of hydrogen ionization over temperature

This curve is plotted to demonstrate the ionization potential for two numbers of hydrogen particle densities N, 10^{16} and $10^{10} cm^{-3}$ [31,36]. Obviously, the ionization fraction is increased sharply, by increasing the temperature. This graph is used to evaluate the fraction of hydrogen ionization for the current study.

2.1.6 Properties of HPSR plasma gases

In HPSR, a mixture of H_2/Ar or H_2/N_2 is injected into the plasma reactor through the hollow graphite electrode. Therefore, they are activated at the high temperatures in the arc zone. Argon is a monoatomic gas, and the generated plasma from argon comprises argon atom, argon ions, and electrons. The ionization and recombination of argon is given as

$$Ar \leftrightarrow Ar^+ + e \tag{21}$$

Nitrogen is a molecular gas, and it should be first dissociated and then ionized. Therefore, nitrogen plasma is composed of molecular, atomic, and ionic nitrogen and electrons. However, it is also possible to form molecular ions. The chemical equation of dissociation and ionization of nitrogen is

$$N_2 \leftrightarrow N + N \tag{22}$$

$$N \leftrightarrow N^+ + e \tag{23}$$

The dissociation and ionization of one mole argon and one mole nitrogen particles were calculated using FactSage™ 7.2 (Database FactPS), and the related diagram is shown in **Figure 2-3**.

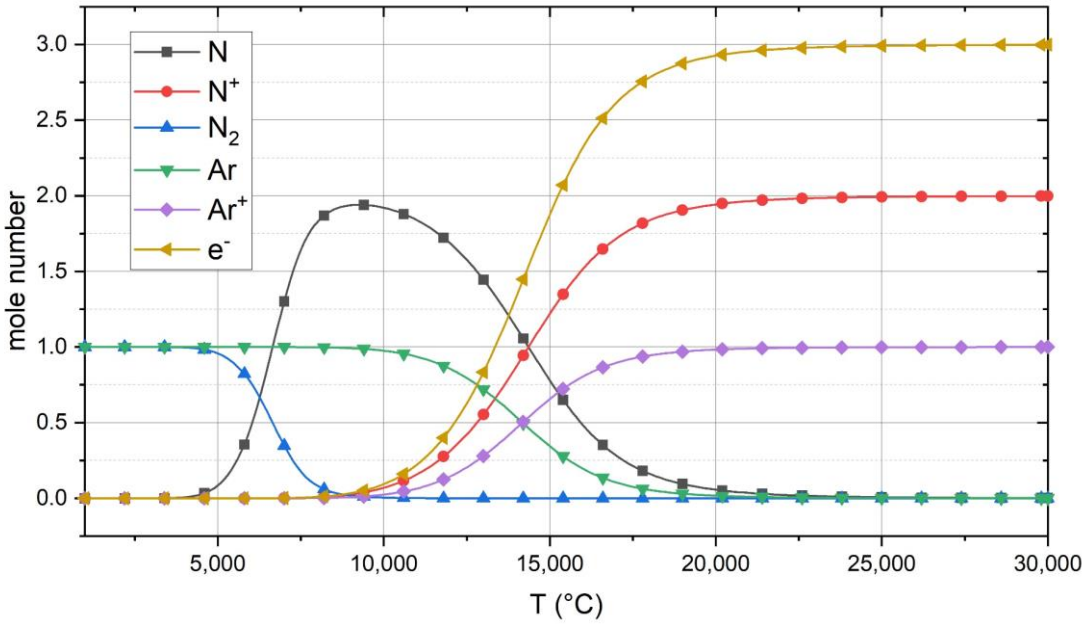

Figure 2-3 Gas composition of a N_2 / Ar mixture over the temperature at 100 kPa, calculated using FactSage™ 7.2, Database FactPS.

This figure shows that the atomization and ionization are two different processes. The dissociation of nitrogen begins at temperatures above 4000 °C, and then at 9000 °C, which is completely atomized, the ionization process begins. At the temperatures above 14,000 °C, the number of ionized particles exceeds the number of atomized nitrogen. Argon is a monoatomic element which is directly ionized. The results are in good agreement with Kanhe et al. [38] and Lisal et al. [39] work. The ionization begins at 9000 °C and at temperatures above 14,200 °C, the ionization process is the dominant process [40,41].

The dissociation, ionization and recombination processes of one mole of hydrogen at equilibrium over temperature are shown in **Figure 2-4**.

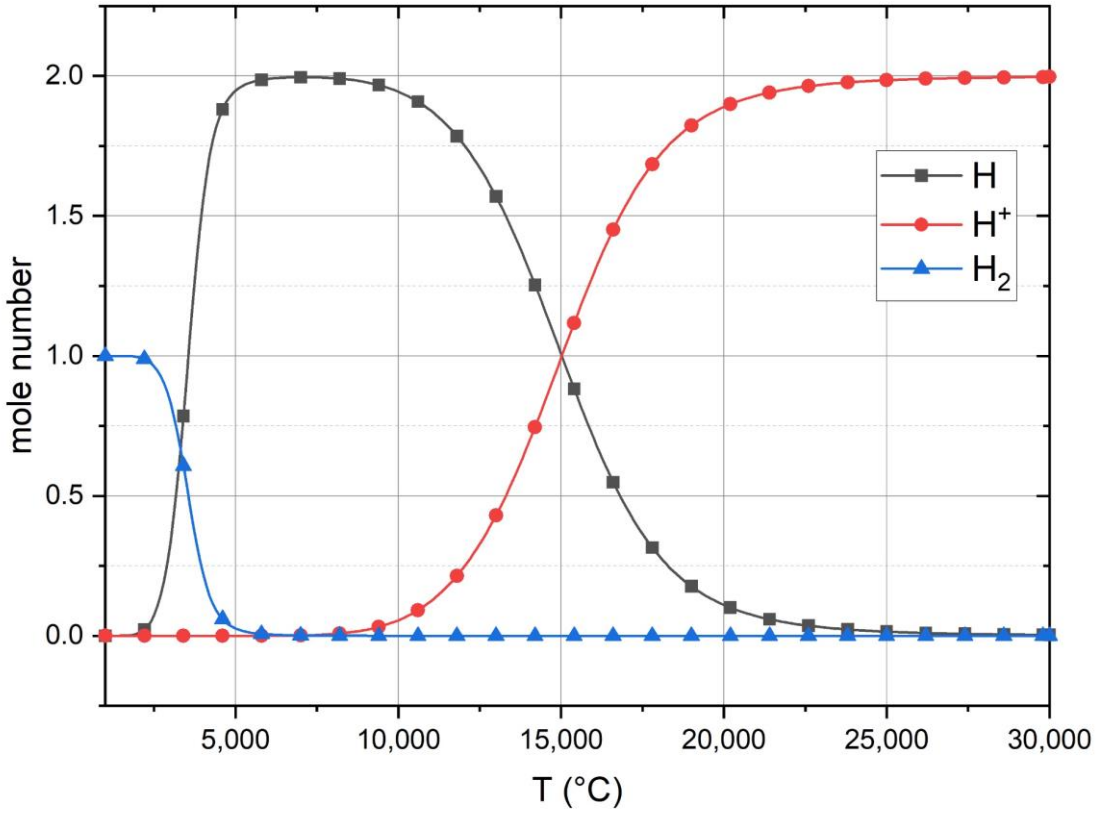

Figure 2-4: Dissociation and ionization of hydrogen over the temperature at 100 kPa (FactSage™ 7.1, Database FactPS).

Hydrogen as a molecular gas is first atomized and then ionized by an increase of temperature [29,31,32]. It is obvious that above 15,000 °C, the amount of ionized hydrogen (H^+) overpasses the amount of dissociated hydrogen (H).

In the following, viscosity, thermal conductivity, electrical conductivity, and heat capacity of various gas mixtures are shown. These are the main properties of the gases that influence the

efficiency of the process. Viscosity influences the collisional integrals for interaction between the particles into the plasma arc zone. The viscosity of argon and nitrogen is greater than that of hydrogen due to their high molecular mass. Figures **Figure 2-5** and **Figure 2-6** show the viscosity of H_2-Ar and H_2-N_2 mixtures over the temperature range, respectively.

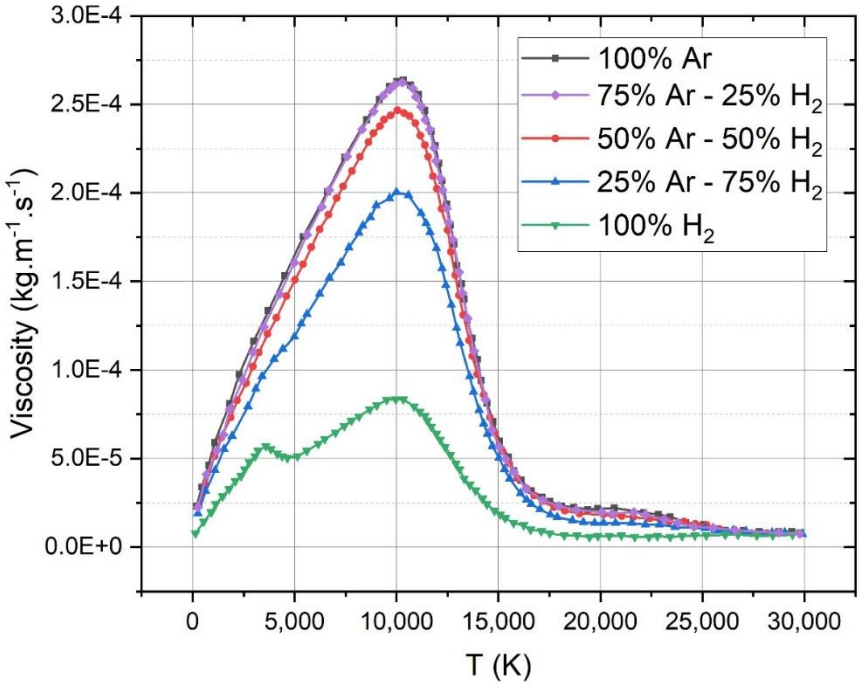

Figure 2-5: Viscosity of hydrogen and argon mixtures vs temperature [12].

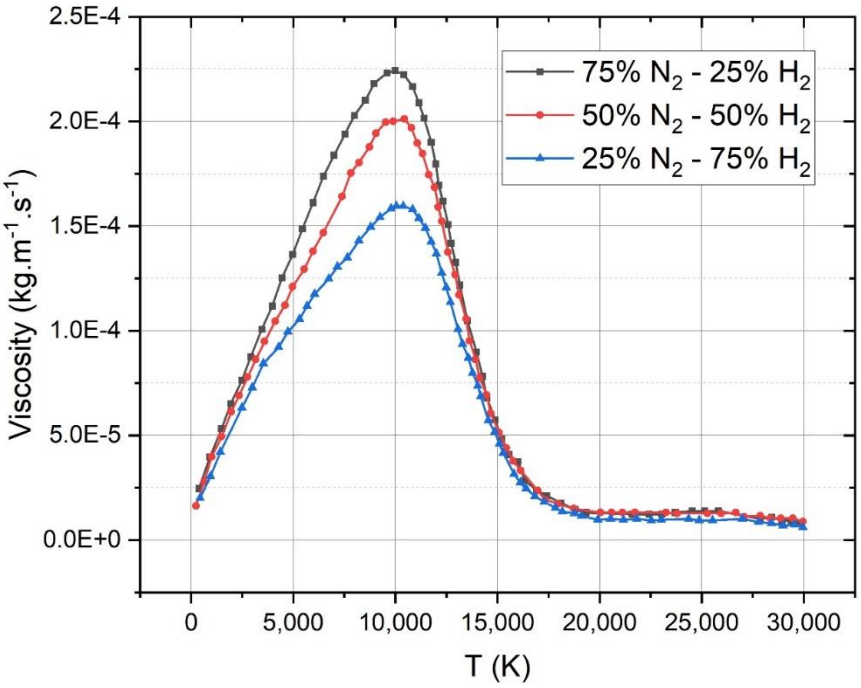

Figure 2-6: Viscosity of hydrogen and nitrogen mixtures vs temperature [42].

The figures show that with the increase in the hydrogen concentration in the mixture, the viscosity decreases. With an increase of the temperature, nitrogen and hydrogen begin to be atomized which caused an increase in viscosity. At temperatures above 10,000 K, the ionization process is started which leads to a decrease in viscosity. At high temperatures, there is no considerable difference between viscosities [17,42]. With the consideration of the viscosity, nitrogen and argon have similar properties to be used in HPSR process. Therefore, viscosity is not an important issue to be considered for the selection of argon or nitrogen [17,42,43].

The reduction reaction rate of iron oxide with hydrogen in the liquid state is higher than that of solid-state [21,44]. In HPSR, the reduction reaction of iron ore occurs in two steps. Firstly, the inflight reduction reaction occurs in the distance between the tip of the hollow graphite electrode (HGE) and the liquid iron oxide [45]. Therefore, if the gas particles can conduct enough heat to melt the iron ore fines in flight, the chance to reduce iron ore in this area would be higher. Moreover, higher thermal conductivity makes the melting of the iron ore particles more feasible. Second, the reduction of iron oxides can occur on the surface of the molten slag, where the higher conductivity leads to an increase in the temperature of the slag.

Figure 2-7 and **Figure 2-8** show the thermal conductivity of H_2-Ar and H_2-N_2 mixtures over the temperature, respectively.

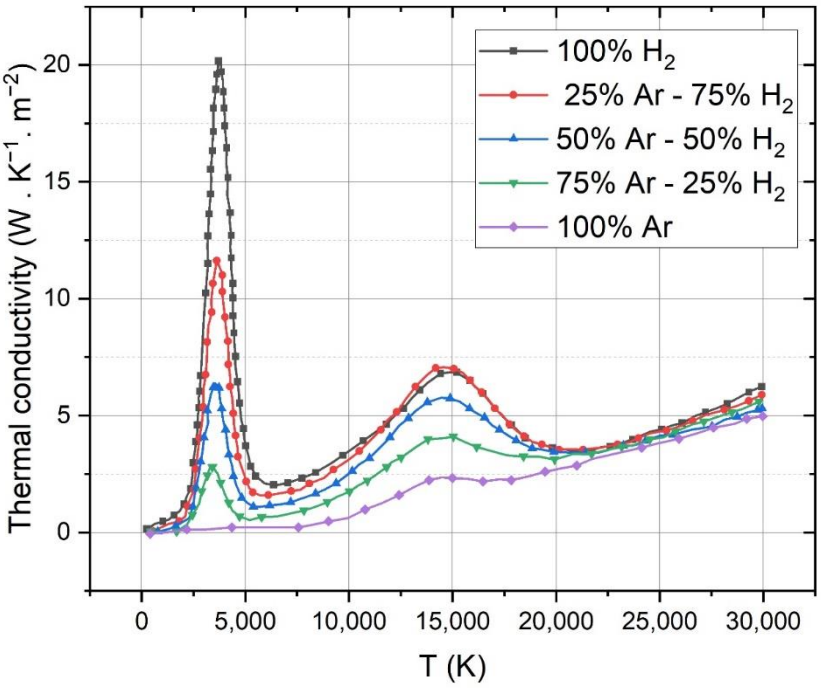

Figure 2-7: Thermal conductivity of hydrogen and argon mixtures vs temperature [17].

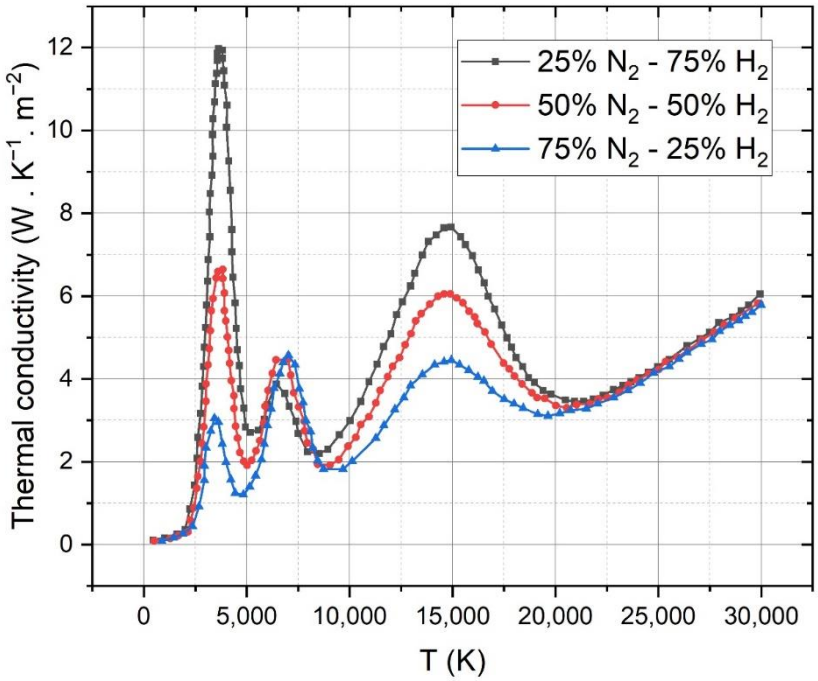

Figure 2-8: Thermal conductivity of hydrogen and nitrogen mixtures vs temperature [42]

In fact, with the increase in temperature, the thermal conductivity of the pure gases or the mixtures increases. However, there are some peaks in the diagram, which belong to the dissociation and ionization of the gases. For instance, the dissociation of hydrogen and nitrogen generates sharp peaks at 3500 K and 7000 K, respectively. The thermal conductivity of hydrogen is considerably higher than that of nitrogen and argon at temperatures below 17,000 K. However, at temperatures above 20,000 °C, there is no considerable difference between thermal conductivities [17,42,43].

The electrical conductivity of H_2-Ar and H_2-N_2 mixtures are shown in **Figure 2-9** and **Figure 2-10** respectively [17,42].

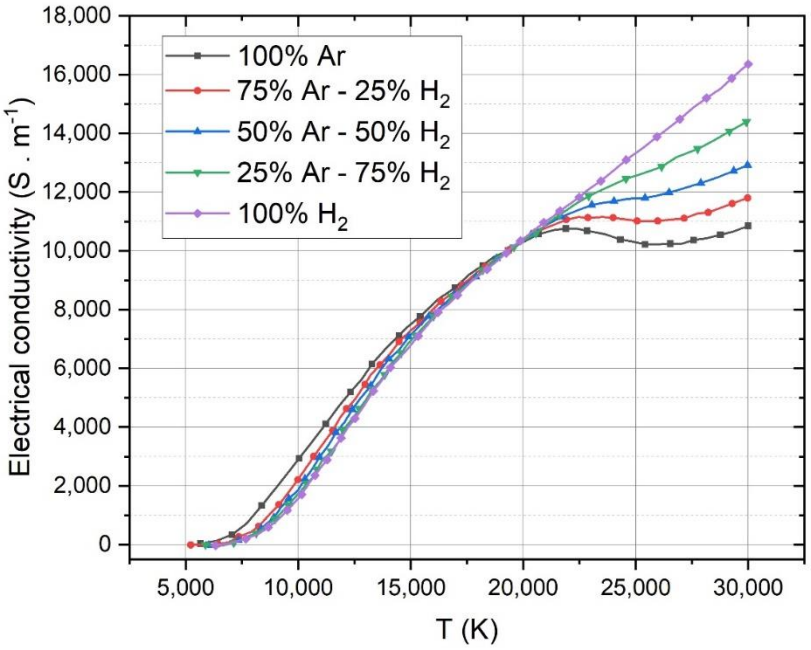

Figure 2-9: Electrical conductivity of hydrogen and argon mixtures vs temperature [17].

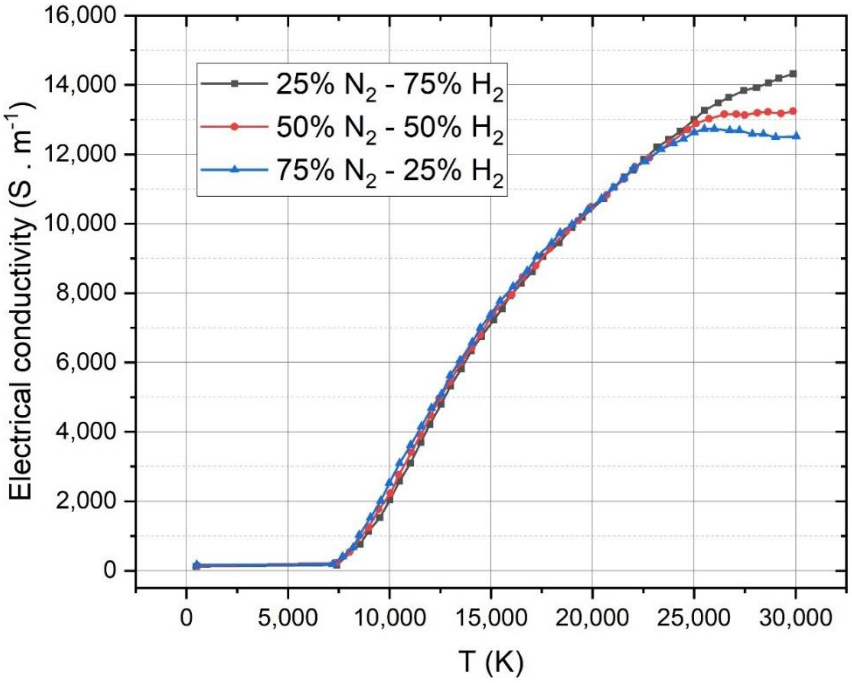

Figure 2-10: Electrical conductivity of hydrogen and nitrogen mixtures vs temperature [42]

The pure gases and their mixtures have almost similar electrical conductivity. The electrical conductivity of argon at temperatures below 20,000 °C is higher than that of hydrogen. However, the electrical conductivity of hydrogen increases with temperature, which makes it a better electrical conductor at temperatures above 20,000 °K in comparison to argon or nitrogen [17,42,43].

The heat capacity of argon, hydrogen, and nitrogen is calculated by FactSage™ 7.2 (Database FactPS), and the results are shown in **Figure 2-11**.

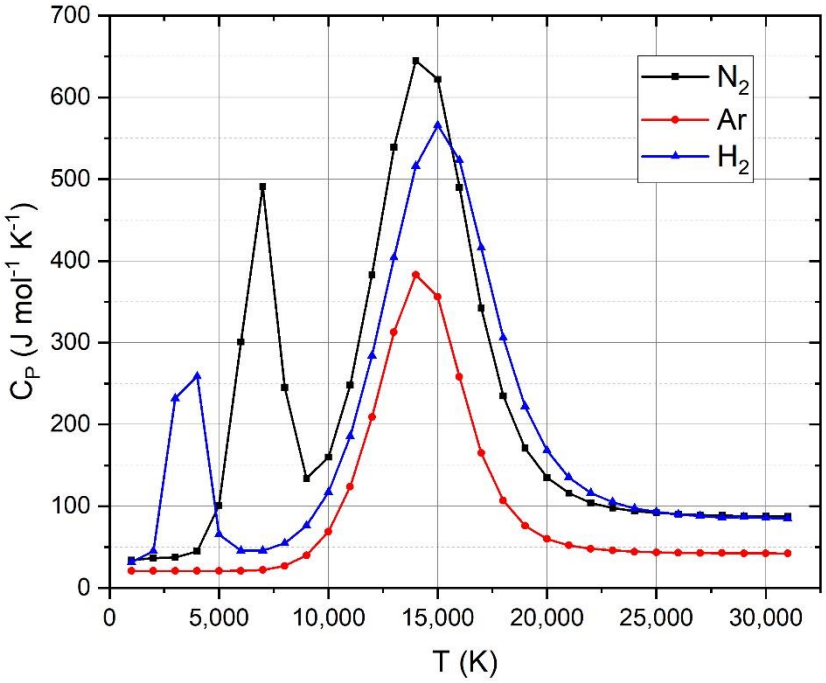

Figure 2-11: C_p of HPSR gases (FactSage™ 7.2, Database FactPS).

The existence of a peak in C_p values of nitrogen and hydrogen at temperatures of less than 10,000 °C is associated with the dissociation of these gases. Nitrogen has a greater heat capacity than argon. Therefore, the flame of the arc is constricted, and the temperature increases in the boundary layer region around the plasma arc. However, to operate the process with H_2-N_2 mixture requires more energy. The mass and energy balance data for the H_2-Ar and H_2-N_2 mixtures of the HPSR operations were calculated theoretically. It showed that in the case of operating the HPSR with a mixture of 50% H_2-50% N_2, the energy consumption will increase by 15% in comparison to the use of 50% H_2-50% Ar mixture.

In HPSR, the thermodynamic calculations show that hydrogen, nitrogen, and argon are not only ionized at the plasma arc zone, but they are also dissociated and partially ionized in the boundary layer region around the plasma arc due to the temperature gradient. Argon and nitrogen are quite similar in viscosity, thermal conductivity, and electrical conductivity. However, the heat capacity of nitrogen and hydrogen is higher than that of argon. Therefore, in the case of the operation of the process with a mixture of H_2-N_2, the energy demand would be more than that of H_2-Ar mixture. Kinetics of the reduction reactions needs further investigations and conducting related trials.

2.1.7 Temperature of the arc

Semenyshyn *et al*. [46] reported the temperature of the plasma arc between 5000 and 8000 C using spectroscopic methods. They generated a free burning electric arc between Ag–SnO_2–ZnO composite electrodes and brass electrodes to measure the temperature of the arc.

Mašláni *et al*. [47] have carried out a spectroscopic measurement of plasma arc cutting using a DC arc. The plasma gas was a vaporized mixture of water and ethanol with a current of 60 A. They reported that the plasma arc temperature in the center of the arc can be exceeded more than 20,000 K. Then in 2 mm from the tip of the electrode, the temperature of the arc was decreased less than 10,000 K.

Dzierżęga *et al*. [48] have used a sub-doppler degenerate four-wave mixing (DFWM) spectroscopy to study the temperature of the argon arc plasma. They have generated an arc discharge between a tungsten electrode as a cathode and a disc as an anode with argon at a pressure of one atm. The plasma temperature was 18570 K and 12770 K at 0.4 and 7.5 mm, respectively, from the tip of the cathode. Other researchers [49,50] have measured the temperature of the electric arc using computational studies. They reported that the temperature was more than 20,000 K in the center of the arc and lower around the plasma arc. The plasma characteristics of AC electric arc furnace in a pilot-scale have been studied [51] using the spectroscopic method and the plasma temperature was reported in the range of 4500 and 9000 K.

Furthermore, several other researchers [52–59] have measured the temperature of the electrons by the spectral relative intensity, in which the procedures in this section are explained. These methods are used to calculate the temperature of the plasma arc in the current study. Regarding the intensity of two wavelengths from the same element, the absolute intensity of a spectral line in an optically thin plasma with the length of L along the light of sight is

$$i_{pr} = {}^{L}/_{4\pi}\, h\upsilon_{pr} A_{pr} N_p \tag{24}$$

$$i_{qr} = {}^{L}/_{4\pi}\, h\upsilon_{qr} A_{qr} N_q \tag{25}$$

where i_{pr} and i_{qr} is the intensity of the spectral line initiated by spontaneous electron transition from the energy level of p or q to r, respectively; h is the Planck constant; υ_{pr} and υ_{qr} are the corresponding frequencies of radiations; A_{pr} and A_{qr} are the corresponding transition probabilities; N_p and N_q are the particle number densities on the energy level of p and q, respectively.

The thermal equilibrium population ratio of the numbers of ions to neutrals $^{N_p}/_{N}$ at the LTE state, which is the uniform temperature distribution among the particles, is given by

$$\frac{N_p}{N} = \frac{g_p}{Z_a(T)} e^{\left(-\frac{E_p}{kT}\right)} \tag{26}$$

where g_p is the statistical weight of the state p; Z_a is the partition function, and E_p is the upper energy level. For the two different energy levels p and q of the same element, the Boltzmann factor relation can be extended by

$$\frac{N_p}{N_q} = \frac{g_p}{g_q} e^{(-\frac{E_p - E_q}{kT_e})} \tag{27}$$

Combining equations 24 and 25, equation 27 can be represented by

$$\frac{i_{pr}\upsilon_{qr}A_{qr}}{i_{qr}\upsilon_{pr}A_{pr}} = \frac{g_p}{g_q} e^{(-\frac{E_p - E_q}{kT_e})} \tag{28}$$

The temperature of the electron is given by

$$T_{e_1} = -\left[\frac{E_p - E_q}{kln(\frac{i_{pr}\upsilon_{qr}A_{qr}g_q}{i_{qr}\upsilon_{pr}A_{pr}g_p})}\right] \tag{29}$$

At the present study, two different methods were used to calculate the temperature of the electrons using optical emission spectra. For this issue, the first method with the use of equation 29 has already been discussed. The second method was presented by Cui *et al.* [54]. They calculated the temperature of the electrons in $CH_4 + H_2$ discharge plasma at atmospheric pressure.

If q is replaced by r in the below equation

$$\frac{N_p}{N_q} = \frac{g_p}{g_q} e^{(-\frac{E_p - E_q}{kT_e})} \quad (27 \tag{30}$$

$$\frac{N_p}{N_q} = \frac{g_p}{g_q} e^{(-\frac{E_p - E_q}{kT_e})} \quad (27 \tag{31}$$

and combining with equation 32

$$i_{pr} = {}^{L}/_{4\pi} h\upsilon_{pr}A_{pr}N_p \quad (24 \tag{32}$$

Therefore

$$i_{pr} = h\upsilon_{pr}A_{pr}N_r \frac{g_p}{g_r} e^{(-\frac{E_p - E_r}{kT_{e_2}})} \tag{33}$$

To obtain the electrons temperature, natural Log is taken of both sides for the two different wavelengths $p \rightarrow r$ and $q \rightarrow r$ of the same element

$$ln\, i_{pr} = ln(h\upsilon_{pr}) + ln(A_{pr}N_r\frac{g_p}{g_r}) - \frac{E_p - E_r}{kT_{e_2}} \quad (34)$$

$$ln\, i_{qr} = ln(h\upsilon_{qr}) + ln(A_{qr}N_r\frac{g_q}{g_r}) - \frac{E_q - E_r}{kT_{e_2}} \quad (35)$$

Subtracting equations 35 and 34

$$ln\left(\frac{i_{pr}}{i_{qr}}\right) = ln\left(\frac{\upsilon_{pr}}{\upsilon_{qr}}\right) + ln\left(\frac{A_{pr}g_p}{A_{qr}g_q}\right) - \frac{E_q - E_p}{kT_{e_2}} \quad (36)$$

This leads to obtaining the equation of electron temperature

$$T_{e_2} = \left[\frac{E_q - E_p}{k\left[ln\left(\frac{\upsilon_{pr}}{\upsilon_{qr}}\right) + ln\left(\frac{A_{pr}g_p}{A_{qr}g_q}\right) - ln\left(\frac{i_{pr}}{i_{qr}}\right)\right]}\right] \quad (37)$$

In the present study, equations 29 and 37 are used to calculate the electron temperatures of different operating conditions.

.

2.2 Thermodynamic aspects of reduction

2.2.1 The thermodynamic principles of iron oxides reduction by hydrogen

Hematite (Fe_2O_3) and magnetite (Fe_3O_4) are the main iron ore oxides, from which metallic iron is extracted in a blast furnace by carbo-thermic reduction. This process includes multiple stages and needs large-scale equipment. Coke is used as a reducing agent to produce pig iron in a blast furnace [25] which leads to produce liquid steel with high amount of carbon. Therefore, to remove carbon from the steel melt, the de-carbonization process is essential. The reduction of iron oxides can be affected by the hydrogen plasma process. Thermal plasma and the application of hydrogen intensify the process and cause not to enter carbon into the steel, which in turn, leads to produce steel in the one-stage process which is shown in **Figure 2-12**.

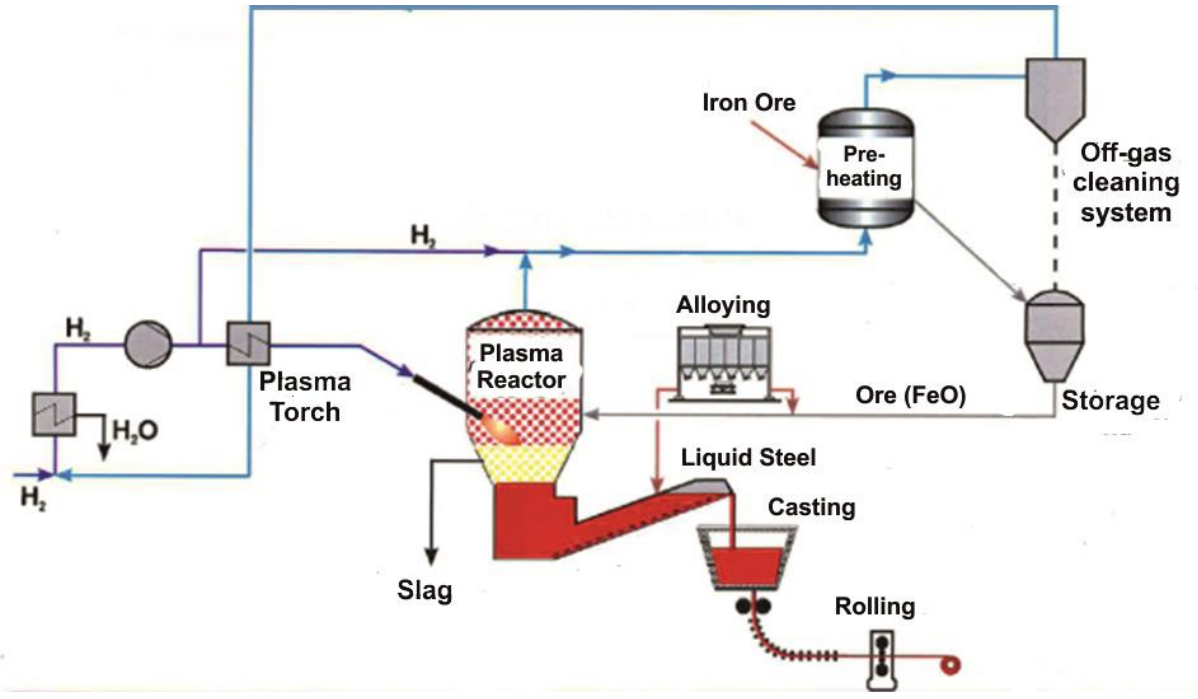

Figure 2-12: Hydrogen plasma smelting process for reduction iron ores

In HPSR process, steel is produced using iron ore fines without pre-agglomeration which is one of the main advantages of this process.

Several studies have been carried out to produce iron from iron ores using hydrogen. Gold *et al*. [20] investigated the one-stage production of iron from iron oxides by hydrogen-helium

thermal discharge plasma. Gilles and Clump [60] studied the reduction of iron ore using hydrogen in a DC plasma jet. They reported that heat transfer to oxide particles is the main factor to identify the kinetics of the reduction process. There is no doubt that hydrogen can be used as a reducing gas in direct reduction processes, but from a design standpoint, it is necessary to establish the kinetics of reduction of iron ore into iron [61].

Stokes reduced iron oxides by hydrogen-helium plasma in a one-stage process. The complete reduction was achieved by injecting Fe_2O_3 powder at a flow rate of 0.3 g/min with hydrogen flowing at 13.6 L/min into the plasma furnace with a power level of 15.5 kW. Other researchers investigated the reduction of iron ore using hydrogen in the plasma state [3,44,60]. They used a DC plasma furnace as a reactor to reduce iron ore, in which the process concept was similar to this study. Mac Rae *et al.* [62] reported the development of a one-stage plasma furnace. They charged iron oxide powders to the liquid iron bath and reduced oxides using a hydrogen and natural gas mixture.

HPSR process has been intensively investigated at the University of Leoben [3,21–24]. Badr *et al*.[3] studied thermodynamics, kinetics, and the scaling up of HPSR process. Their results approved the observations of previous researchers [44,63–66]. One of the main results is the lower degree of hydrogen utilization in the case of using a high concentration of hydrogen in H_2-Ar mixture. Their results are discussed in section 4.

Figure 2-13 shows of the Bauer-Glaessner diagram for H_2/H_2O and CO/CO_2.

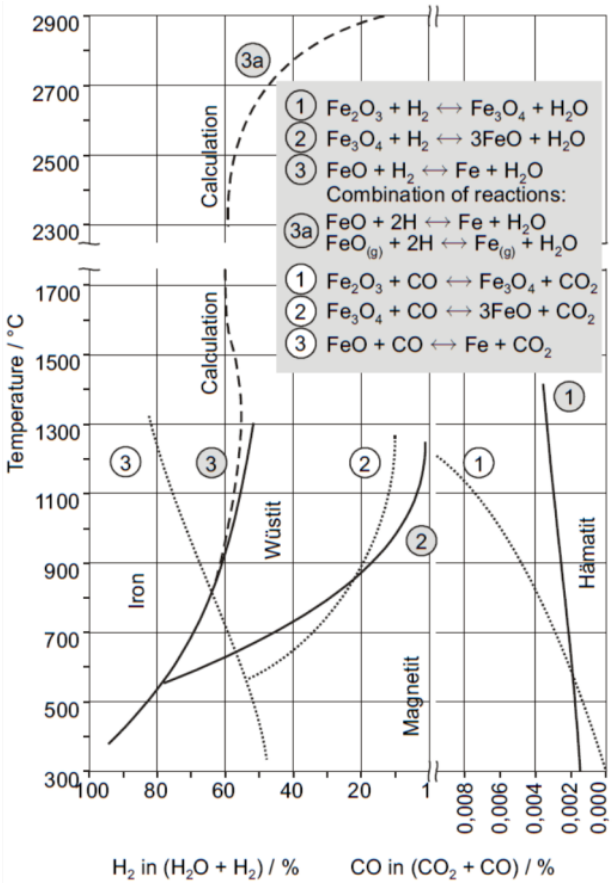

Figure 2-13: Combination of the Bauer-Glaessner diagram for H_2/H_2O and CO/CO_2 atmosphere [67]

It is indicated that below 570 ℃, the magnetite phase is directly reduced to iron. The reduction reactions of wustite and hematite are represented in the Bauer-Glaessner diagrams for hydrogen and carbon monoxide reduction. At the temperatures above 810 ℃, the reduction of wustite is possible by hydrogen at a lower hydrogen concentration in the mixture of H_2/H_2O than that of carbon monoxide in the mixture of CO/CO_2. As an example, at 1100 ℃, 54% H_2 can reduce wustite, in contrast, 75% of monoxide carbon in the corresponding mixture is required [3,21,67]. Hence, in these terms of view, hydrogen is the preferred agent for the smelting reduction of iron oxides.

In 1970, Gilles and Clump [60] showed that the reduction rate of iron oxides in a direct current hydrogen plasma jet depends on the heat transfer to the iron oxide particles. The rate of reduction of liquid FeO and its bearing slags was reported by Kamiya *et al.* [44], who represented that the rate of FeO reduction using H_2–Ar plasma is significantly higher than that of the other reducing agents such as carbon and carbon monoxide. Uchikoshi *et al.* [68] used

the hydrogen plasma arc discharge smelting process to produce high purity of semiconductor grade Fe in 2004.

Rajput *et al.* [61] reported that iron oxide reduction using hydrogen takes place at the temperature of 1473–1773 K in some seconds. This finding is in good agreement with the results of the experiments presented in publication 1 in the attachment of this paper [69]. The chemical composition of both sides of a slag layer with a thickness of one millimeter was measured. The chemical compositions showed that iron oxide fines existed only on the upper side of the slag, and on the lower side, the reduction degree was more than 90%. Therefore, the iron oxide particles were reduced immediately by hydrogen thermal plasma.

2.2.2 Thermodynamics reduction using hydrogen plasma

In the plasma state, hydrogen in the molecular form is supplied. Plasma causes molecular hydrogen to change to atomic, ionic, or other excited forms. The reduction reaction of metal oxide by hydrogen is given by:

$$MeO_x + xH_2 \rightarrow Me + xH_2O,\ \Delta G_1 > 0 \tag{38}$$

ΔG denotes the Gibbs free energy changes. Molecular hydrogen is activated by plasma

$$H_2(gas) \leftrightarrow HydrogenPlasma\left(2H, 2H^+, H_2^+, 2/3\, H_3^+, or\ H_2^*\right),\ \Delta G_2 >> 0 \tag{39}$$

Therefore, the reduction reaction of metal oxide ($\mathrm{MeO_x}$) with hydrogen plasma is represented as:

$$MeO_x + xHydrogenPlasma(2H, 2H^+, H_2^+, 2/3\, H_3^+, or\ H_2^*) \rightarrow Me + xH_2O$$

$$\Delta G_3 \leftrightarrow \Delta G_1 - x\Delta G_2 < 0 \tag{40}$$

In the case of hematite reduction using hydrogen plasma

$$Fe_2O_3 + 3\ Hydrogen\ plasma\ (2H, 2H^+, H_2^+, 2/3\, H_3^+, or\ H_2^*) \leftrightarrow 2Fe + 3H_2O(g)$$

$$\Delta G < 0 \tag{41}$$

$\Delta G_1$is positive, in other words, metal oxides are not reduced by hydrogen at the ambient temperature. ΔG_3, which defines the spontaneity or possibility of the reduction reaction by hydrogen plasma, is negative because ΔG_2 is more positive than ΔG_1. As a consequence, hydrogen plasma reduces metal oxides more feasible and even at low temperatures [70].

Ellingham diagram, calculated using FactSage™ 7.2, is shown in **Figure 2-14** for metal-oxide and H_2O–H_2, H_2O–H and H_2O–H^+ lines over the temperature.

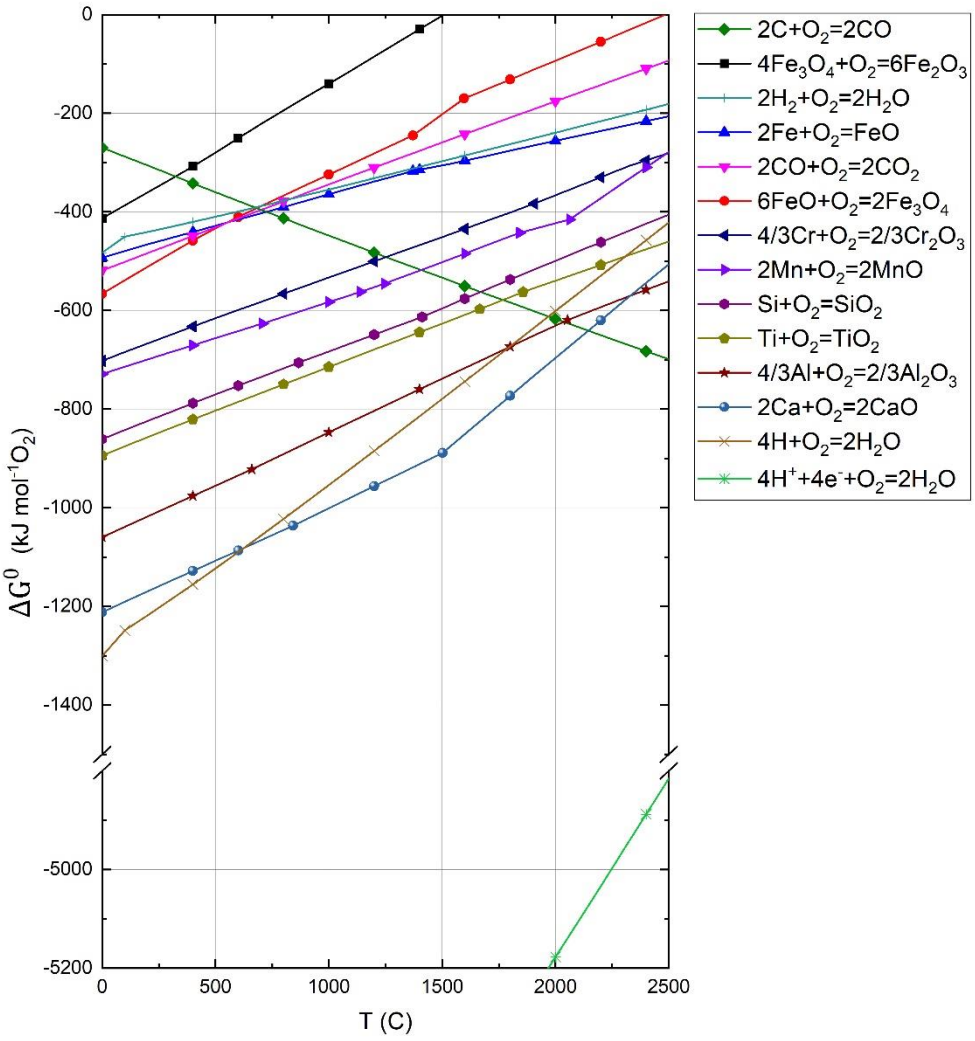

Figure 2-14: Ellingham-Richardson diagram for various metal oxides calculated using FactSage™ 7.2, Database FACT oxide compounds (2019)

Ellingham diagram provides an estimation of the possibility of metal oxides reduction in terms of thermodynamic aspects. It shows that H_2O–H^+ line lies below the lines of other metals and their oxide. As a consequence, the reduction of metal oxide using hydrogen in the plasma state is thermodynamically favorable [21,70]. There are many possible processes not only to reduce iron ores but also other metal oxides using hydrogen plasma. Because hydrogen plasma contains different species, namely, the hydrogen molecule, excited hydrogen molecule, monoatomic hydrogen, and ionic hydrogen, which are all able to reduce metal oxides in the different range of temperatures [61].

2.2.3 Thermodynamics of reduction using monoatomic hydrogen agent

Monoatomic hydrogen is one of the most powerful agents to reduce different metal oxides. **Figure 2-14** shows that ΔG^0 values of H_2O–H is 3 times lower than that of H_2O–H_2, and is located below the oxide-metal lines. Rajput *et al.* [61] studied the reduction of iron oxides using hydrogen monoatomic. They showed that monoatomic hydrogen can reduce iron oxides at low partial pressures and low temperatures [61].

Thermodynamics calculations have been carried out by Robino [71] to compare the reduction ability of molecular and atomic hydrogen in terms of Gibbs free energy changes. The basic reaction for producing water from molecular hydrogen is

$$2H_2 + O_2 \leftrightarrow 2H_2O, \Delta G_1^0 = -492.9 + 0.1096\,T \tag{42}$$

The equilibrium between molecular and atomic hydrogen and the related Gibbs free energy is

$$4H \leftrightarrow 2H_2\,, \Delta G_2^0 = -875.61 + 0.21205\,T \tag{43}$$

Uniting equation 42 and 43, water is formed by monoatomic hydrogen by

$$4H + O_2 \leftrightarrow 2H_2O\,, \Delta G_3^0 = -1368{,}51 + 0{,}32167\,T \tag{44}$$

If the mixtures of H and H_2 is assumed to follow the ideal gas rules, henceforth,

$$\frac{P_H}{P_{H_2}} = \frac{n_H}{n_{H_2}} = \frac{V_H}{V_{H_2}} \tag{45}$$

where P_H and P_{H2} are the partial pressure, n_H and n_{H2} are the numbers of moles, and V_H and V_{H2} are the volume of H and H_2, respectively. The formation of water using a mixture of H and H_2 is

$$n_H H + n_{H_2} H_2 + \left(n_H/4 + n_{H_2}/2\right) O_2 \leftrightarrow \left(n_H/2 + n_{H_2}\right) H_2O \tag{46}$$

If the molar fraction of H in the mixture is n, then

$$n = n_H/\left(n_H + n_{H_2}\right) \tag{47}$$

Obtaining n_{H_2} from n gives:

$$n_{H_2} = n_H(1-n)/n \tag{48}$$

Uniting equation 46 and 48 yields

$$n_H H + \frac{n_H(1-n)}{n} H_2 + (n_H/4 + \frac{n_H(1-n)}{2n}) O_2 \leftrightarrow (n_H/2 + n_H(1-n)/n) H_2O \tag{49}$$

Solving and normalizing the reaction 49 yields

$$\frac{4n}{2-n}H + \frac{4(1-n)}{2-n}H_2 + O_2 \leftrightarrow 2H_2O \quad (50)$$

From ΔG_1^0 and ΔG_3^0, the Gibbs free energy changes for this reaction is given by:

$$\Delta G_4^0 = \frac{1}{2-n}(-985.75 - 382.75\,n + (0.21924 + 0.10242\,n)\,T) \quad (51)$$

Figure 2-15 represents the standard Gibbs free energy changes for different mole fraction of monoatomic hydrogen (n) over the temperature in increments of 0.1.

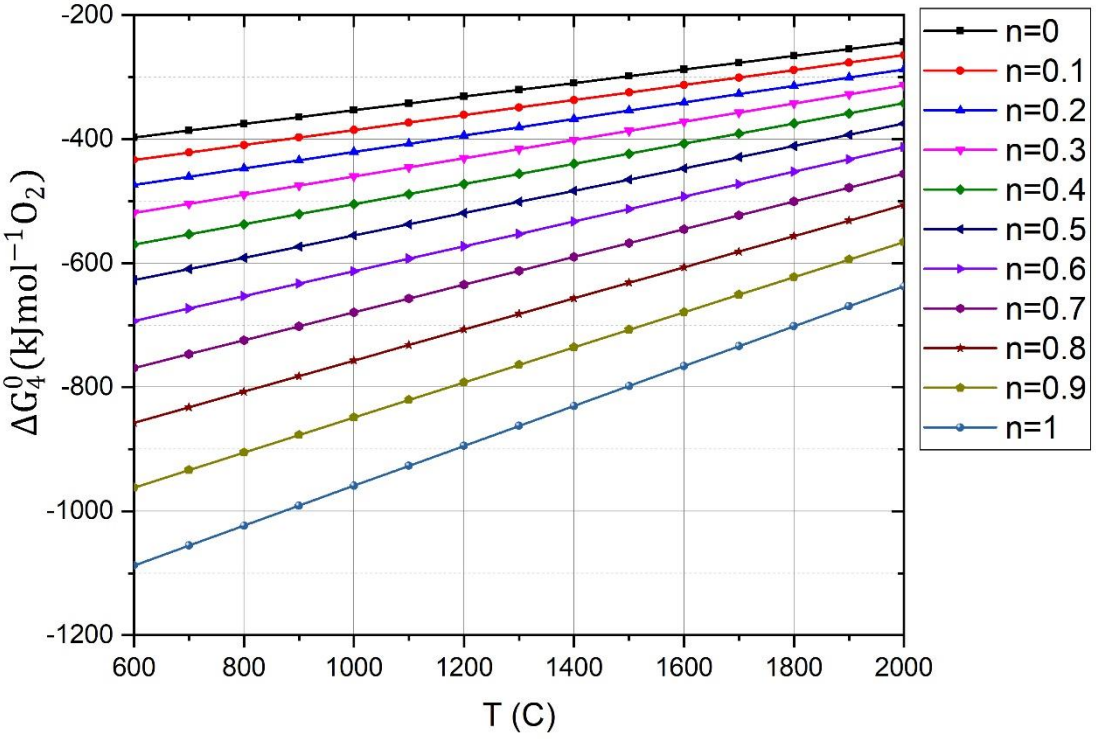

Figure 2-15: The temperature variation of the standard free energy for the equation 50 [58]

It shows that with an increase of the mole fraction of monoatomic hydrogen, the standard Gibbs free energy significantly declines. Nevertheless, the mole fraction of ionic hydrogen is low, its reduction potential is significantly high. In other words, monoatomic hydrogen (H) can reduce metal oxides more readily.

Assuming that the oxidation reaction of metals is described as follows:

$$2x/y\,M + O_2 \leftrightarrow 2/y\;M_xO_y\,,\;\Delta G_5^0 \quad (52)$$

ΔG_5^0 is the free energy change for the above reaction.

Therefore, the reduction reaction of metal oxide in a mixture of H and H_2 is written by

$$\frac{4n}{2-n}H + \frac{4(1-n)}{2-n}H_2 + 2/y\ M_x O_y \leftrightarrow 2H_2O + 2x/y\ M \tag{53}$$

After all, the general Gibbs free energy changes for the reduction reaction of metals using molecular and monoatomic hydrogen is

$$\Delta G = \Delta G_4^0 - \Delta G_5^0 \tag{54}$$

By replacing ΔG_4^0 and ΔG_5^0 in equation 54,

$$\Delta G = \frac{1}{2-n}(-985.75 - 382.75\,n + (0.21924 + 0.10242\,n)\,T) - \Delta G_5^0 \tag{55}$$

As has been noted, in the hydrogen plasma state, besides the molecular and monoatomic hydrogen, ionic hydrogen species also exist. Zhang et al. [30] presented that the main hydrogen species in a hydrogen plasma at moderate pressures are H, H^+, H_2^+, H_3^+. They studied the Gibbs free energies changes for the formation of H_2O using hydrogen species over temperature. As a conclusion, the ordered the reduction potentials as follows

$$H^+ > H_2^+ > H_3^+ > H > H_2 \tag{56}$$

Figure 2-16 shows the reduction potential of hydrogen species for the reduction of iron oxides as a function of temperature calculated using FactSage™ 7.1 (Database: FactPS 2017).

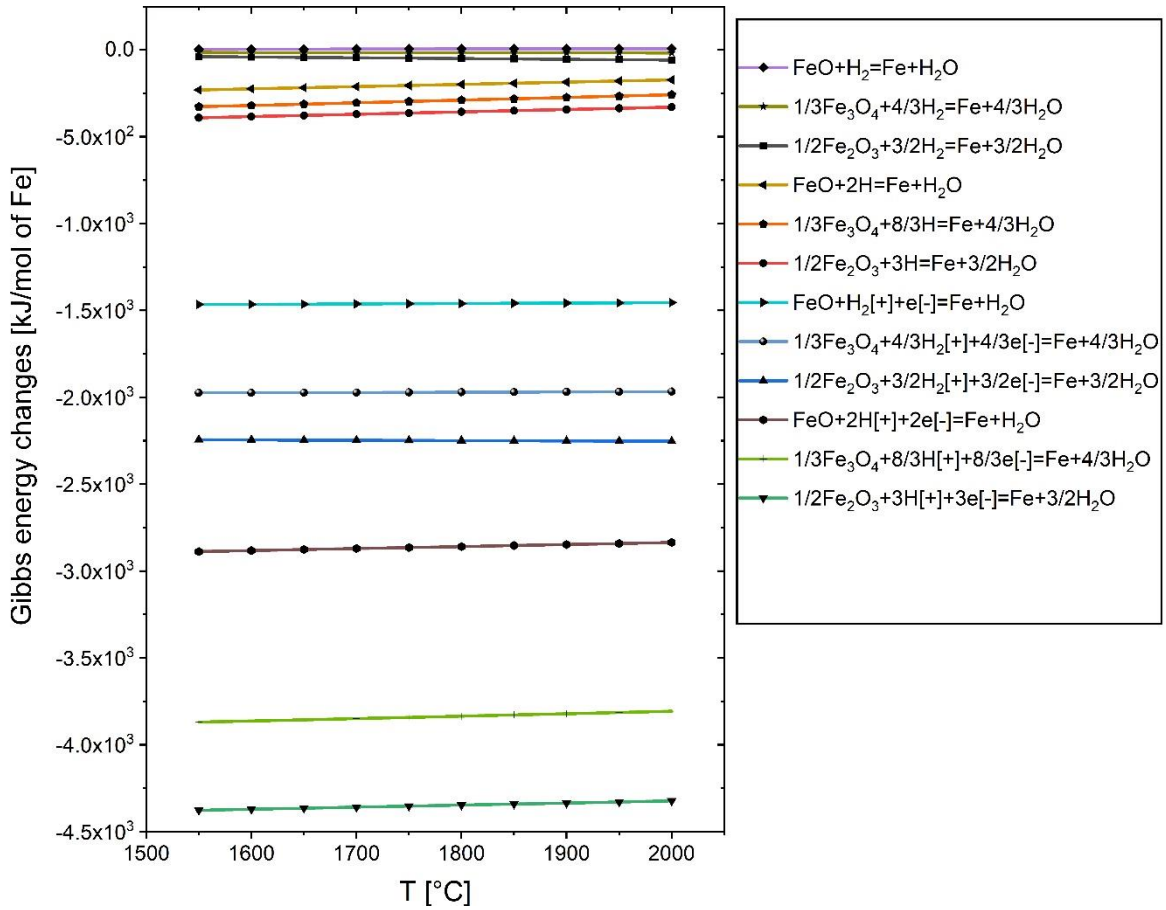

Figure 2-16: Gibbs free energy changes as a function of the temperature for the reduction of Fe_2O_3, Fe_3O_4, and FeO using hydrogen species at plasma state (FactSage™ 7.1, Database: FactPS and FtOxide 2019).

The order of reduction potential of hydrogen plasma presented in this diagram is in good agreement with that of the Zhang *et al.* [30]. The figure shows a comparison of iron oxides stability in terms of the reduction process using hydrogen. As a result, FeO is the most stable form of iron oxide. Consequently, to have a high potential of reduction, the reduction reaction of iron oxides should occur using hydrogen-activated particles (i.e., atomized, ionized, and excited state of hydrogen particles).

2.2.4 Polarity of charge

The polarity of plasma charge can be positive, negative, or neutral. Upon the polarity of charge, the density of ions and electrons changes during approaching the charged surface. The boundary layer is closed to the plasma surface where the plasma sheath is on the bottom. In the plasma sheath, the charged particles are influenced by the polarity of the plasma

surface, in such a way that the oppositely charged particles are attracted and the same charges repelled [2,70,72].

The order of magnitude Debye length determines the density of the charged particles in the plasma sheath [36]. The Debye length is given by

$$\lambda_D = (\frac{\varepsilon_0 k T_e}{e^2 n_e})^{1/2} == 69.1(\frac{T_e}{n_e})\ [m] \quad (57)$$

where λ_D is the Debye length in m, *e* is the electron charge and equals 1.6×10^{-19} As, ε_0 is dielectric constant and equals 8.86× $10^{-12}\ F/m$, and k is Boltzmann constant. The thickness of the plasma sheath in thermal plasma is between 10^{-8} to 10^{-7} m [36]. The average temperature of the electrons in the plasma sheath of a thermal plasma is approximately 25,000 K with an electron density of $10^{23}\ \mathrm{m}^{-3}$, which is a layer closed to the slag surface in HPSR process. Therefore, the Debye length is 3.5×10^{-8} m. In a typical plasma process, the thickness of the plasma sheath and the Debye length are approximately equal. Nevertheless, the sheath edge, which is a transition layer between plasma and sheath with a low collision rate, is in the range of 1 to 10 times of Debye length [36,73]. The thermal boundary layer lied above the plasma sheath is thicker than that of the plasma sheath. In this layer, the recombination process leads to a decrease in the concentration of the active particles.

The thermodynamics of surface charged polarity in metallurgical processes was studied by Dembovsky [72] He outlined that electrons with higher velocity can first reach the neutral surface which caused the surface to be negatively charged. Therefore, a neutral surface attracts the ions and repels the negative electrons.

A schematic of the concentration of the ions and electrons in the vicinity of plasma charged surfaces is shown in **Figure 2-17** and **Figure 2-18**. When the surface is positively charged, the density of the electrons is higher than the density of the ions in the plasma sheath, and vice versa.

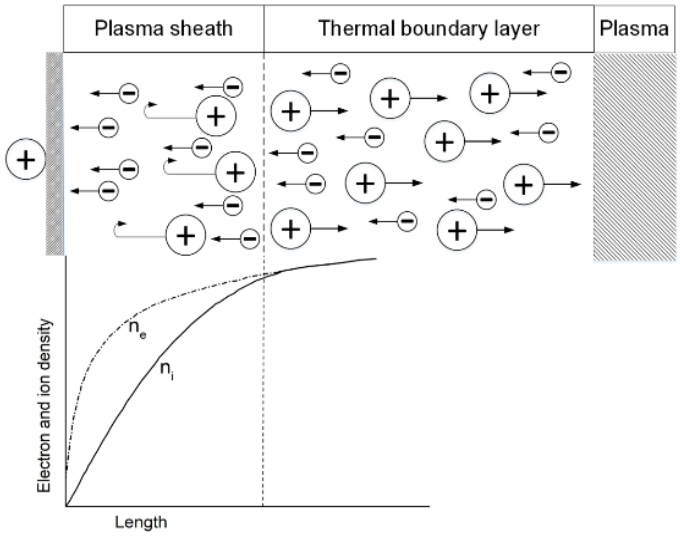

Figure 2-17: Concentration of the ions and electrons in the plasma sheath and thermal boundary layer of a positively charged surface [36,72].

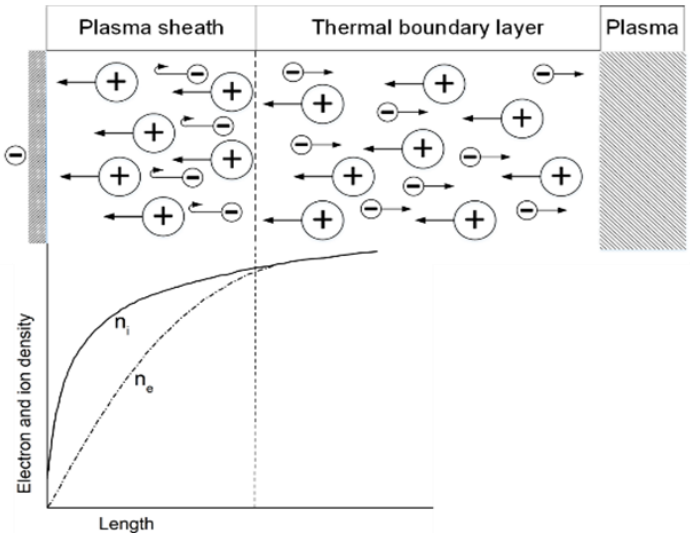

Figure 2-18: Concentration of the ions and electrons in the plasma sheath and thermal boundary layer of a negatively charged surface [36,72].

With the consideration of the direct current straight polarity (DCSP) of the HPSR process, the hollow graphite electrode is the negative pole, and in contrast, the liquid slag is the positive pole. Therefore, positive ions of hydrogen are repelled by the liquid slag, caused a decrease in the reduction rate. Dembovsky [72] studied the Gibbs free energy changes with the consideration of the surface polarity during the reduction of iron oxides using hydrogen thermal plasma at 10,000 K. The reduction reaction of FeO using hydrogen thermal plasma is

$$FeO + xH_2 + yH + zH^+ + ze^- \rightarrow Fe + H_2O \quad (58)$$

where x, y, and z are the molar fractions of molecular, atomic, and ionized particles of hydrogen, respectively. At high temperatures, hydrogen is activated. Therefore, the temperature of the particles and the polarity of charge are the main two influencing parameters on the reduction rates of iron oxide [2,70,72]. Dembovsky [72] showed that if the surface polarity of charge is negative, the reduction rate of iron oxide would be higher.

In the current work, the Gibbs free energy changes of the iron oxide reduction considering the charge polarity was studied using FactSage™ 7.2 (Database: FactPS 2019). **Figure 2-19** shows the results of the thermodynamics calculations.

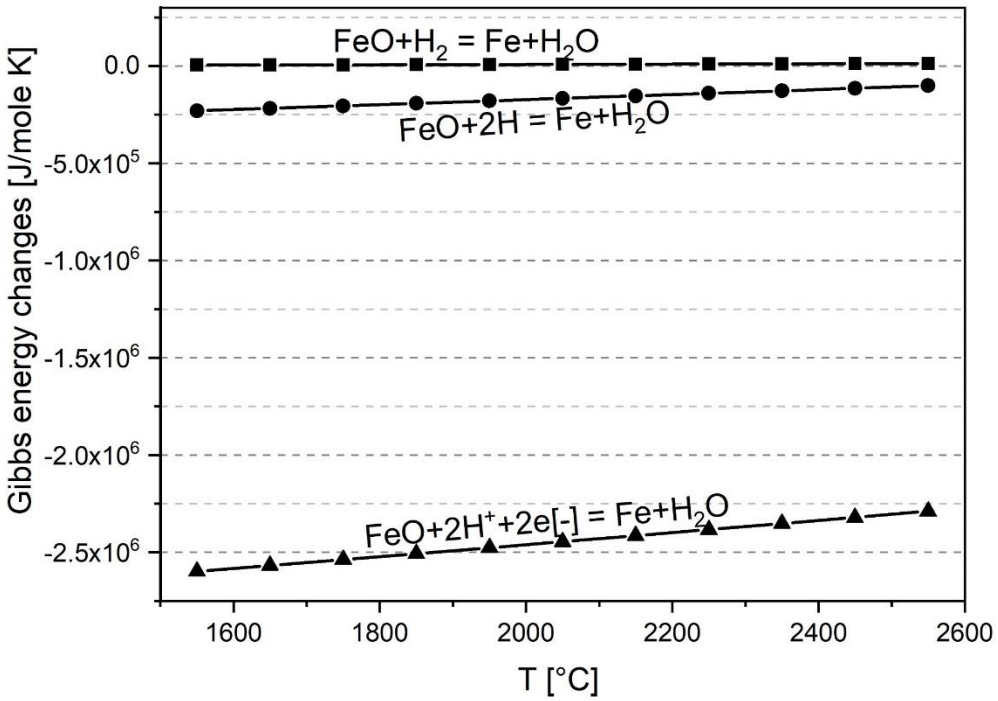

Figure 2-19: Gibbs free energy changes over temperature for the reduction of iron oxide

In the case of applying the positive polarity in HPSR process, the positive ions of hydrogen cannot touch the liquid slag surface, which leads to an increase in the Gibbs free energy changes and be more positive.

2.3 Review of literature on the kinetics of molten iron oxide reduction using different reducing agents

Several investigations have been carried out to evaluate the reduction rate of solid iron oxides in conventional steelmaking processes. However, a study on the kinetics of the reduction of iron ore in the liquid state is scarce [20,60,74,75]. Nowadays, conventional iron making processes are the main source of CO_2 emission in the steel industry. Therefore, the hydrogen plasma smelting reduction of iron oxides is one of the new iron making processes for the next generation. Hence, kinetic aspects of understanding and controlling the process play an essential and extremely important role. Katayama et al. [76] studied the reduction of molten iron oxide using a mixture of H_2 and H_2O. Nagasaka et al. [65] showed that the reduction rate of molten iron oxide using hydrogen was high and the mass transfer in the gas-phase was of uppermost importance.

In the plasma state, the role of ro-vibrationally excited hydrogen molecules has been emphasized in investigations [77,78]. Ro-vibrational transition is a transition including changes in both vibrational and rotational states. Molecules in the ro-vibrationally excited state can have an internal energy up to 4.5 eV [77]. In those circumstances, inelastic collisions and chemical reactions cause to transfer internal energy of excited particles to other molecules and atoms in the gas phase. Therefore, increasing the internal energy of the reactants and declining of the activation barrier making the reactions easier.

The reduction of hematite in a non-thermal hydrogen plasma was studied by Rajput *et al.* [61], they indicated that hematite is reduced by excited hydrogen molecules even at temperatures below 573 °K, however, in absence of plasma, hydrogen molecule gas is not able to reduce hematite at the same conditions. The reason is that the plasma state causes to create excited hydrogen particles which, in turn, decline the activation energy from 46 to 5.36 KJ/mol [70].

Plasma not only makes the reduction reaction more readily by decreasing the activation energy but also, affects the surface interactions. Contacting excited hydrogen molecules with the reaction surface causes the surface to overheat, which leads to an increase in the reduction rates [70].

2.3.1 Kinetics of iron oxide reduction using hydrogen

To take place a reaction, the reactants must first collide to cope with the activation barrier. Going up the temperature of the system causes an increase in the number of molecules with enough energy to react. The reduction rate is defined by the slowest event at the process, which restricts the overall reaction rate. Kamiya *et al.* [44] proposed a mechanism of iron oxides reduction reactions using hydrogen plasma which is given by the following steps:

1- Gas-phase mass transfer of hydrogen to reach the reaction interface

2- Liquid-phase mass transfer of oxygen from molten iron oxide to the reaction zone

3- Touch and adsorption of hydrogen on the reaction surface

4- Dissociation of iron oxide particles at the reaction zone

5- Reduction reaction of iron oxide at the reaction interface

6- Desorption of the reduction product, which is water, from the surface

7- Mass transfer of water in the gas phase

Nagasaka *et al.* [65] presented the three limiting steps regarding the reduction of FeO using hydrogen

1. Mass transfer in gas flow
2. Interfacial reduction reaction
3. Liquid-phase mass transfer of oxygen through the liquid film to the reaction interface

By preparing enough flow rate of reducing agent, the effect of step (1) on the overall reaction rate would be negligible and can be eliminated. In the case of reducing pure liquid Fe_tO, the effect of step (3) could be neglected. However, this step becomes important in the reduction process of liquid Fe_tO containing additives [65].

The reduction of liquid FeO, using different mixtures of hydrogen and an inert gas such as argon, nitrogen, or helium at 1400 °C, has been carried out by Ban-ya et al. [74]. They reported that the reduction rate of liquid wustite was influenced by the partial pressure of H_2 in the mixture of H_2-Ar, H_2-He, or H_2-N_2. The empirical equation of the reduction rate was given by

$$r = k[H_2]P_{H_2}\ (kg_{O_2}/m^2 s) \tag{59}$$

where r is the specific reduction rate, $k[H_2]$ is the apparent rate constant for the reduction reaction by hydrogen $(kg_{O_2}/m^2 s\ Pa)$. P_{H_2} is the partial pressure of hydrogen. Moreover, the gas flow rate was another important influencing parameter on the reduction rate. If the gas flow

rate with a mixture of H_2-Ar or H_2-N_2 was less than 4 L/min and for H_2-He mixture less than 7 L/min, the reduction rate was controlled by the mass transfer in the gas phase. For the flow rates higher than 28 L/min, it was restricted by the chemical reaction at the interface. Furthermore, for a range of 4-28 and 7-28 L/min, both steps were limiting the reduction rate.

Figure 2-20 shows the reduction rate of liquid FeO at 1400 °C regarding the partial pressure of hydrogen.

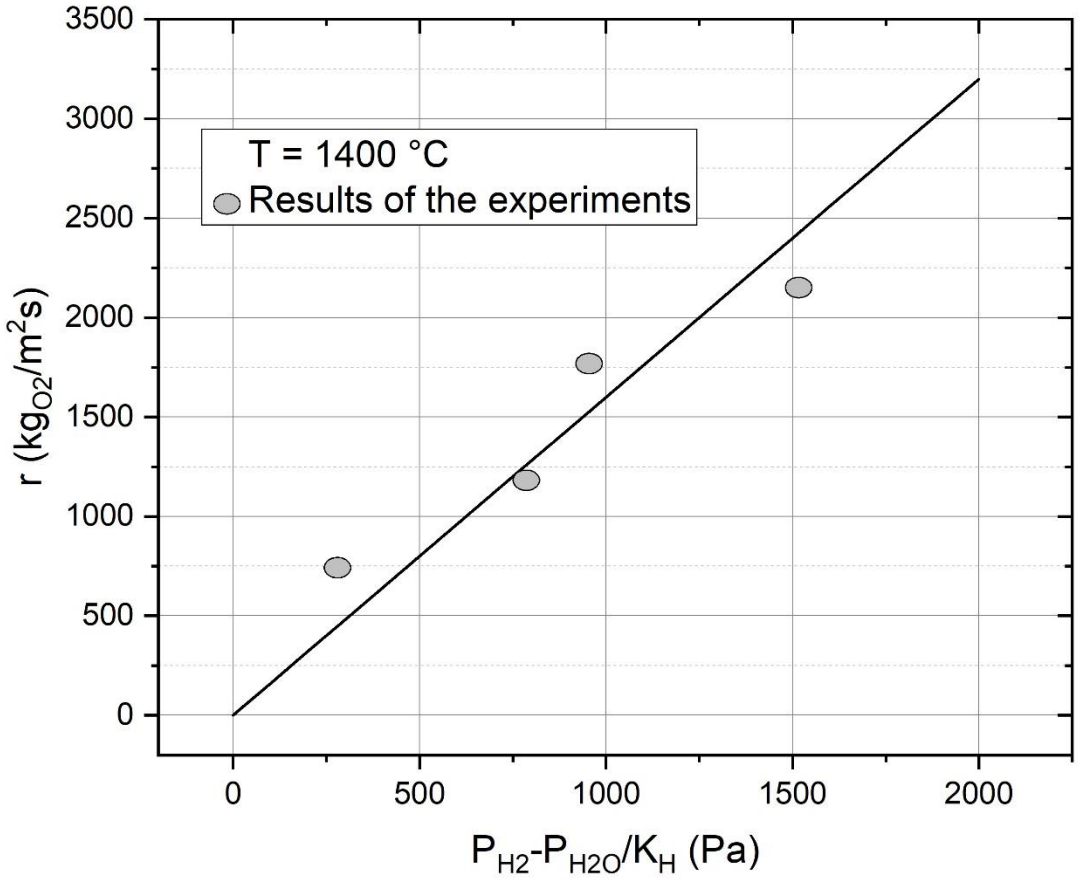

Figure 2-20: Reduction rate of pure liquid FeO using hydrogen at 1673 K [74]

The results of the experiments were marked out by four circles on the graph. Then, based on the results, the regression line was drawn.

The reduction rate of pure liquid FeO at 1400 °C can be presented by the following empirical equation

$$r = k[H_2]\left(P_{H_2} - P_{H_2O}/K_H\right) = 1.6 \times 10^{-6}\left(P_{H_2} - P_{H_2O}/K_H\right) \quad (60)$$

where K_H is the gas ratio of (P_{H_2O} / P_{H_2}) at equilibrium with liquid FeO. As shown in equation 60, the driving force of the chemical reaction is the partial pressure of hydrogen. The apparent rate constant was 1.6 x $10^{-6}(kg - oxygen/m^2 s\ Pa)$ at 1400 °C, which is approximately two orders of magnitude larger than that of CO. It means that the reduction of liquid FeO using hydrogen is much faster than that of using CO.

Furthermore, Hayashi and Iguchi [75] studied the reduction rate of pure liquid Fe_tO by hydrogen at 1500 °C. They reduced fines of FeO by the means of a gas conveying system using H_2-N_2 mixture. Due to high temperature, very fine Fe_tO droplets were formed and reacted with hydrogen in the gas mixture. In those conditions, the limiting factor of the reduction rate was the interfacial chemical reaction, and the influence of the gas phase mass transfer became negligible. They showed that the chemical reaction rate was first order with respect to the partial pressure of hydrogen. The apparent rate constant was $1.58 \times 10^{-6}(kg - oxygen/m^2 s\ Pa)$ at 1500 °C. Although, the temperature of their experiments was 100 °C higher than that of Nagasaka *et al*. [74] work, the result was in a good agreement.

2.3.2 The reduction rate of iron oxide using hydrogen at high temperatures

Hydrogen plasma smelting process to reduce iron ores has been studied since the late 1970s [19,22–24,60]. Kamiya *et al.* [44] constructed a simple experimental plasma furnace to investigate of the reduction of iron ore, which is shown in **Figure 2-21**.

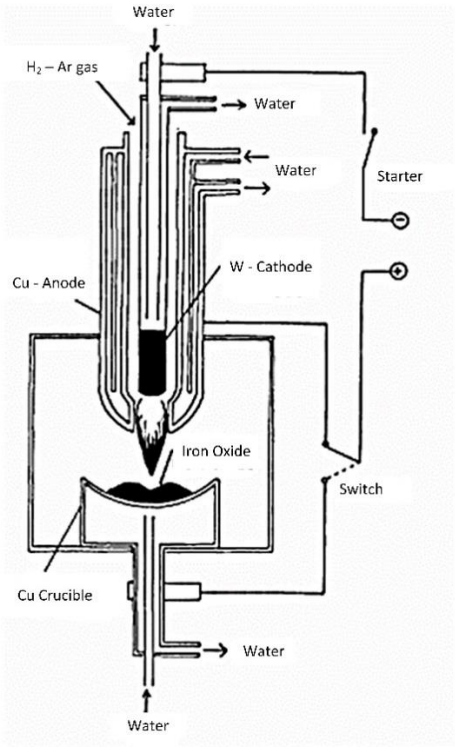

Figure 2-21: Schematic diagram of the experimental apparatus [44]

It is made of a DC plasma torch with a water-cooled tungsten electrode. A water-cooled copper crucible with a diameter of 60 mm as an anode was used for the experiments. It was a transferred-arc plasma furnace worked under an argon atmosphere. Similar to our previous study [45], at the beginning of the experiments, only argon was injected into the plasma zone to melt iron ore inside the crucible, and then, after completely melting of iron ore, a mixture of hydrogen and argon was then injected into the furnace. The mass of the samples was in a range between 25 and 75 g, the flow rate of the gas mixture was 20 NL/min and the power of the plasma torch was 8.3 kW. A series of experiments have been carried out to demonstrate the influence of gas flow rate on the degree of reduction.

10, 20, and 30 L/min were selected as gas flow rates with a mixture of 7% H_2 / 93% Ar. They reported that the degree of reduction increased linearly over operation time and the highest degree of reduction could be achieved by a flow rate of 20 L/min [44]. Furthermore, they studied the effect of CaO and SiO_2 addition on the reduction rate of liquid Fe_tO. As a result, with the addition of CaO to Fe_tO, the apparent rate constant of liquid Fe_tO reduction increased. In contrast, it was decreased when SiO_2 was added to Fe_tO. **Figure 2-22** shows the degree of hydrogen utilization for the reduction of 50 g Fe_tO with a basicity of 1.5.

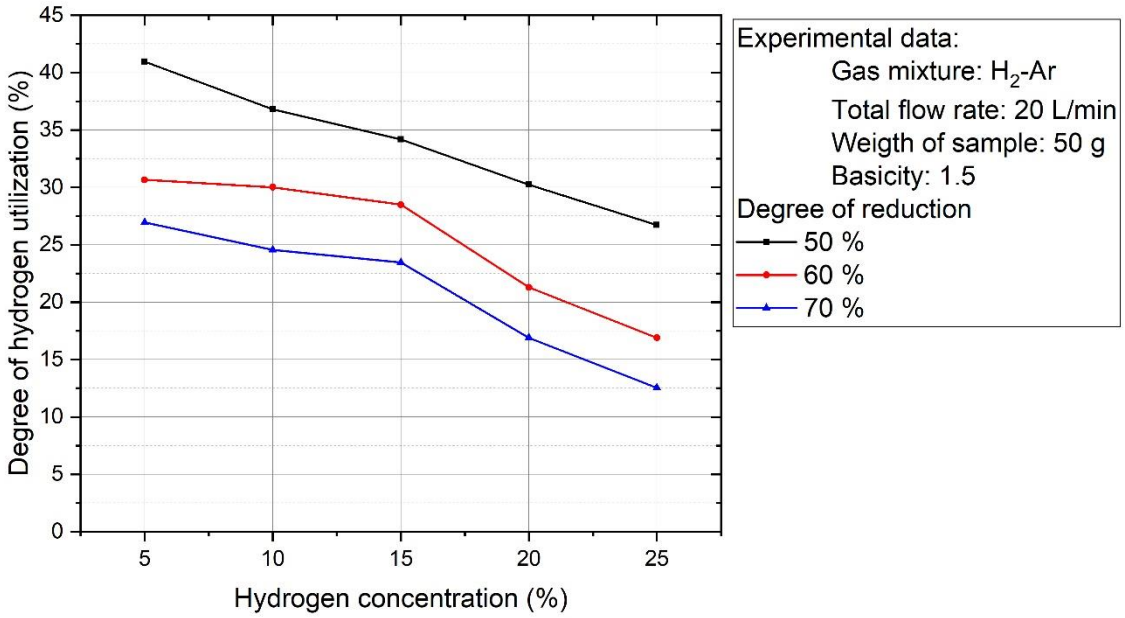

Figure 2-22: Degree of hydrogen utilization over the hydrogen concentration [44]

Three series of experiments were carried out with a total flow rate of 20 L/min and four different concentrations of hydrogen in the gas mixtures. The experiments were stopped when the degree of reduction could achieve 50, 60, and 70%. They reported that the degree of hydrogen utilization was high when hydrogen concentration in the gas mixture was low. For example, with 70% of the degree of reduction and 15% of hydrogen concentration, the degree of reduction was approximately 22%.

Figure 2-23. shows the reduction rate of FeO in solid and liquid states by H_2 and CO reported by different studies [74,75,79–81].

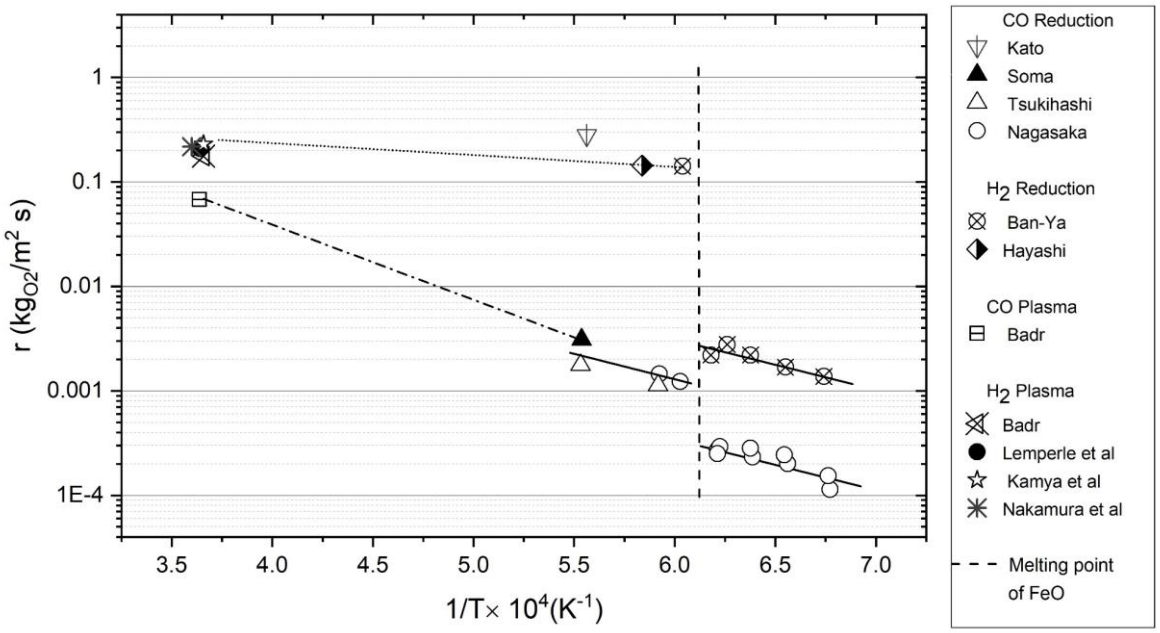

Figure 2-23: Reduction rates of liquid FeO using hydrogen over temperature [3]

The plot shows that the reduction rate of pure liquid Fe_tO using CO and H_2 depends on temperature. The reported results by various researchers for the reduction by CO are in good agreement except for Kato *et al's* work [82]. They reported a high reduction rate of pure liquid Fe_tO using CO in 1977. Then, Soma [81] corrected their results and reported a slower rate. As can be seen in **Figure 2-23**, Soma's value is in good agreement with that of other researchers [79,80]. As can be seen, the reduction potential of hydrogen increased significantly above the FeO melting point. However, at temperatures above the melting point of FeO, with an increase of the temperature, the logarithms of the reduction rate increased linearly.

2.3.3 Reduction rates of liquid iron oxide using different reducing agents

The reduction of molten iron oxide by CO was discussed in the previous section. As a result, at the temperature just above the melting point of iron oxide, the reduction rate of FeO using CO increased by one order of magnitude.

Several researchers have investigated the reduction of liquid iron oxide using carbon [80,83–85]. They showed that the reduction rate of liquid oxid using carbon was significantly affected by temperature. Moreover, the reduction rate of liquid iron oxide by $\mathrm{Fe-C}$ was significantly higher than that by solid carbon up to 1620 °C.

Figure 2-24. Shows a comparison of the reduction rates of Fe_tO using hydrogen, carbon, $Fe-C$ melt, and CO.

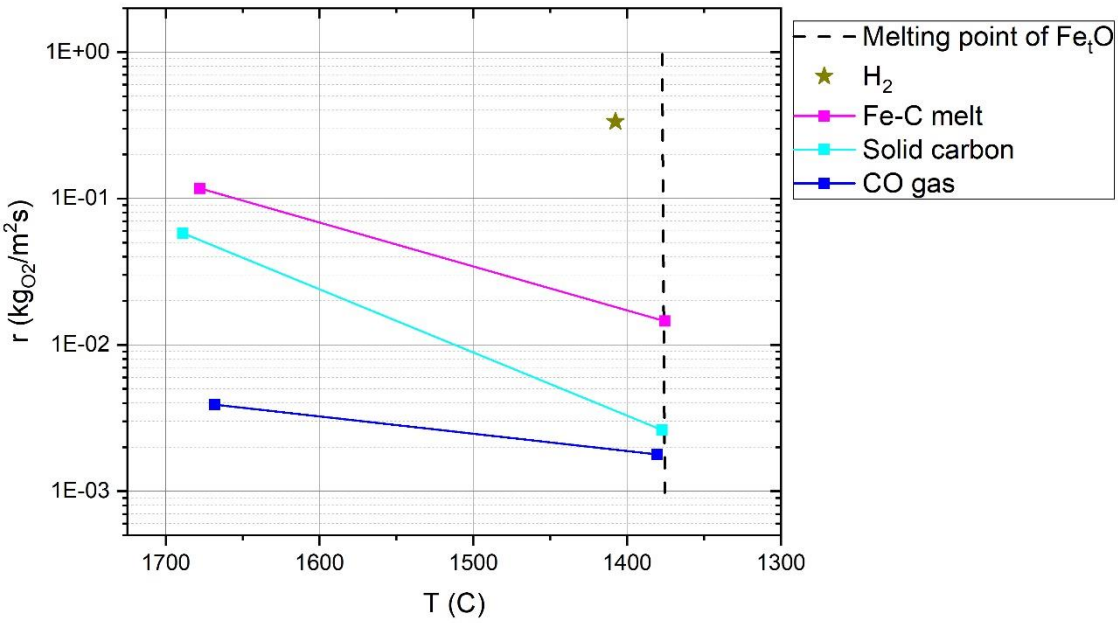

Figure 2-24: Reduction rates of pure liquid Fe_tO using different reducing agents [65]

The reductions by H_2 and CO was referred to the interfacial chemical reaction. Whereas, regarding the reductions using carbon and $Fe-C$ melt, the overall rates were taken into account. As a main result, the reduction rate of iron oxide using hydrogen was one or two orders of magnitude greater than those by the other reducing agents [65]. For instance, the reduction rate of Fe_tO using H_2 was two orders of magnitude greater than that of CO.

2.4 Patterns of flow in hydrogen plasma reactor compartment

To do the experiments for the present study, argon and hydrogen are injected into the reactor. Argon left the reactor without any reaction; in contrast, hydrogen reduced iron oxide and produced water vapor. Furthermore, carbon reduced iron ore and produced CO and CO_2 [45]. Therefore, the composition and flow rate of the inlet and outlet gas was different. To do the mass balance, the flow pattern of the gases should have been prepared.

The flow pattern can give different behavior which depends on the volume of the reactor and distribution of the gases. The flow pattern is mainly defined by three factors. First, the residence time distribution (RTD) of the gases, which is the time of residence of gas particles inside the reactor. Second is the state of the aggregation of the flowing stream and the third is the earliness and lateness of mixing. The plasma reactor is a real reactor in experimental conditions, which deviates from the ideal reactors. Hence, the flow elements spend different lengths of time in the reactor. Therefore, to define the flow pattern, the outlet concentration curve should be found experimentally. Levenspiel et al. [86] presented a schematic of the inlet and outlet concentration curve for a step experiment like the experiments carried out for the present study, in which there is one-step input of a gas into a reactor. **Figure 2-25** shows the plasma reactor and a schematic of the inlet and outlet concentration curve of hydrogen.

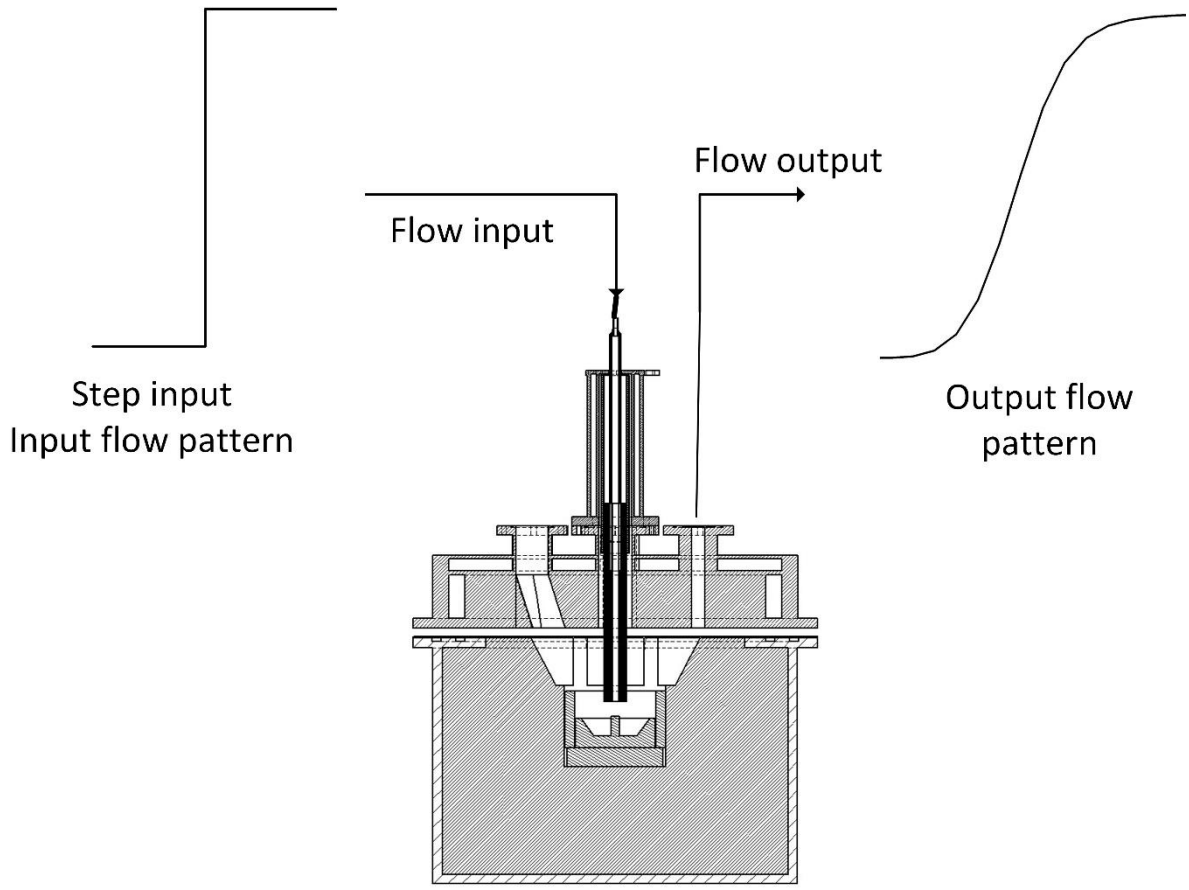

Figure 2-25: Schematic of an input and output flow pattern into the gas compartment of the plasma reactor

The figure shows the hydrogen concentration curve when the gas composition was switched from pure argon to a mixture of argon and hydrogen. Because of low turbulence in the pipe, the inlet curve was a step input with a constant volumetric flow rate. The concentration of hydrogen in the inlet to the reactor is kept constant until the concentration in the outlet is in the same range from that in the inlet.

The mean residence time is defined by

$$\tau_H[s] = \frac{V\ [L]}{\dot{V}\ [L/min]\times 60} \tag{61}$$

Where τ_H is the residence time of hydrogen particles inside the plasma reactor and V is the volume of the plasma reactor, and $\dot{V}$ is the flow rate of the gas. The non-dimensional time is defined by

$$\bar{t} = \frac{t\ [s]}{\tau\ [s]} \tag{62}$$

t is the time of the process, and $\bar{t}$ is mean residence time which is a non-dimensional number as a ratio of times.

For the experiments, in the pre-melting step, argon was injected into the furnace. In the reduction step, hydrogen gas injected into the plasma reactor which was already filled with argon. **Figure 2-26** shows the fraction of the hydrogen concentration curve as a percentage in the inlet and outlet of the plasma reactor.

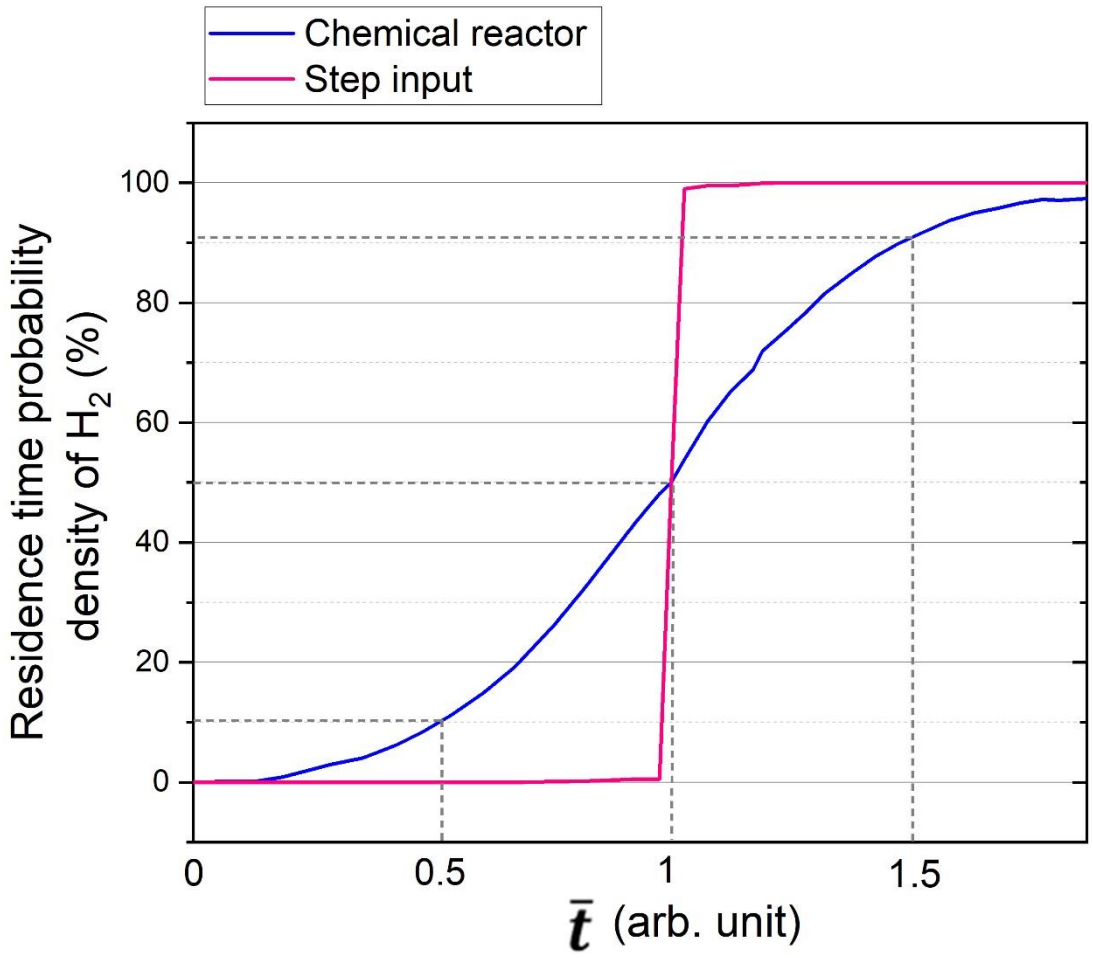

Figure 2-26: Schematic of inlet and outlet residence time response of the plasma reactor compartment

Y-axis shows the fraction as a percent of hydrogen concentration that has a residence time in the plasma reactor. The figure shows that with the injection of hydrogen, according to a step input, hydrogen particles leave the plasma reactor showing a spread of residence. At $\bar{t}$ larger than the mean residence time, approximately more than half of hydrogen particles will have left the reactor.

The real hydrogen flow pattern in the plasma reactor for this study was defined experimentally, which is explained in section 3.5 and both methods are discussed in section 4.1.

2.5 Summary of the statement of the art

The topics of know-how to develop an HPSR industrial plant are discussed in this section. The existing knowledge, findings of the current study and the required future investigations in different sections are listed below.

1- **Gases:** The optimal compositions of the gas mixture for the use in this process have already been studied. For this issue, argon and nitrogen are the best gases to be mixed with hydrogen to be injected into the plasma arc zone. The properties, advantages, and disadvantages of different mixtures of these gases are explained in the literature review of the current study. However, the gas composition and the optimal flow rate should be evaluated by carrying out experiments using the HPSR testing plant. Moreover, the parameters of the recycling process of the gases should be further investigated.

2- **Reduction behavior:** Nevertheless, the reduction parameters had already been investigated, in the present study, the main reduction parameters included degree of reduction and hydrogen utilization, reduction rate, slag formation, and produced amount of metallic iron have been studied, and the values of the parameters have been suggested to develop an HPSR testing plant.

3- **Refractory materials:** Because of high radiation to the furnace wall, the refractory lining of the plasma reactor is one of the main challenges of the development of this process, which is essential to be investigated in the future. Moreover, the possibility of the generation of the foamy slag during operation also should be studied.

4- **Plasma arc specifications:** The degree of hydrogen ionization and its effect on the reduction behavior of iron ore is one of the main parameters for the development of this process. The temperature of the arc defines the degree of hydrogen ionization and accordingly influences the reduction rate. Unfortunately, despite the importance of this topic, enough investigations have not been carried out. As the first step, in the present study, the methodology of the measurement of the plasma arc temperature has been developed and the temperature was calculated. This topic requires an intensive investigation to acquire enough knowledge for the development of this process. Moreover, the degree of hydrogen ionization can be optimized by the optimization of the plasma arc generation system. Therefore, the optimal arcing

parameters such as arc length, power of the electrical supply, voltage and amperage should be determined.

5- **Specification of raw materials**: The specifications of iron ore fines and the additives had already been investigated. In the current study, based on the results of the former researchers, the optimal grain size of fines has been selected and the relevant experiments have been carried out. However, it needs to be further investigated using the HPSR testing plant. Furthermore, preheating and pre-reducing of iron ore fines should be investigated.

3 Apparatus and procedure

The Experiments were carried out in two groups, the first group was to study the reduction behavior and the second was to monitor the plasma arc. In this section, the experimental facilities are introduced, and then the experimental program and the materials specifications are presented. Finally, the methodology and operation procedure are described.

3.1 Facilities

The facilities utilized for this study have been introduced in detail in publications 1 and 2 in the attachment of this paper [45,69]. Nevertheless, the laboratory-scale hydrogen plasma facility is briefly described in this section. **Figure 3-1** shows a schematic of the process flowsheet and the laboratory set up of the plasma reactor facilities.

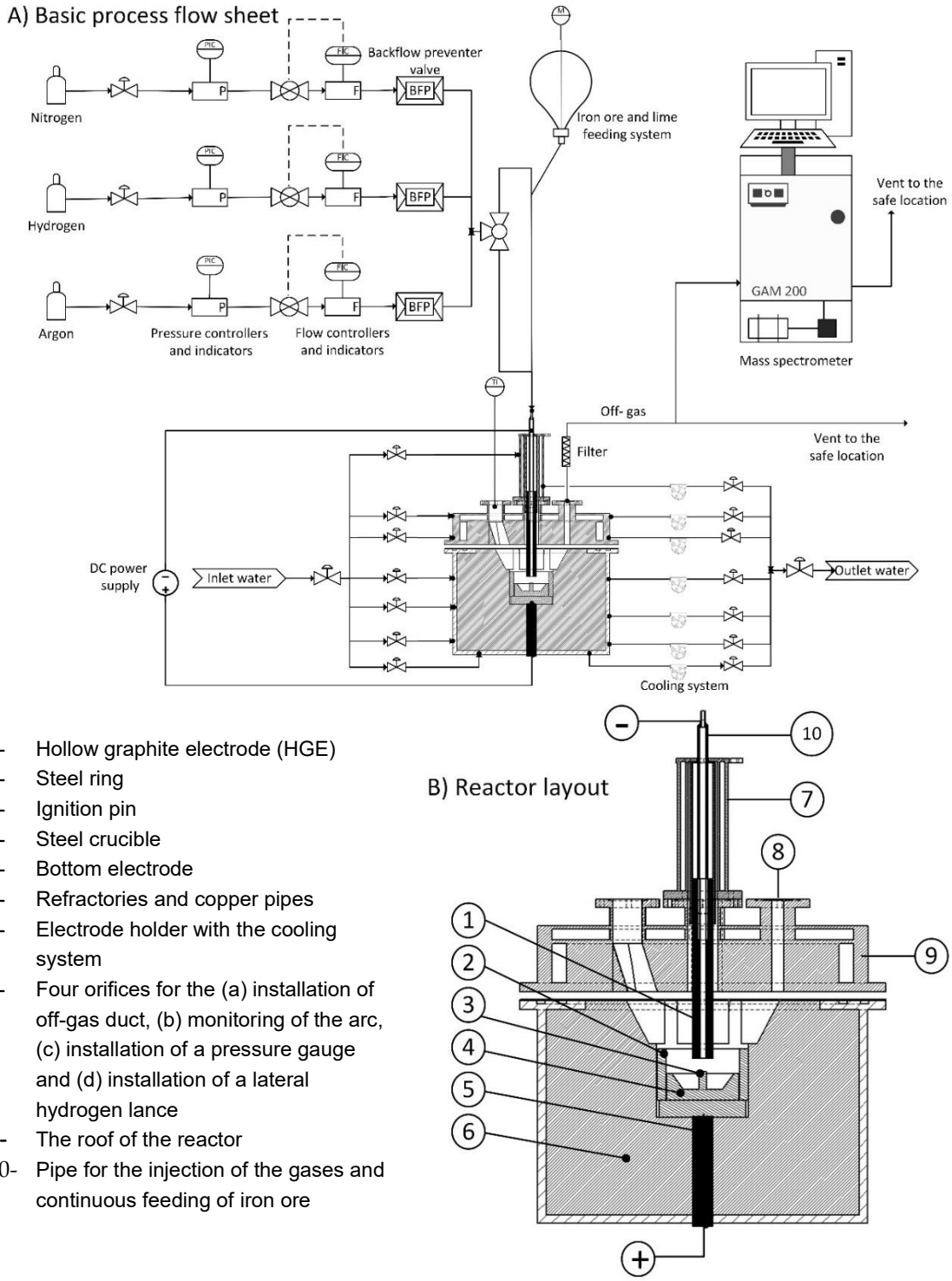

Figure 3-1: Schematic of the laboratory-scale plasma facility at Montanuniversitaet Leoben: (A) process flow diagram and (B) reactor layout [45].

For an operation, hydrogen, nitrogen, argon or premix gas with different flow rates can be injected into the reactor. Fines of iron ore are charged batch-wise or continuously into the steel crucible and are smelted and reduced by hydrogen plasma. Hollow graphite electrode (HGE), as a cathode, and the steel crucible connected to the bottom electrode, as an anode, generated a transferred-DC arc to melt iron oxide particles. The steel crucible was located inside the steel ring, in which the inner section was covered by the refractory lining to prevent it from heat exposure. Because of the generation of heat from plasm arc, the reactor and the electrode holder were-cooled by a water-cooling system during the test runs.

Off-gas was cooled and cleaned before entering MS in a gas cleaning system, in which the setup is shown in **Figure 3-2**.

Figure 3-2: Setup of the off-gas cleaning system

Off-gas cleaning system comprised of a steel grid, glass wool, two water bottles, and molecular sieves to collect the dust and to remove the water vapor.

To calculate the mass balance, the chemical composition of off-gas was analyzed by GAM 200 mass spectrometer produced by InProcess Instruments Gesellschaft für Prozessanalytik mbH. To study the reduction behavior of iron oxide, a solid powder feeding system, Hi-Doser 1l powder dosing instrument manufactured by LAMBDA Laboratory Instruments, was used to charge the mixture of iron ore and additives fines continuously into the steel crucible during the test runs.

An optical microscope, Nikon MM 40 with image analysis CLEMEX Vision 7, was used to study the microstructure of the produced iron and the heat affected and melted zone of the

steel crucible. The Quanta 200 Mk2 scanning electron microscope (SEM) equipped with an EDX-device in low vacuum mode was used to study the topographical and chemical analysis of the slags.

To monitor the emission of plasma arc, an integrated optical spectrometer manufactured by Avantes BV was used. It was three spectrometers in one box. The technical data of the spectrometers are presented in **Table 3-1**.

Table 3-1: Technical specifications of spectrometers

Specification	Spectrometer No. 1	Spectrometer No. 2	Spectrometer No. 3
Model	AVASPEC - ULS3648		
Wavelength range	300 – 535 nm	530 – 742 nm	740 – 1040 nm
Grating	UC – 1200 l/mm	VC – 1200 l/mm	SI – 830 l/mm
Resolution	0.14 – 0.18 nm	0.14 – 0.18 nm	0.25 nm
Integrated time	10 µs - 10 minutes		
Detector lens	AvaSpec 2048 L - 3648		
Slit	10 um entry, 75 mm bench		
Order sorting filter	300 nm	515 nm	600 nm

Figure 3-3 shows the experimental set up of the spectrometer and the position of the fiber installed on the side of the reactor.

Figure 3-3: Setup of the plasma arc monitoring experiment

The experimental setup comprised the fiber probe, three spectrometers, and data processing software. A 400-micron diameter solarisation-resistant fiber was installed on the side of the reactor where there was an orifice to monitor the arc. One visible glass was installed on the orifice to seal the reactor. The fiber probe was used to take the light sample from the arc to send to the optical spectrometry. The sight angle of the fiber was able to monitor the whole area of the arc zone. Avasoft-Full spectrometer software was used to readout and process the data generated by the spectrometer.

Hematite ore produced by the Carajas mine was used to carry out the experiments with the total Fe content of 65.81%. Its chemical composition measured by flame atomic absorption spectrometry is shown in **Table 3-2**..

Table 3-2: Chemical composition of the iron ore

No.	Element	(wt.%)
1	Fe (III) oxide	92.83
2	Fe (II) oxide	1.07
3	Silica	1.694
4	Aluminium oxide	1.01
5	Manganese (II) oxide	0.22
6	Calcium oxide	0.01
7	Magnesium oxide	0.01
8	Total phosphorus	0.057
9	Sodium oxide	0.019
10	Carbon	0.098
11	Zinc	0.004
12	Total sulfur	0.014
13	Potassium oxide	0.017
14	LOI[1]	2.947
[1] Loss of ignition		

To adjust the basicity, fines of Carajas iron ore were mixed with lime which had already been calcined at 1100 °C. Its composition is shown in **Table 3-3**.

Table 3-3: Chemical composition of the calcined lime

No.	Element	(wt.%)
1	CaO	86.41
2	SiO_2	4.76
3	MgO	1.05
4	Al_2O_3	1.87
5	Fe_2O_3	2.50
6	P_2O_5	0.11
7	C	0.11
8	S	0.02
9	LOI	3.17

Lime and iron oxide were separately classified and mixed. **Table 3-4** shows the grain size distributions of the mixture.

Table 3-4: Grain size distribution of Carajas iron ore and lime

Mesh Size (µm)	Fraction (wt.%)	Cumulative (wt.%)
63–125	34	34
25–63	60	94
0–25	6	100

During the experiment, the ignition pin and a part of the steel crucible were melted which caused the carbon content of those parts to be introduced to the melt. Hence, the compositions of these steel components should have been considered during the calculations of the mass balance. The chemical composition of the steel crucible and the ignition pin is shown in **Table 2-1Table 3-5**.

.

Table 3-5: Composition of the ignition pin and steel crucible

Element	Unit	C	Si	Mn	P	S	Cr	Mo	Ni	Al	Cu
Steel crucible	(wt.%)	0.178	0.261	1.325	0.009	0.005	0.083	0.031	0.168	0.027	0.179
Ignition pin	(wt.%)	0.441	0.217	0.85	0.008	0.028	0.985	0.162	0.085	0.021	0.116

3.2 Experimental method

In this section, the methods of the experiments are outlined, and all parameters of the experiments are explained. In the present work, in a series of experiments, the reduction behavior of iron ore was studied. Moreover, the temperature of the plasma arc was assessed using an optical spectrometer.

The reduction behavior related experiments have carried out in three different groups namely sample weight, the basicity of the slag and continuous feeding of iron ore. **Table 3-6** shows the experimental program with the main parameters.

Table 3-6: Experimental program

Set of Experiments	Experiment	Weight (g)	Lime (g) / Iron Ore (g)	B_2 (CaO/SiO_2)	Gas Flow Rate (NL/min), 1 atm, 25 °C	H_2/Ar Ratio (molar %)
Basicity	Ex. 1	100	0 / 100	0	5	50/50
	Ex. 2	100	1.7 / 98.3	0.8		
	Ex. 3	100	3.3 / 96.7	1.6		
	Ex. 4	100	4.9 / 95.1	2.3		
	Ex. 5	100	6.4 / 93.6	2.9		
Continuous feeding	Ex. 6	100	3.3 / 96.7	1.6		
Sample weight	Ex. 7	50	3.3 / 96.7	1.6		
	Ex. 8	75	3.3 / 96.7	1.6		

A premixed 50% H_2-50% Ar gas with a total flow rate of 5 NL/min was used for all experiments to reduce iron oxides melted inside the steel crucible.

Five experiments with different basicities (0, 0.8, 1.6, 2.3, and 2.9) have been carried out to study the slag formation and reduction behavior of iron oxides. The procedure of the experiments was outlined in publication 1 in the attachment of this paper [69]. Two samples with a weight of 50 and 75 g of premixed iron ore and lime were prepared for this series of experiments. They were compared with Ex. 3 with a weight of 100 g, in which all other parameters were the same.

To scale up the HPSR process from the laboratory scale to the testing plant and industrial scale, iron ore should be continuously charged into the reactor. Therefore, the reduction behavior of iron oxide was studied during the continuous charging of material. For this purpose, 20 g of the premixed fines were directly charged into the steel crucible and 80 g was charged to the glass vessel to be fed continuously into the plasma reactor.

3.3 Description of the operation

In terms of the operation, the experiments have been divided into two groups namely batch-wise charge and continuous feeding of iron ore. **Figure 3-4** and **Figure 3-5** show the operation steps of the batch-wise and continuous feeding experiments, respectively.

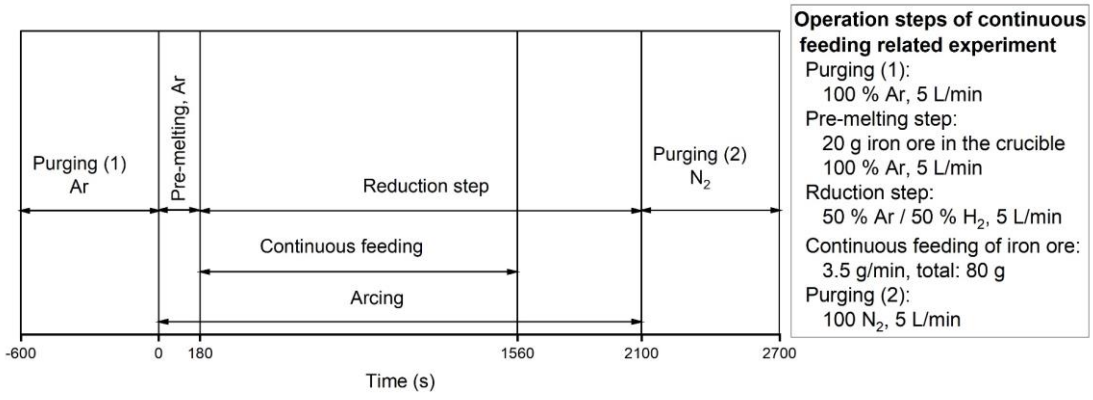

Figure 3-4: Process steps of experiments with batch-wise charge of iron ore, EX. 1, 2, 3, 4, 5, 7 and 8

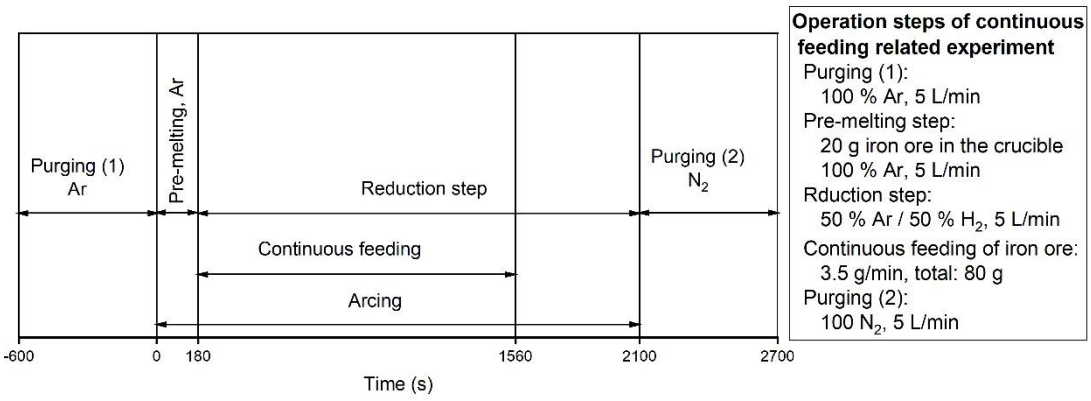

Figure 3-5: Process steps of experiment with continuous feeding of iron ore, Ex. 6

For conducting the experiments with the batch-wise charge of iron ore, 100 g of material was charged into the crucible and located inside the reactor. For the Ex. 6, 20 g of iron ore was poured into the steel crucible and 80 g was poured into the glass vessel of the continuous feeder system to be fed continuously during the operation.

Oxygen was removed from the reactor and other sections of the process before the start of arcing by the injection of 5 NL/min argon for 600 s. During this process, the exit stream was analyzed by using the MS. After that, the pre-melting step, run for 180 s, was started by the injection of pure argon with the same flow rate. Then, the reduction step was started by the switch of the feed gas to premixed H_2/Ar with a flow rate of 2.5/2.5 NL/min. During the reduction step, the gas flow rate and the composition were kept constant. The voltage of the arc was fluctuating during the arcing because of changing the gas composition inside the plasma reactor and the arc zone. During the reduction process, the concentration of hydrogen inside the plasma zone was changing due to the fluctuations of the degree of hydrogen utilization. Molecular hydrogen needs more energy to be atomized and ionized than pure argon [87,88]. It led to fluctuating energy consumption and accordingly caused changes in the voltage.

Ex. 3 and 7 were stopped at 1500 s because of heating the transformer of the power supply. To assess the reduction parameters for longer operation time, the time of experiments Ex. 1, 2, and 5 was extended to 1980 s, and experiments 4 and 6 were carried out in 2220 s. Ex. 8 was carried out in 1380 s because of existing only 50 g of powder inside the crucible. Therefore, the reduction step lasted until η_{H_2} decreased to less than 10%, which is a low degree of hydrogen utilization. After finishing the reduction, the feed gas was switched to pure nitrogen with a flow rate of 5 NL/min to remove hydrogen.

To check the results of the mass balance calculation using off-gas composition, the crucible, and electrode were weighed before and after each test run. To study the reduction behavior, the chemical composition of slag was analyzed by using EDX or XRF. Furthermore, the crucible was cut from the middle and analyzed by using a spectrometer. Its microstructure was studied to estimate the weight of the melted section during the operation to determine the carbon amount contributed to the reduction process.

3.4 Optical spectrum of plasma arc

Avantes spectrometer with a multi-furcated fiber-optic cable and Avasoft-Full spectrometer software was installed to monitor the plasma arc. **Figure 3-6** shows the setup of the optical spectrometer to monitor the arc.

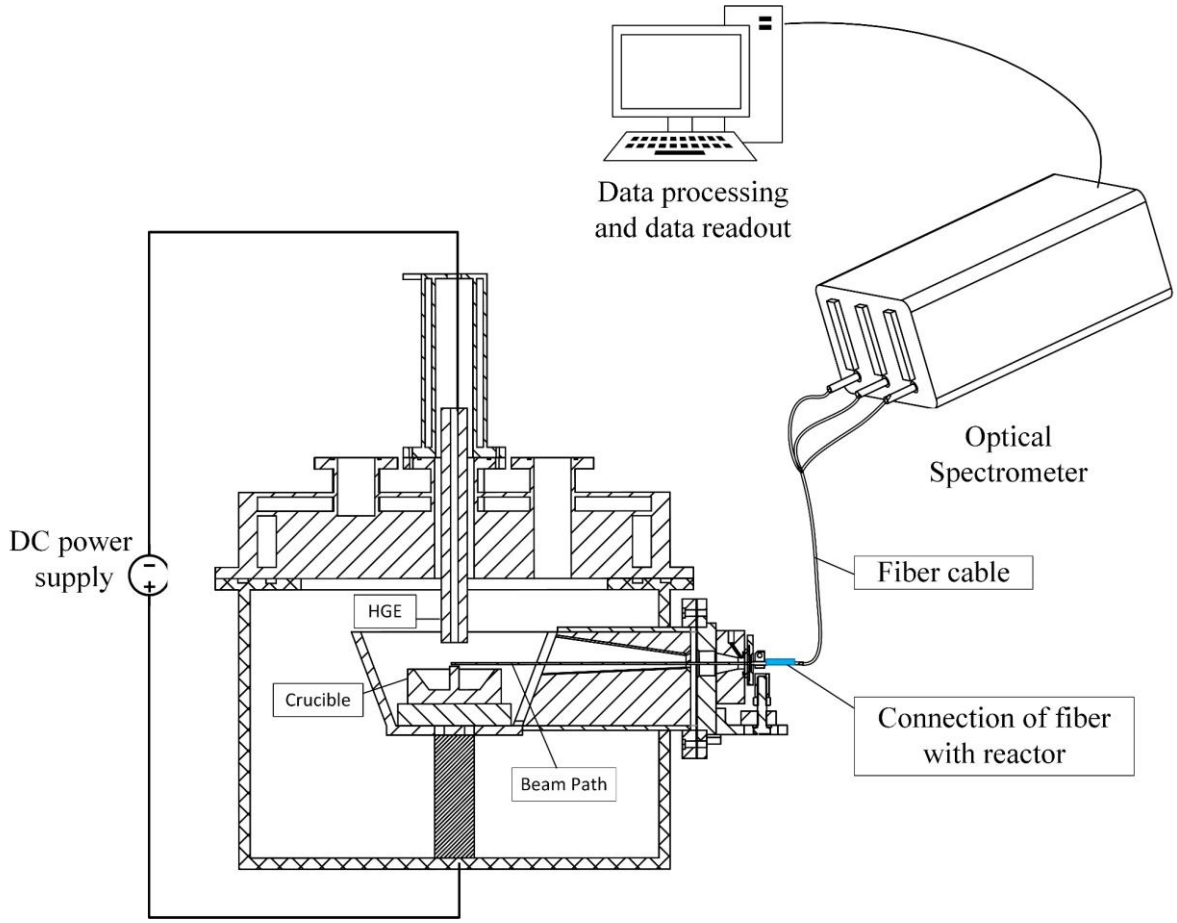

Figure 3-6: Schematic setup of the optical spectrometer

The fiber was installed on the side of the plasma reactor to catch the light beam from the arc. The fiber used for the experiment was a normal fiber which was not possible to focus only on one point. Therefore, the whole zone of the plasma arc was monitored instead of a point. The fiber was connected to the integrated optical spectrometer and then to the computer to readout and process the data by Avasoft-Full spectrometer software. For this experiment, scrap was charged into the crucible instead of iron ore. The process steps of monitoring of plasma arc are shown in **Figure 3-7**.

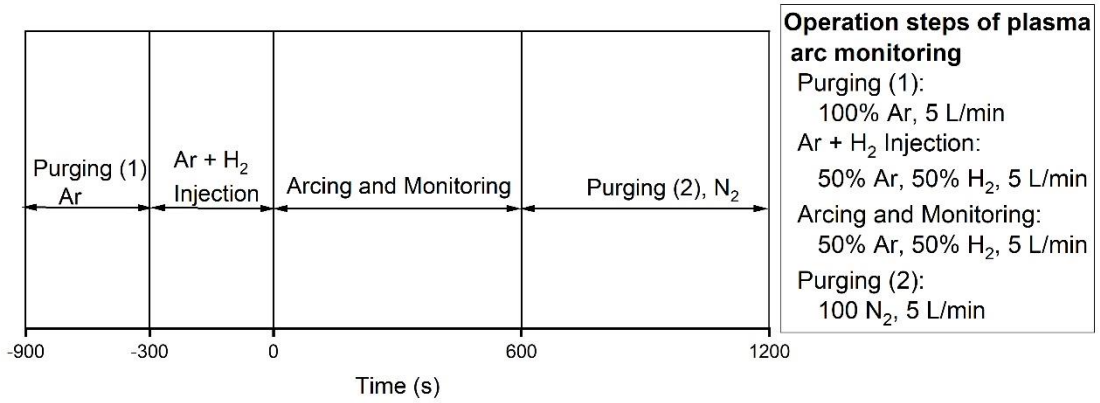

Figure 3-7: Operation steps of monitoring the plasma arc

At first, the whole system was purged by argon to remove oxygen from the system. Then, to fill the reactor with hydrogen and argon with a ratio of 50% / 50%, the injection gas was switched to 50% Ar / 50% H_2 with a total flow rate of 5 NL/min. After approximately 300 s, the gas was uniformly distributed into the reactor. The next step was arcing and monitoring of plasma arc. During arcing, the arc was continuously monitored, and the data was saved. At the end of the experiment, the whole system was purged by nitrogen to remove hydrogen from the system. Please note that instead of charging iron ore, scrap was charged into the steel crucible to reduce dust.

3.5 Method of calculation of the reduction parameters

The input material comprises of premixed iron ore and lime, carbon from HGE and steel crucible and premixed 50% H_2 / 50% Ar gas. The products included off-gas, slag, produced iron, and unreduced ore. Mass balance has been closed by the calculations of the amount of products using the chemical composition of the off-gas.

The chemical composition of the off-gas was shown by MS which comprised Ar, H_2, CO, and CO_2. CO and CO_2 were the products of iron oxide reduction by carbon. H_2O was not shown

by MS due to the condensation inside the off-gas duct and cleaning system. The amount of all components was calculated by mass balance equations using the chemical composition of off-gas.

To calculate the total flow rate and flow rate of each component in off-gas, the flow pattern should have been developed. Because the flow pattern of the real equipment deviates from the ideals, for the current study, it has been experimentally developed. However, the mean residence time of the hydrogen particle inside the plasma reactor was calculated theoretically and discussed in section 4.1.

To develop the flow curve experimentally, a gas with the same flow rate and composition was injected into the reactor without a reduction reaction. The arc was created between HGE and only steel scrap to simulate the process. **Figure 3-8** shows the flow transient of hydrogen and argon in the start-up phase called the Reference diagram.

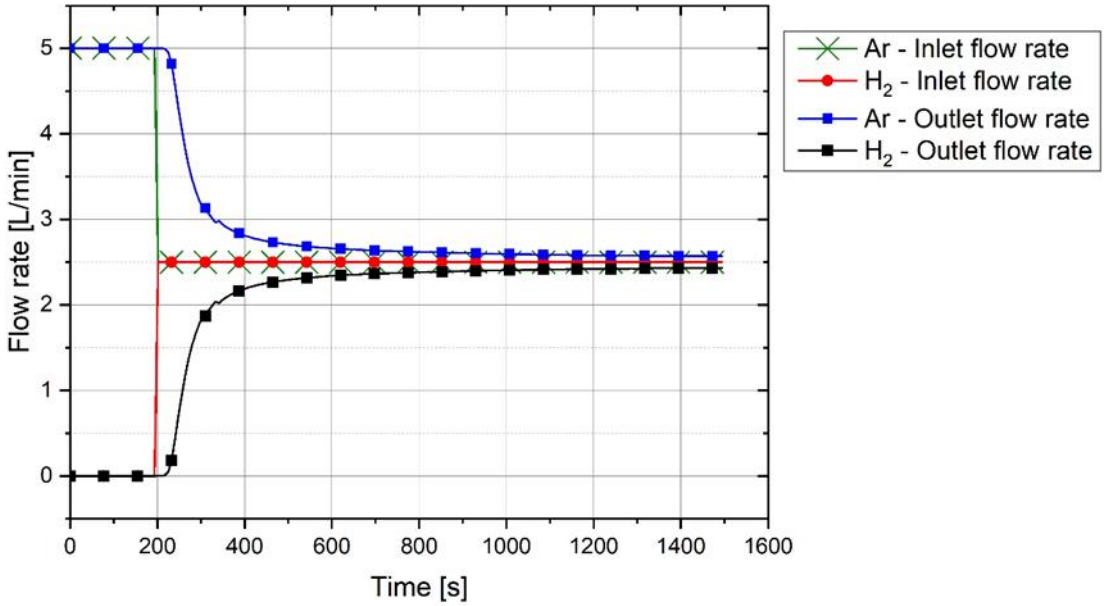

Figure 3-8: Reference diagram of hydrogen and argon during start of hydrogen injection

In 180 s as pre-melting step, only argon was injected into the reactor with a flow rate of 5 L/min, and then switched to 50% H / 50% Ar. Over the injection time, the concentration of hydrogen increased. After 1200 s, the composition of the exit stream was different from that of the feed gas due to the residence time distribution of hydrogen and argon. Therefore, this exit flow pattern was considered as a reference point to compare the exit gas composition of the experiments to calculate the produced water.

The flow chart for the calculations of the reduction parameters from the chemical composition of off-gas in 10 steps is shown in **Figure 3-9**.

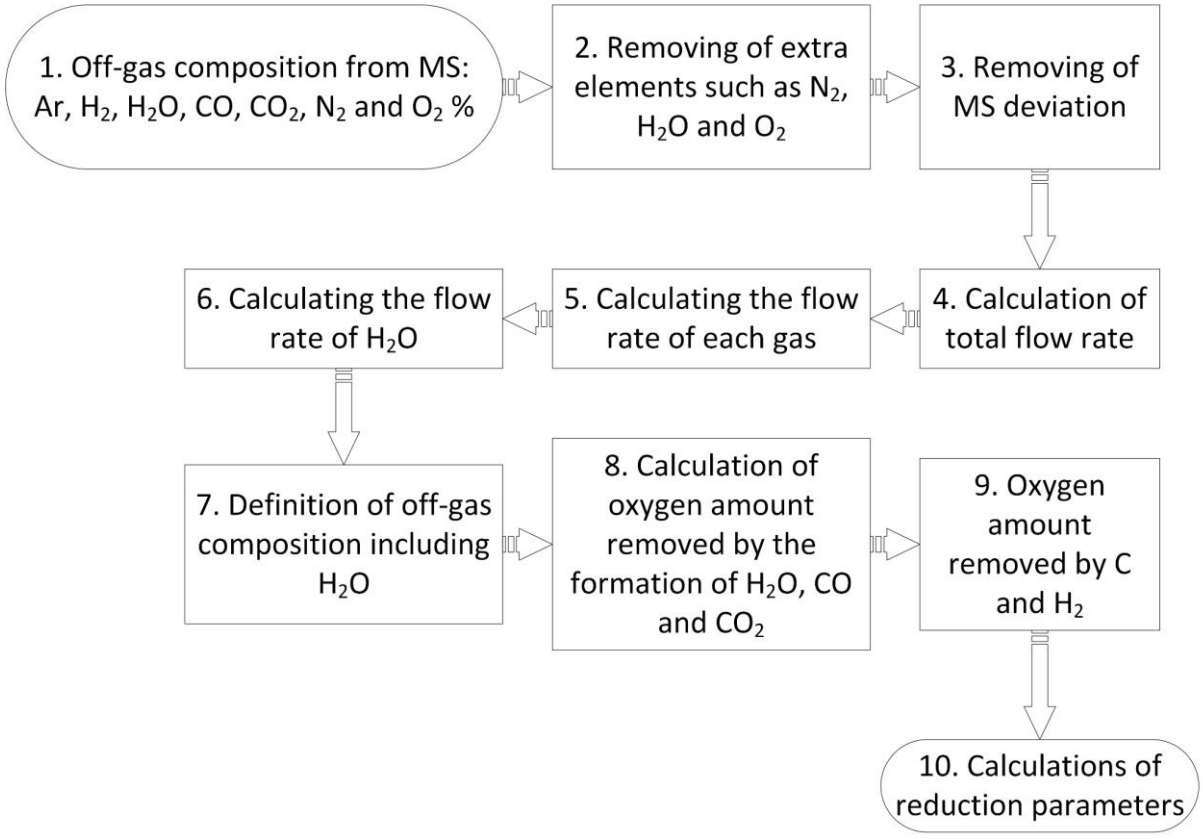

Figure 3-9: Flowchart for the calculation of reduction parameters

This figure shows the procedure for the calculation of reduction parameters from the chemical composition of off-gas. To minimize the deviations and errors, the raw chemical composition shown by MS was corrected in two steps. In the first step, the unwanted elements, namely N_2, O_2, and H_2O, were removed from the exit gas composition. After removing water from the off-gas in the cleaning system, less than 0.2% of water was still shown by MS as remaining in the off-gas. Small amounts of nitrogen (in a range between 0.2 and 0.5%) and oxygen (less than 0.06%) were also shown in MS. In the next step, the deviations of the MS should have been determined by comparing the results with the Reference diagram and then were removed.

Corresponding to the argon concentration in the Reference diagram, the total flow rate (step 4) was calculated by

$$\text{Total flow rate [L/min]} = \text{Ar outlet flow rate [L/min]}/(\text{Ar in the off} - \text{gas [\%]}) \times 100 \qquad (63)$$

Then, the flow rate of each element was defined (step 5). Water vapor was removed from the exit gas in the cleaning system. Therefore, to calculate the produced water, the hydrogen flow rate from the Reference diagram was subtracted from that of off-gas (step 6).

$$\begin{aligned} &H_2O\ flow\ rate\ [L/min] \\ &\quad = (H_2\ flow\ rate from\ off-gas\ [L/min]) \\ &\quad - (H_2\ flow\ rate\ from\ the\ reference\ diagram\ [L/min]) \end{aligned} \tag{64}$$

Then, the off-gas composition was determined which H_2O concentration was included (step 7).

The degree of hydrogen utilization was calculated by

$$\eta_{H_2}[\%] = \frac{\%H_2O}{(\%H_2 + \%H_2O)} \times 100 \tag{65}$$

Iron oxide was reduced by carbon and hydrogen during the reduction process and oxygen was removed from iron ore. The amount of reduced oxygen was defined by (step 8)

$$m_{O,H_2O} = \sum_{C=1}^{n} \left[\frac{H_2O\ flow\ rate\ [L/min]}{22.4} \times 16 \times (C_n - C_{n-1})(s)/60 \right] [g] \tag{66}$$

$$m_{O,CO} = \sum_{C=1}^{n} \left[\frac{CO\ flow\ rate\ [L/min]}{22.4} \times 16 \times (C_n - C_{n-1})(s)/60 \right] [g] \tag{67}$$

$$m_{O,CO_2} = \sum_{C=1}^{n} \left[\frac{CO_2\ flow\ rate\ [L/min]}{22.4} \times 32 \times (C_n - C_{n-1})(s)/60 \right] [g] \tag{68}$$

$$m_{O,tot} = (m_{O,H_2O} + m_{O,CO} + m_{O,CO_2})[g] \tag{69}$$

where m_{O,H_2O}, $m_{O,CO}$ and m_{O,CO_2} are the mass of oxygen in H_2O, CO, and CO_2 respectively, $m_{O,tot}$ is the total mass of oxygen, and C_n, C_{n-1} (s) are the cycles n and n − 1 from MS, respectively. The measurement cycle of the MS was 8.4 s.

The degree of reduction (R_D), which was the amount of oxygen reduced by carbon or hydrogen during the experiment, was defined by (step 9)

$$R_{D,\ H_2} = m_{O,H_2O}/m_{O,in\ iron\ ore} \times 100 \tag{70}$$

$$R_{D,\ C} = (m_{O,CO} + m_{O,CO_2})/m_{O,in\ iron\ ore} \times 100 \tag{71}$$

Hence, the total degree of reduction was defined by

$$R_{D,total} = R_{D,H_2} + R_{D,C} \quad (72)$$

Carbon was introduced to the melt from the hollow graphite electrode, ignition pin, and steel crucible. The amount of carbon from HGE was calculated by subtracting the weight of the electrode before and after each experiment run. The ignition pin was completely melted, therefore, the whole carbon content was considered to be introduced to the melt. To calculate the amount of carbon contributed to the melt from steel crucible, the steel crucible was cut in half and was analyzed, and then the microstructure was studied using optical microscopy to estimate the amount of melted section. **Figure 3-10** shows the cross-section of the crucible.

Figure 3-10: Cross-section of the crucible for Ex. 3.

The reduction rate by hydrogen was the rate of oxygen removed from iron oxide with the formation of water. It was calculated by

$$Reduction\ rate = dm_{O,H2O}\,(g)\ /\ dt\ (min) \quad (73)$$

The produced iron was calculated by the balance of the masses. The degree of metallization (M_D) was defined by

$$M_D = {Produced\ iron\ (g)}\Big/{Total\ Fe\ (g)} \times 100 \quad (74)$$

Moreover, M_D was also calculated by the other method

$$M_D = \frac{R_D - 33.3}{66.6} \times 100 \quad (75)$$

The M_D calculated from those two methods were compared and interpreted for each test run in the next section.

4 Results and discussions

In the present work, the reduction behavior of hematite using hydrogen thermal plasma has been studied. For this purpose, the effect of some parameters included sample weight, the basicity of the slag and continuous feeding of iron ore on the reduction behavior have been investigated. The reduction parameters of each experiment consist of the degree of hydrogen utilization (η_{H_2}), degree of reduction (R_D), reduction rate, degree of metallization (M_D), and the produced iron and slag have been assessed.

Plasma arc radiation generated during the operation with 50% H_2 / 50% Ar gas was captured utilizing an optical spectrometer system. The relevant software processed the data from the optical spectrometer, and the intensity of each wavelength during the arcing process was defined. Accordingly, the temperature of the arc was calculated based on the intensity of the wavelengths, and the results are presented in this section.

4.1 Chemical composition of off-gas

Reference diagram was used to calculate the off-gas composition. Before beginning the discussion of the chemical composition, the residence time of the hydrogen particles inside the plasma reactor is evaluated.

Equation (61) was used to calculate the mean residence time. The denominator is the flow rate of gas if the flow rate of the inlet and outlet are the same. In this process, the reduction reactions took place inside the reactor and the gas products such as CO and CO_2 caused changes in the outlet flowrate. Therefore, the flow rate of the inlet gas cannot be used for the

calculations. For simplicity, the average gas flow rate $\dot{V}_A$, average of inlet and outlet gas flow rate was considered for the calculations of $\tau_{H,A}$, which is the average mean residence time.

The volume of the free space of the plasma reactor was about 3.78 L. The inlet flow rate for all experiments was 5 NL/min at the atmospheric pressure and ambient temperature and the outlet flow rate, $\dot{V}_O$, was shown in **Table 4-1** for each time of the process for each test run. The $\tau_{H,A}$ of hydrogen particles for Ex. 2, 5, 6 and 8 were calculated and are shown in **Table 4-1**.

Table 4-1: $\tau_{H,A}$ of hydrogen particles in plasma reactor

Experiment	t_O (s)	t_H(s)	$\dot{V}_O$ (NL/min)	$\dot{V}_A$ (NL/min)	$\tau_{H,A}$ (s)
Ex. 2	255	31	6.0	5.5	41.1
	503	279	6.3	5.7	40.1
Ex. 5	255	31	6.5	5.7	39.6
	503	279	5.6	5.3	42.8
Ex. 6	255	31	5.4	5.2	43.7
	503	279	5.5	5.2	43.3
Ex. 8	256	31	6.1	5.6	40.8
	504	279	5.4	5.1	43.8

t_O is the operation time, t_H is the time of introducing hydrogen into the plasma reactor, which was started with the reduction step. The results show that $\tau_{H,A}$ was between 39.9 s and 43.8 s, which depends on the outlet flow rate of the gas. Furthermore, the mean residence time was measured experimentally. For the laboratory setup, there were some other reactor compartments in the off-gas cleaning system including two bottles of water, and compartments of glass wool molecular sieves, which caused a deviation between calculated and measured τ_H values. The mean residence time of hydrogen for the whole system was approximately 70 s. The other source of deviation was the temperature of the gas inside the reactor. With an increase in temperature, the residence time was decreased. Inside the reactor, there was considerably severe turbulence because of the high temperature of the plasma arc and the chemical reduction reactions. The temperature of the central arc cone is above 20,000 K and decreases considerably in the surroundings of arc. The temperature of the gas in the freeboard of the plasma reactor was measured using Type K thermocouple wires, which was in the range of 380 – 410 °C. However, off-gas was cooled in the off-gas cleaning system before entering to the MS.

Three test runs, Ex. 3, 7 and 8, have been carried out to study the influence of the sample weight on the reduction behavior of iron ore. The experiments and the results were presented

and discussed in publication 2 in the attachment of this paper [45], and in this section, a supplementary discussion is presented. The chemical composition of off-gas for Ex. 7 and 8 are shown in **Figure 4-1** and **Figure 4-2** and for that of Ex. 3 was shown in the paper [45].

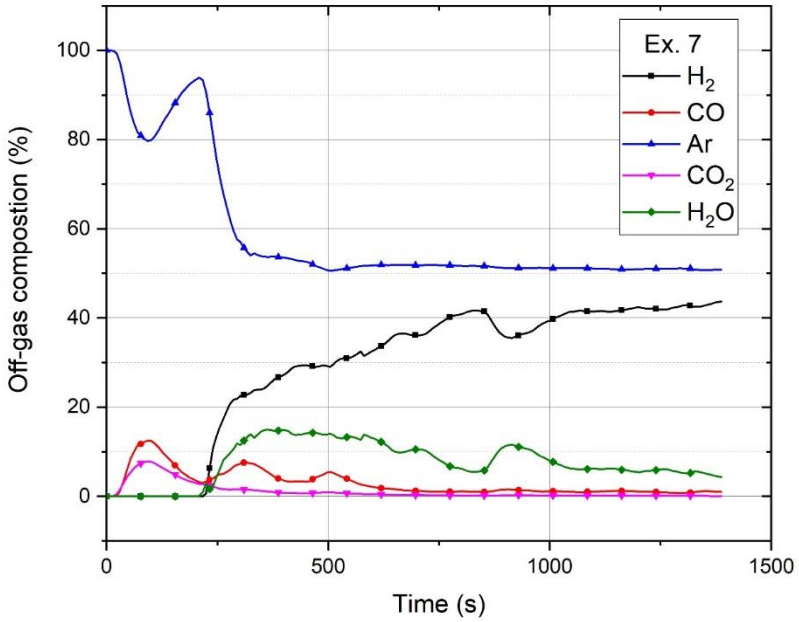

Figure 4-1: Chemical composition of off-gas for Ex. 7

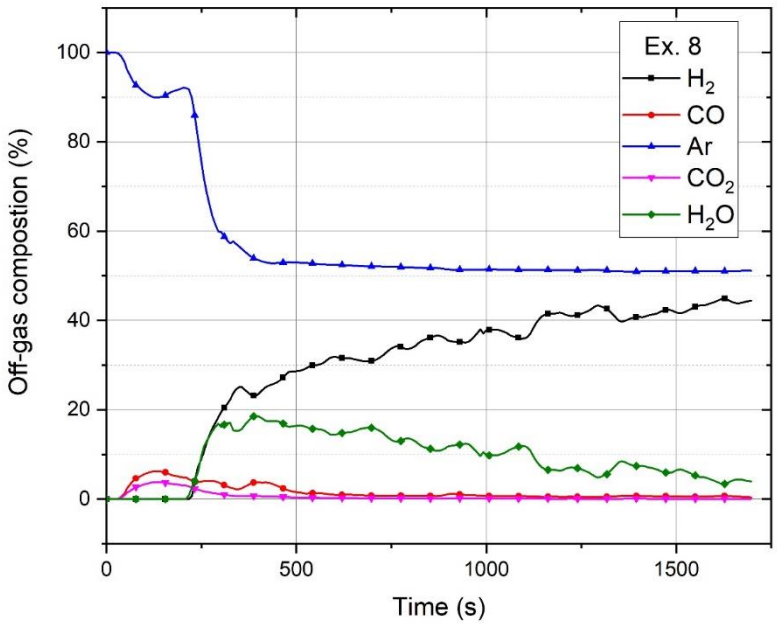

Figure 4-2: Chemical composition of off-gas for Ex. 8

Before starting the operation, the plasma reactor was purged out with argon to remove oxygen from the inside of the system. Then in the pre-melting step (0-180 s), only argon was injected to the reactor with a flow rate of 5 NL/min to generate the plasma arc. In this part of the process, there was a possibility that fines, inside the steel crucible, to be reduced by carbon initiated from ignition pin, steel crucible, or HGE. This subject was discussed in detail in publication 1 in the attachment of this paper [69]. Regarding the reduction of iron ore with carbon, off-gas consisted of Ar, CO, and CO_2, which can be seen in these figures in the pre-melting step. Ex. 7 was carried out by 50 g and Ex. 8 by 75 g of mixed fines charged into the steel crucible. Hence, it was expected that the amount of CO and CO_2 emitted by Ex. 8 to be more than that of Ex. 7. Nevertheless, the results contrast with our expectation and the compositions of the gases show that Ex. 8 emitted less amount of CO and CO_2 than that of Ex. 7. The possible reason could be the generation of arc on the edge of the steel crucible. In those conditions, instead of melting iron ore, mainly steel crucible was melted and mixed with iron oxide. Mixing of iron with Fe^{3+} caused the formation of Fe^{2+}. Accordingly, the concentration of Fe^{3+} in the melt became low and the chance of reduction by carbon decreased.

The next step of the operation was the reduction process started with the switching of the injection gas from pure argon to a mixture of 50% Ar / 50% H_2 with a total flow rate of 5 NL/min at 180 s. From this moment, the amount of hydrogen and water vapor increased, and the amount of other gases decreased. However, after 350 s, the amount of water vapor decreased

because of a decrease in the reduction rate. Ex. 7 was terminated at 1387 s because only 50 g of fines were charged into the crucible and there was a risk of melting the wall of the steel crucible, and accordingly, the penetration of the melt into the refractories.

The off-gas composition of the other experiments was discussed in detail in publications 1 and 2 in the attachment of this paper [45,69]. The trends of those were similar to these two experiments except Ex. 6 which was continuous feeding of iron ore and was discussed in publication 1 in the attachment of this paper [69].

There was some difference between the methods of the measuring and calculation of the chemical composition of off-gas by the previous researchers [3,22,24] and this study. First, they have not removed water in the off-gas system; instead, they guided water vapor by heating the off-gas duct to be captured by the MS. Second, they have not compared the results of the MS with a Reference diagram. For instance, an off-gas composition of Badr work [3] shows 5% of H_2O and 5% of H_2 at the beginning of the experiment (time=0 s), however, the results of the current study show that it takes some seconds for hydrogen to reach the MS.

4.2 Degree of hydrogen utilization (η_{H_2})

One of the main parameters of reduction behavior is the degree of hydrogen utilization (η_{H_2}). Not only the degree of hydrogen utilization over the operation time but also the average amount of η_{H_2} regarding the total operation time of each experiment was calculated and the results were discussed in publications 1 and 2 in the attachment of this paper [45,69]. Furthermore, in this section, η_{H_2} of all experiments for a comparison are presented.

η_{H_2} of all experiments were calculated and the results are shown in **Figure 4-3** and **Figure 4-4**. They outlined in two figures to be more legible.

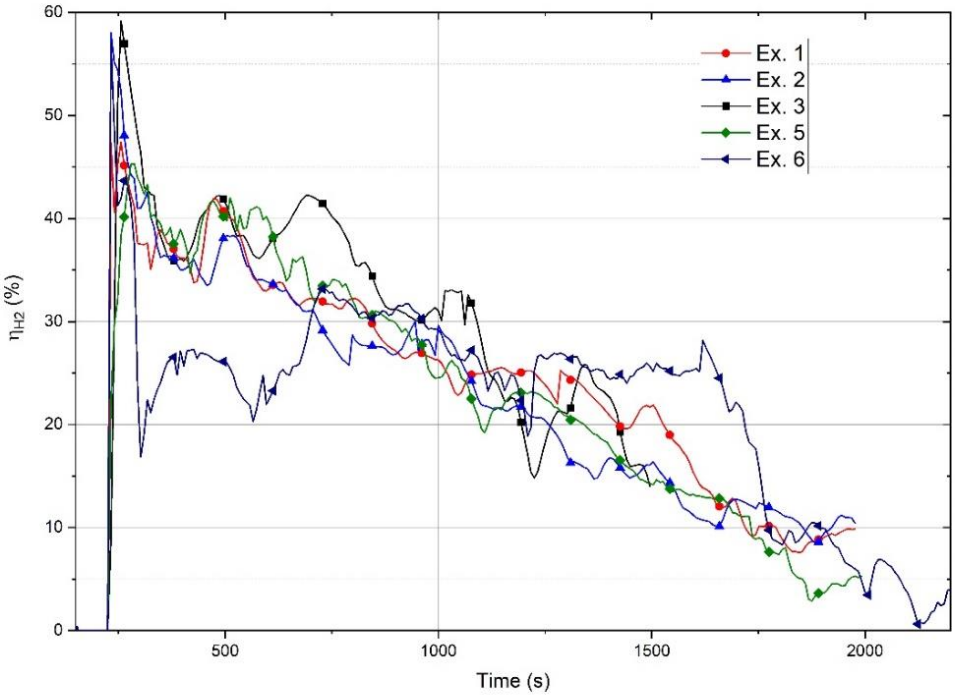

Figure 4-3: Degree of hydrogen utilization of Ex. 1, 2, 3, 5 and 6

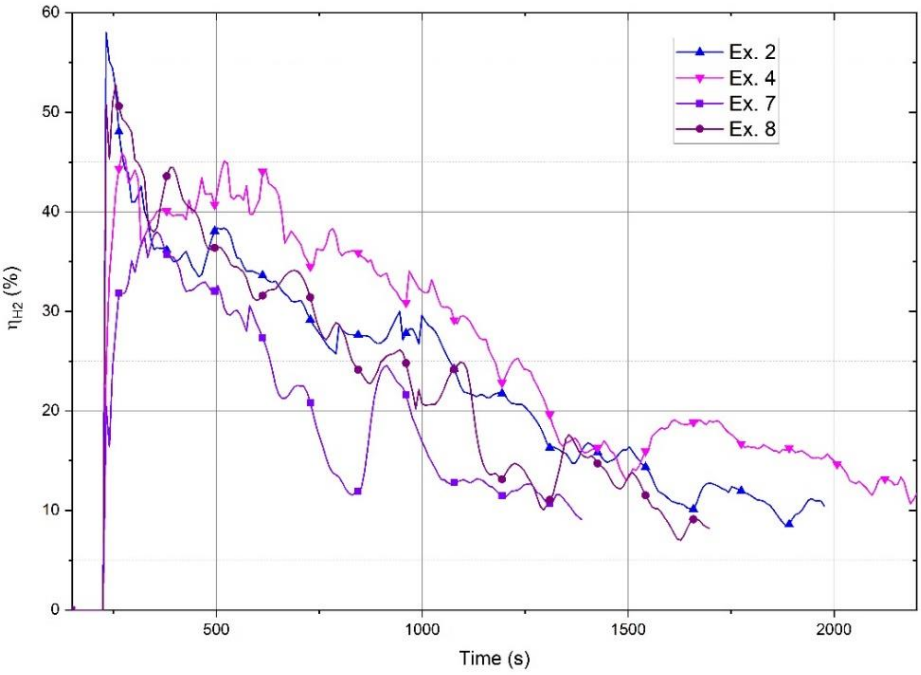

Figure 4-4: Degree of hydrogen utilization of Ex. 2, 4, 7 and 8

At the beginning of the reduction step in the time range of 190 – 300 s, η_{H_2} was between 44 and 58% for all experiments except Ex. 7, and then sharply decreased. Because there was a low amount of hydrogen inside the reactor versus a liquid pool of iron oxide. Hence, a large part of hydrogen could contribute to reduction reactions to form H_2O. Ex. 7 with only 50 g of fines inside the steel crucible illustrated the minimum amount of η_{H_2} (less than 40%) among all the other experiments. The reason might be the production of a liquid pool with a low amount of Fe^{3+}. It could happen when the arc was generated on the edge of the steel crucible or an already reduced section. However, the generation of arc on the edge of the crucible, in this case, is more acceptable because of the low amount of iron ore inside the crucible.

Plasma arc was not completely stable; therefore, it was turning around while arcing. The optimal case was the generation of the arc on the fines of iron ore instead of on the edge of the steel crucible. The movement and changing the position of the arc was the main reasons for η_{H_2} fluctuations. The fluctuation was more obvious for the Ex. 7 and 8 due to a lower amount of iron oxide inside the steel crucible. There was not any fluctuation in η_{H_2} presented by Plaul [22].

Badr [3] divided the process into three phases. The first phase was started from the beginning of the experiment until the slope of the hydrogen line got approximately zero or the

line was horizontal. He reported for an experiment with 3 NL/min of argon and 2 NL/min of hydrogen and 100 g of iron ore, η_{H_2} was more than 90% at the start and more than 40% at the end of the phase one. His results were not in good agreement with the present study. In the second phase, which was more stable, the line was horizontal. For the mentioned experiment, η_{H_2} was in the range between 25% and 35%, which the trends were not in good agreement with this study. The third phase started when the slope of the line began to decrease. However, the results of this study showed that the slope of the curve after 200 s was decreasing.

Plaul [22] experimented with a gas mixture of 30% H_2 / 70% Ar with a total flow rate of 5 NL/min, and 100 g of iron ore from Chador Malu mine. **Figure 4-5** shows the degree of reduction and hydrogen utilization of that experiment.

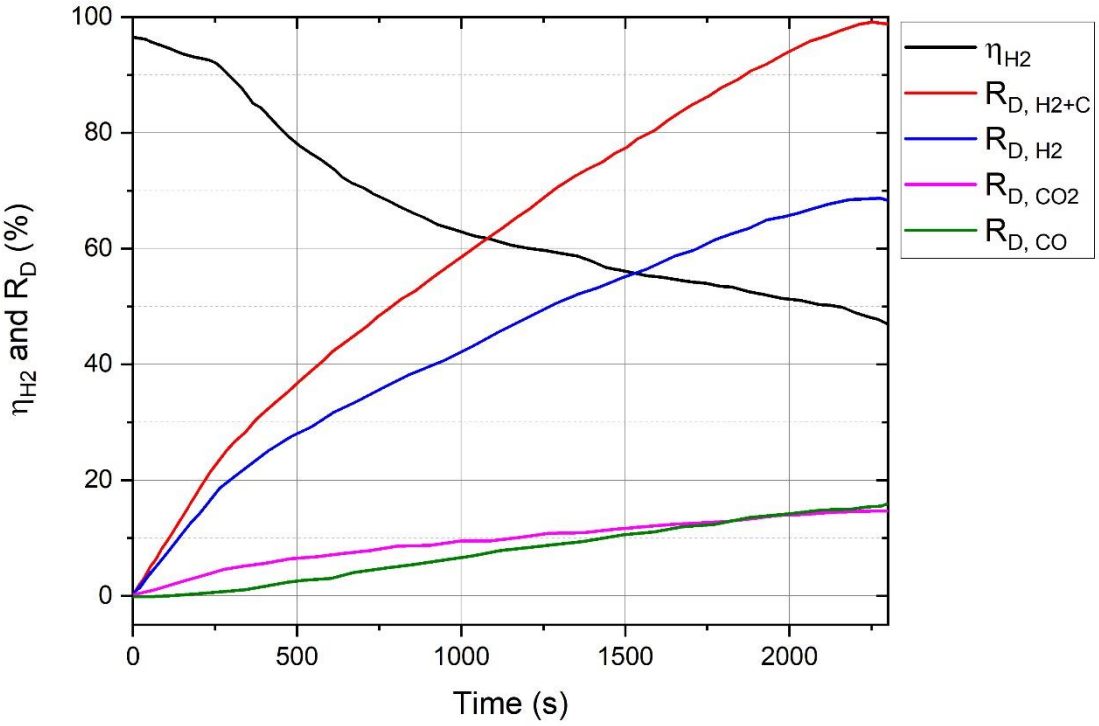

Figure 4-5: The degree of reduction and hydrogen utilization versus time [22]

The degree of hydrogen utilization was approximately 96% at the beginning of the experiment and then decreased. At the end of the experiment, η_{H_2} was approximately 47%, and at the same time, the total reduction degree was more than 99%. This statement cannot be true, because, with 99% of the degree of reduction, there was not iron oxide inside the crucible to be reduced by hydrogen.

Bäck [24] studied the reduction behavior of iron ore using hydrogen thermal plasma. He carried out some experiments with 45%, 35%, 25%, and 15% of hydrogen in a mixture of argon and hydrogen with a constant argon flow rate of 4 NL/min and 100 g of iron ore. He reported that η_{H_2} was more than 40% in all experiments until when the total degree of reduction was less than 65%. Furthermore, when the degree of reduction was more than 97%, the η_{H_2} was more than 25% for all the experiments. Consequently, the reported values of the η_{H_2} was much higher than the results of the present study.

4.3 Degree of reduction (R_D)

In this process, hydrogen and carbon attended to the reduction reactions. The products of the reductions were H_2O, CO, and CO_2. The degree of reduction by the formation of these products for the experiments Ex. 4, 6 and 7 are shown in **Figure 4-6**, **Figure 4-7** and **Figure 4-8**, respectively.

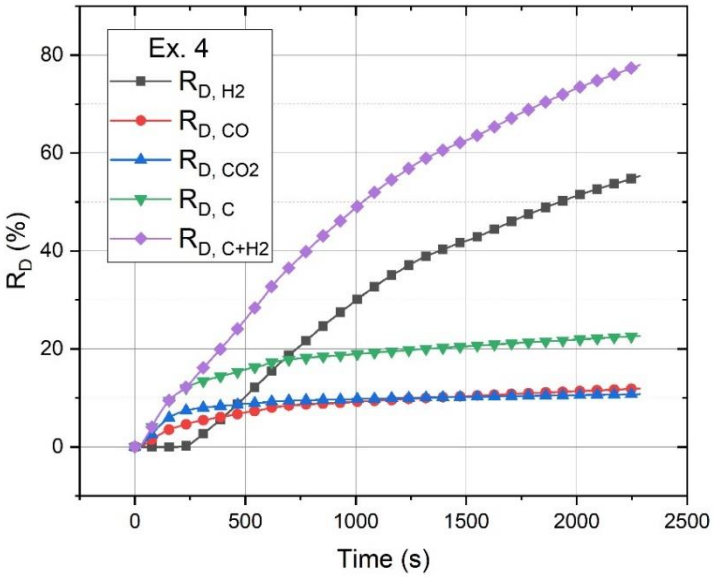

Figure 4-6: R_D of Ex. 4

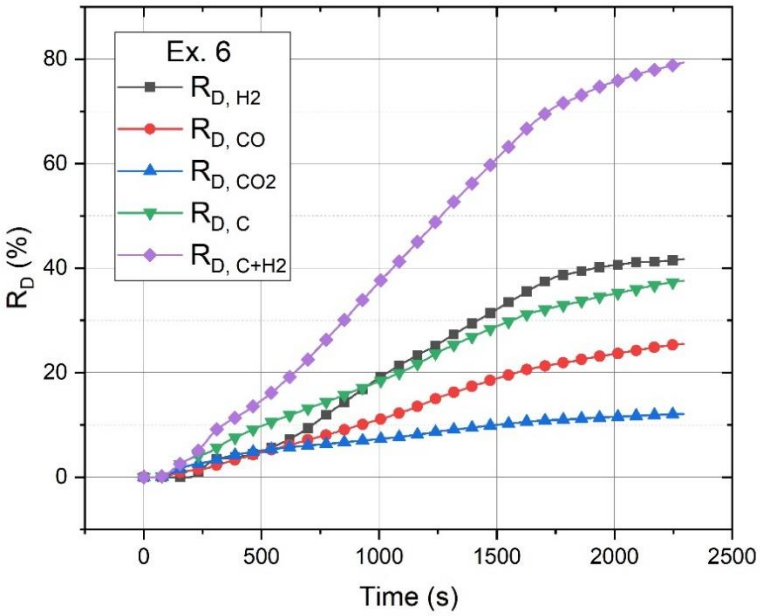

Figure 4-7: R_D of Ex. 6

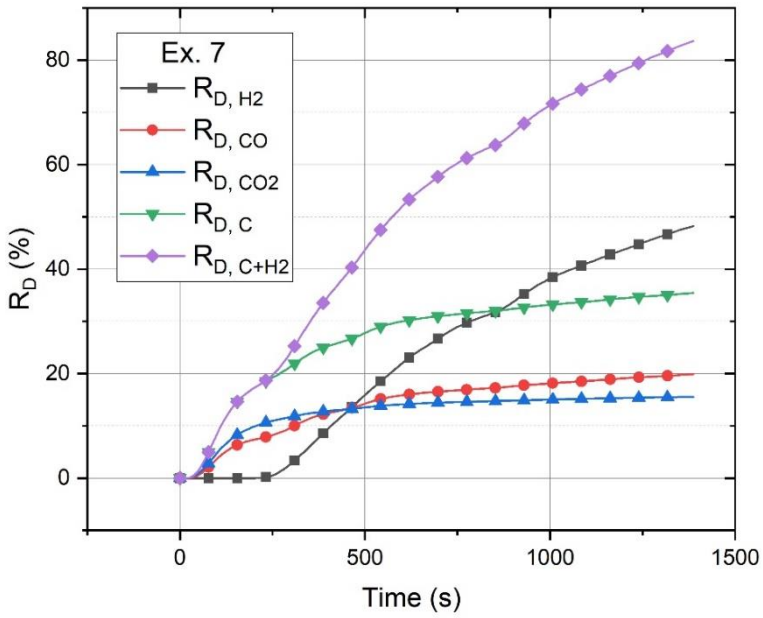

Figure 4-8: R_D of Ex. 7

It was expected that the amount of carbon contributed to the reduction reactions to be approximately in the same range for all experiments because of the operation with the same operation parameters such as the power of the arc, arc length and the carbon content of the

crucible and ignition pin. However, as it has already been mentioned, it could be different from experiment to experiment because of the generation of the plasma arc in different places. $R_{D,C}$ of Ex. 4, 6, and 7 after 1000 s were 18%, 18%, and 33%, respectively. $R_{D,C}$ of Ex. 7 was more than that of the two others because the released carbon was approximately in the same range, but 50 g of iron oxide was inside the crucible instead of 100 g.

The ratio of CO/CO_2 was different in these experiments. This ratio of CO/CO_2 in Ex. 6 was greater than that of the two other experiments because of the continuous feeding of iron ore through the HGE. During the continuous charging of iron ore, the powders were stuck on the inner surface of the HGE and then reduced. Regarding these fines on the inner surface of the HGE, a low amount of iron oxide contacted with a high amount of carbon. Therefore, the ratio of CO/CO_2 increased. For instance, the products of one mole of Fe_2O_3 with two moles of carbon at equilibrium at 1600 °C was assessed using FactSage™ 7.2, and the results showed the production of 1.7 mole CO and 0.3 mole CO_2. Therefore, the ratio of CO/CO_2 is much more than one. In contrast, when carbon was introduced to the melt from the steel crucible or ignition pin, the carbon concentration in the melt was low and CO_2 was the dominant product, which caused the ratio to be decreased.

Degree of reduction by hydrogen of Ex. 4, 6 and 7 until 700, 900, and 850 s respectively were less than that of by carbon. Because carbon started to reduce iron ore from pre-melting step (0 - 180 s). The other reason was that at the beginning of the experiments, the contribution of carbon to the reduction reactions was high. The lather reason was explained in detail in publication 1 in the attachment of this paper [69].

Figure 4-9 shows the degree of reduction by hydrogen for Ex. 1, 3, 4, 6 and 7.

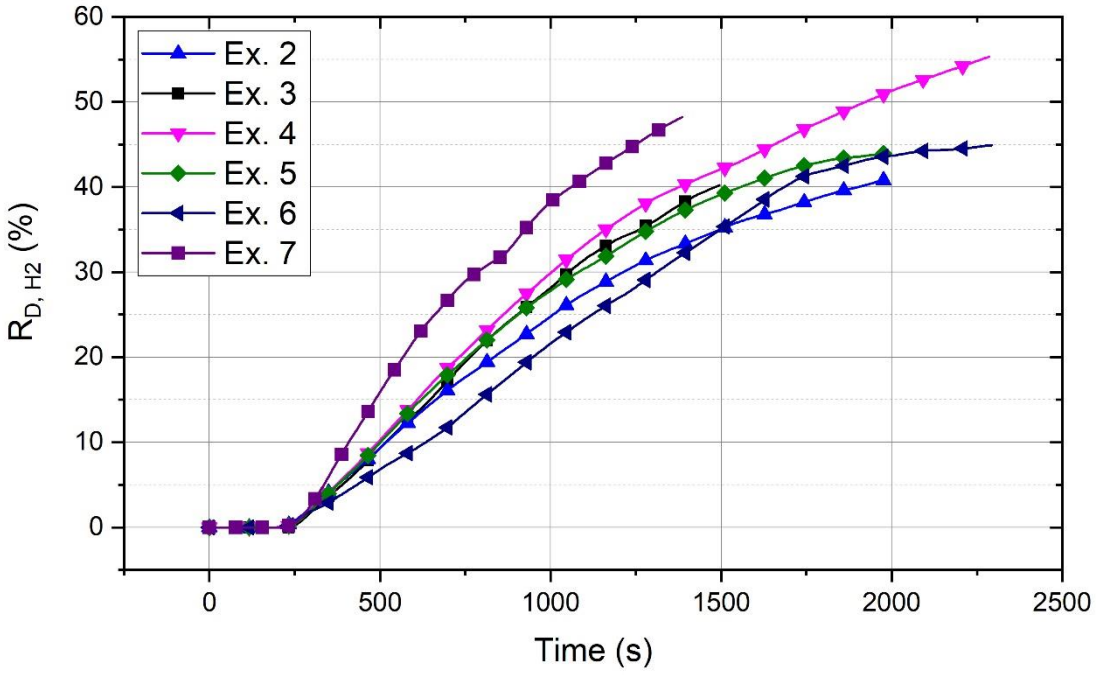

Figure 4-9: $R_{D, H2}$ for the Ex. 1, 3, 4, 6 and 7

Figure 4-9 shows that the degree of reduction by hydrogen for the Ex. 7 was more than that of the other experiments because of the low sample weight. The only difference between experiments Ex. 2, 3, 4 and 5 was the basicity of the slag. Ex. 4 with basicity B_2= 2.3 had a greater value of the degree of reduction than that of Ex. 2, 3 and 5 with a basicity of 0.8, 1.6, 2.9, respectively. Therefore, it can be suggested that B_2=2.3 could be the optimal amount of the slag basicity for the operation in terms of reduction behavior.

The trends of Ex. 6 were different from the other experiments. At the beginning of the experiments, the reduction degree was lower than the other experiments. Because only 20 g of sample was inside the crucible and a large portion of the crucible was empty, which led to generating an arc on the surface of the steel crucible instead of fines, and then with continuously charging of fines, the reduction degree increased. Consequently, it is expected to have the highest degree of reduction using a continuous feeding system, if the process would be started with more fines inside the crucible.

$R_{D, C}$ of the other experiments have also been assessed and the results are shown in **Figure 4-10**.

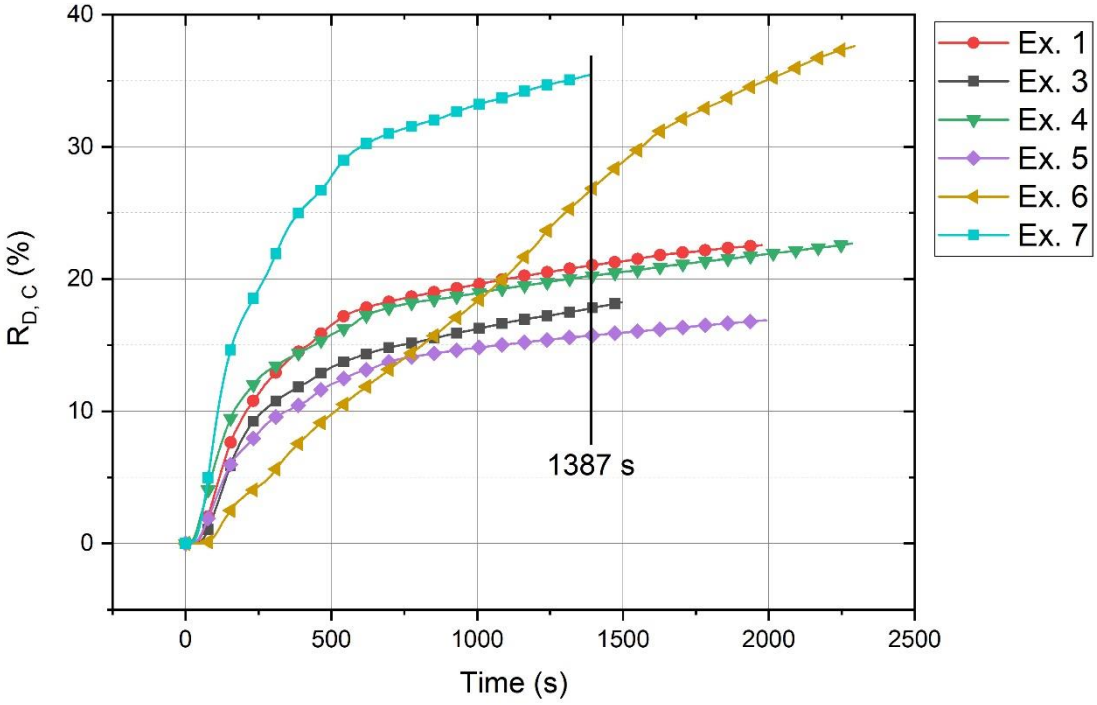

Figure 4-10: $R_{D,C}$ for the Ex. 1, 3, 4, 5, 6 and 7

Degree of reduction by carbon after 1387 s for the Ex. 1, 3, 4, 5, 6 and 7 were 22%, 18%, 21%, 16%, 27% and 36%. The reason for the high $R_{D,C}$ for Ex. 6 and 7 were discussed in **Figure 4-7** and **Figure 4-8**. However, there was not a large difference between the values of $R_{D,C}$ for the other experiments.

The total degree of reduction for Ex. 1, 3, 4, 5, 6, and 7 is shown in **Figure 4-11**.

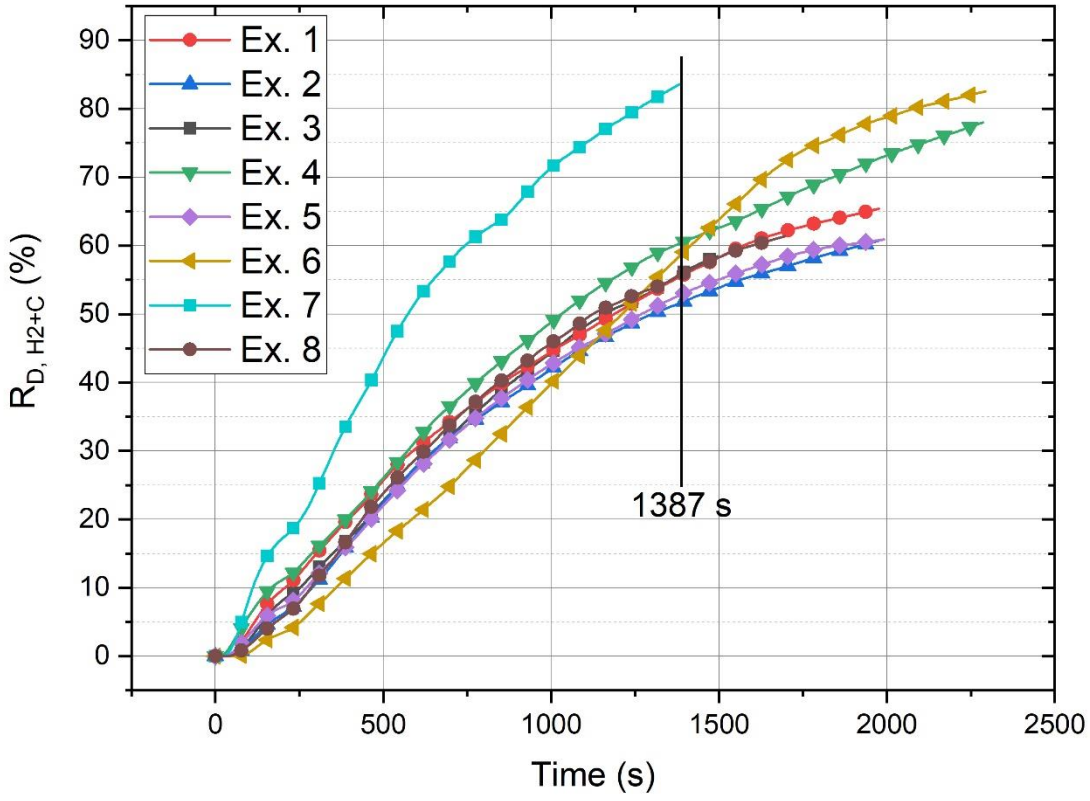

Figure 4-11: $R_{D, H2+C}$ for the Ex. 1, 3, 4, 5, 6 and 7

The total degree of reduction was the sum of the degree of reduction by carbon and hydrogen. After 1387 s, $R_{D, H2+C}$ of the experiments with a 100 g of sample weight was between 52 and 62%. However, with the extension of the operation time to 2000 s, it could not achieve higher than 80%. The main reason was the use of steel crucible instead of refractory lining. When steel crucible was used, only a section of the materials under the arc was in a liquid state and the rest was in solid-state. Moreover, iron ore powder before the reduction might be buried under a layer of melt. To observe the unreduced material buried under a layer of produced iron, the steel crucible of the experiments after the test runs were cut off from the middle and the microstructures have been observed by optical microscopy. **Figure 4-12** shows buried iron oxide inside the crucible after the operation.

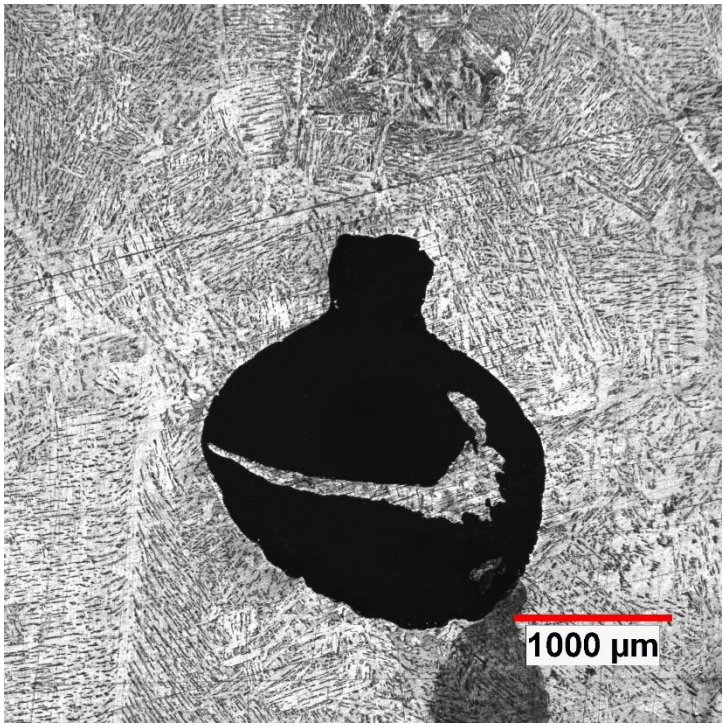

Figure 4-12: A cross section of the crucible, a portion of slag or iron ore, black area, under a layer of produced iron, Ex. 3.

A black section was the slag entrapped inside the solidified produced iron. The chance of the reduction of this slag was low. Because, the produced iron surrounded the slag should have been re-melted to prepare the conditions to solve the unreduced material into the melt, and then the reduction process could occur. However, there was a poor possibility because of the use of the steel crucible and cooling system.

Badr [3] carried out an experiment with 3 NL/min of argon and 2 NL/min of hydrogen, and 100 g of iron ore in an approximately 2250 s of operation. He reported an approximately 97% degree of reduction, which was much higher than that of all experiments of the current study.

Bäck [24] carried out some experiments which were explained in the previous section. He could achieve a 100% degree of reduction by an experiment with 100 g of iron ore and a gas mixture of 3.3 NL/min H_2 and 4 NL/min Ar in an operation time of 1750 s. He reported a degree of reduction 97%, 97%, and 87% for the experiments with 35%, 25%, and 15% of hydrogen, respectively. The reported values were much higher than those of the current study.

4.4 Reduction rate

The reduction rate by hydrogen and carbon and total reduction rate by the sum of carbon and hydrogen for all experiments were presented in publication 1 and 2 in the attachment of this paper [45,69]. Furthermore, in this section, the reduction rate by hydrogen of all experiments are compared.

Figure 4-13 shows the reduction rate by hydrogen of all the experiments.

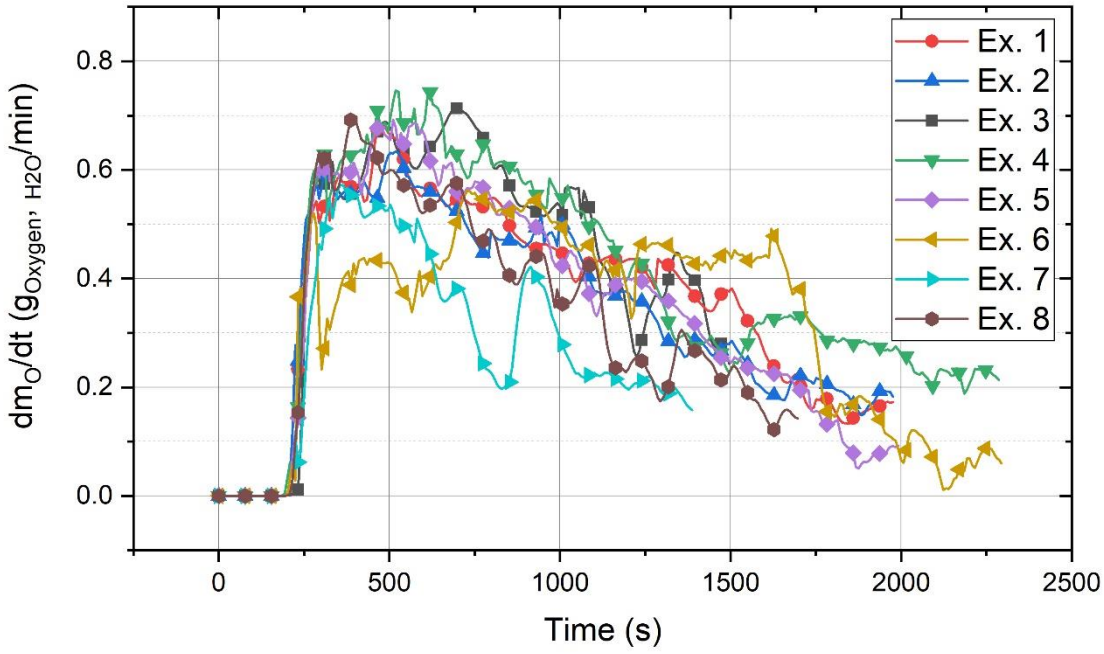

Figure 4-13: Reduction rate by hydrogen of the Ex. 1, 2, 3, 4, 5, 6, 7 and 8.

The reduction rates at the beginning of the experiments were high, and then they gradually decreased. The trends of the changes for all experiments were similar except that of Ex. 6 and 7. The reasons were similar to the reasons for the degree of hydrogen utilization, which has already been explained in **Figure 4-9**.

One of the main results was the reduction rate of Ex. 6, which was approximately between 0.4 and 0.6 $g_{Oxygen,H2O}$/min in the time range of 750 – 1560 s. It proofed that with continuous feeding of iron ore, the reduction rate could be kept constant. Furthermore, the risk of burring material during operation decreased.

Badr [3] reported the average 0.4 g_{Oxygen}/min reduction rate for the second phase of the experiment explained in the previous section.

4.5 Plasma arc temperature

Optical thickness of the plasma arc is important to be considered for the arc measurements with a spectrometer. Optical thickness defines the distance that photons travel before reaching the analysis instruments. Hence, optical thickness limits the photos analyzing from the plasma arc [89]. However, it causes to prevent radiation heat transfer to the reactor refractories. In HPSR, iron ore with additives is continuously injected into the plasma arc zone which leads to creating a high amount of dust. The creation of a high amount of dust in the plasma reactor causes an increase in the optical thicknesses. In the present study, the main objective was the assessment of the plasma arc temperature, and not the reduction behavior. Therefore, scrap was charged into the crucible instead of charging of iron oxide. As a result, the optical thickness was not an influencing parameter for the analyzing process.

To monitor the arc, a plasma arc was generated between the HGE and steel scrap. The reactor has already been filled with 50% Ar / 50% H_2 and during the arcing; 5 L/min of that gas mixture was injected into the plasma zone. The arc length was approximately 20 mm. the voltage of the arc was not stable and was between 50 V and 80 V and the amperage was between 90 A and 100 A.

The integration time of the spectrometers was 10^{-5} s, and the arc was monitored for 600 s. As an example, a spectrum of the hydrogen plasma arc is shown in **Figure 4-14**.

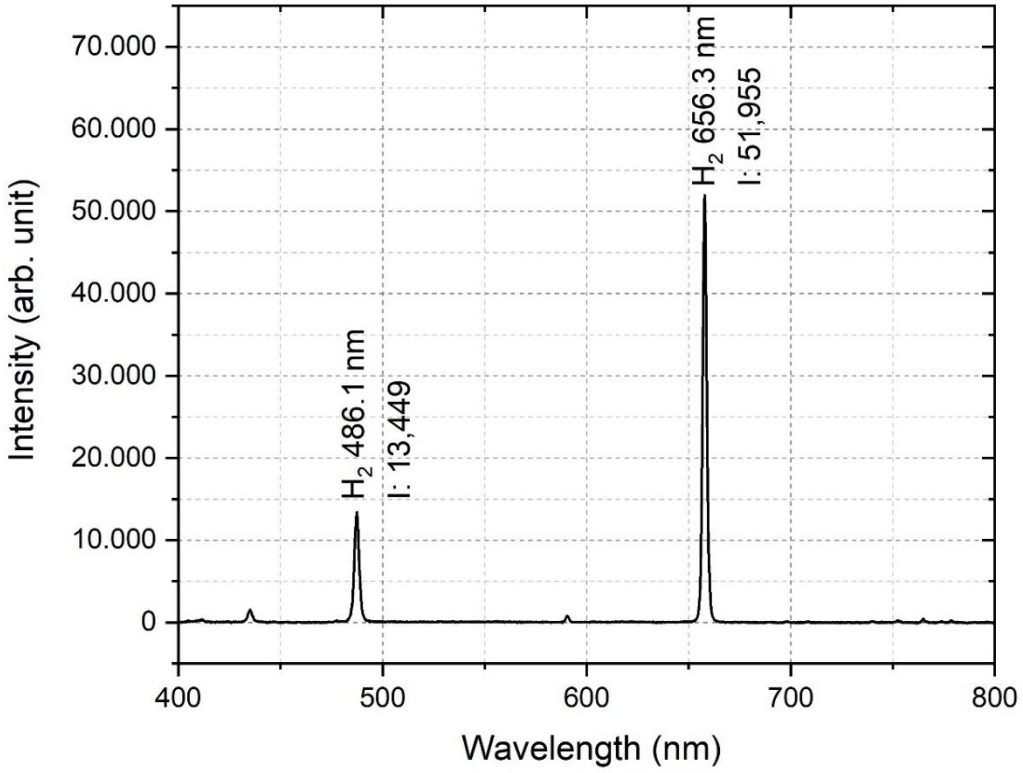

Figure 4-14: An optical emission spectrum of 50% Ar / 50% H_2

Two wavelengths are with high intensity in the figure that belongs to hydrogen. These two wavelengths, 486.1 nm, and 656.3 nm were selected to calculate the temperature of the arc. The temperature of the arc was calculated using two methods with the following equations.

$$T_{e_1} = -\left[\frac{E_p - E_q}{k ln(\frac{i_{pr} \upsilon_{qr} A_{qr} g_q}{i_{qr} \upsilon_{pr} A_{pr} g_p})}\right] \tag{76}$$

$$T_{e_2} = \left[\frac{E_q - E_p}{k\left[ln\left(\frac{\upsilon_{pr}}{\upsilon_{qr}}\right) + ln\left(\frac{A_{pr} g_p}{A_{qr} g_q}\right) - ln\left(\frac{i_{pr}}{i_{qr}}\right)\right]}\right] \tag{77}$$

The wavelength data from the atomic spectra database are listed in **Table 4-2** [35].

Table 4-2: Spectral parameters and diagnosis of the hydrogen plasma temperature

p	*q*	*r*	*c (m/s)*	E_p	E_q
3	4	2	3E8	2.04E-18	1.94E-18

Table 4-2a: Continued table 4-1

λ_{pr} *(nm)*	λ_{qr} *(nm)*	υ_{pr} *(s^{-1})*	υ_{qr} *(s^{-1})*
656.3	486.1	4.57E+14	6.17E+14

Table 4-2b: Continued table 4-1

A_{pr} *(s^{-1})*	A_{qr} *(s^{-1})*	g_p	g_q	*H (J. s)*	*k (J/K)*
4.41E+7	8.42E+6	18	32	6.63E-34	1.38E-23

Table 4-2c: Continued table 4-1

i_{pr} (arb.uni.)	i_{qr} (arb.uni.)	Equation	T_e (K)
51,955.43	13,449.52	77	13,435
51,955.43	13,449.52	76	13,406

The highest temperature of the arc was calculated using the two different equations, although the results were close to each other. It was expected the temperature of the arc to be higher. For this monitoring, a multi-furcated fiber-optic cable with a wide-angle was used. Therefore, the whole zone of the arc zone was monitored. If a microfiber would be used for the monitoring, it would be possible to measure the temperature of the arc point by point. Because the angle of sight of microfiber is zero, and then can monitor a point with a diameter of 2 mm. in the following, the results of other researchers are presented for the comparison.

As it was discussed, the ionization of hydrogen particles was a function of temperature and the density of the electron. The density of the electrons in a plasma arc presented by Pauna *et al.* [51] was in the range of 10^{18} - 10^{20} cm^{-3}. Therefore, the degree of hydrogen ionization for all possible values of electrons density in a plasma arc is shown in **Figure 4-15:** The degree of hydrogen plasma ionization x for different particle densities over the ionization potential. It shows the fraction of hydrogen ionization with different electron density over the ionization potential.

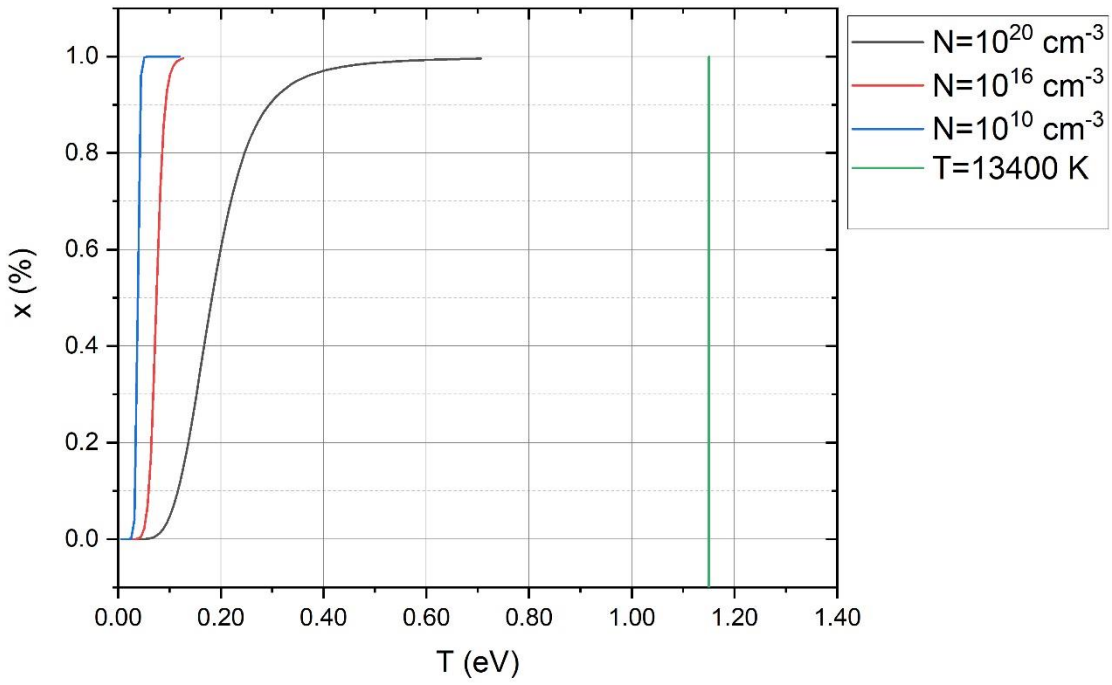

Figure 4-15: The degree of hydrogen plasma ionization x for different particle densities over the ionization potential

At the temperature of 13,406 K and an electron density less than 10^{20} cm^{-3}, the degree of hydrogen ionization is 100%. Therefore, it is expected that in this process, all hydrogen particles in the plasma arc zone to be ionized. However, it needs more investigations to determine the temperature gradient inside the hydrogen plasma reactor and to determine the electron density in different sections of the plasma arc.

5 Summary and conclusion

1. Activated particles, like electrons and ions, exist in a plasma arc zone. The ionization degree of hydrogen particles defines the reduction rate of iron oxide. Gibbs free energy was calculated for iron oxide reduction reactions by different hydrogen species. As a result, The reduction ability of hydrogen species is different and the order of reduction ability is represented as: $H^+ > H_2^+ > H_3^+ > H > H_2$. Therefore, the temperature of arc and the density of hydrogen particles are the main parameters influencing the degree of hydrogen ionization and the reduction rate. Above 15,000 °C, hydrogen, and argon are in the ionized state, which leads to reduce iron ore more readily.
2. The characteristics of the hydrogen plasma smelting reduction of hematite were studied included the degree of hydrogen utilization, the reduction rate, and the degree of reduction. Those parameters have been studied by carrying out a series of experiments regarding various sample weights, slag basicity, and continuous feeding of fines. Thermodynamic calculations of the reduction at equilibrium were carried out using FactSage™ 7.2.
3. An increase of 60% in the degree of hydrogen utilization observed at the beginning of the experiment runs, and then by the passage of the reduction operation, upon to the diminishing of hematite, it then decreased. The average η_{H_2} the value was approximately 28% for the samples with a basicity of 1.6 and 2.3.
4. The conducting of the plasma arc between the edge of the steel crucible and the hollow graphite electrode led to generate fluctuations in the degree of hydrogen

utilization. Because of using the crucible made by refractory materials in the testing plant and industrial plant, it is expected to achieve a greater value of η_{H_2}

5. The use of the steel crucible and the graphite electrode led to introduce carbon to the melt. The share of carbon in the reduction of hematite was approximately 30% of the total degree of reduction.
6. The possibility of dephosphorization in this process was studied. The phosphorus content could be reduced by 0.01% because of the high basicity of the slag.
7. HPSR produces a small amount of CO_2 due to the contribution of carbon, from the graphite electrode to the reduction reactions. The average consumption of the electrode was approximately 31 kg/t liquid steel which led to emit 114 kg CO_2/t liquid steel. However, it is expected that the production of CO_2 during the operation of the testing plant or industrial plant of this process would be much lower than those of other steel-making processes.
8. During the continuous feeding process of iron ore, the η_{H_2} value could be kept constant. Therefore, we expect to achieve a high η_{H_2} value in an industrial scale of this process.
9. The un-melted iron oxide fines buried by the melted iron oxide, could not be reduced. Therefore, to achieve a high degree of reduction was not possible when using a laboratory-scale facility.
10. Upon the low amount of FeO content in the slags, it is expected to reach a high degree of reduction if iron ore fines could be melted. It can be achieved using crucible with refractory materials and high power of the arc. Therefore, operation with the testing plant and industrial plant of HPSR prepare the conditions to keep iron oxide in the liquid phase inside the crucible.
11. The methodology of monitoring of the plasma arc was defined, and the experimental setup was introduced and the method of the calculation of the plasma arc temperature was in detail explained.
12. The results of the plasma arc temperature showed that the maximum temperature was 13,400 K. To calculate the plasma arc temperature the whole plasma arc zone was monitored. Therefore, it is expected that the maximum temperature of the arc would be higher if the arc would be monitored in a spatial resolved manner.

6 Outlook

HPSR has a high potential for the reduction of iron oxides. Further investigations have to be done to find the strengths of the production of steel using this process. During the execution of the present work, the following topics were found to be valuable for further work:

- In the plasma state, excited particles such as electrons and ions are existing. Therefore, to manage the reduction process of iron ores using the HPSR process requires knowledge of plasma physics and the thermodynamic aspect of reduction reactions.
- Electrons, which are accelerated particles, are responsible to transfer energy in the plasma atmosphere. Electron collision with hydrogen molecules leads to exciting hydrogen particles. Therefore, the density of electrons in the plasma arc zone, degree of hydrogen ionization and the lifetime of excited particles should be studied.
- The density of the activated particles in the plasma arc zone and hence, the ionization rate of hydrogen atoms is a function of temperature, the mass of particles and the number of particles in specific volume. The temperature of the plasma arc was studied using the optical spectrometer method. However, the temperature in the plasma arc zone should be measured spatially resolved and the temperature gradient developed. Furthermore, the effect of the degree of hydrogen ionization on the reduction behavior of iron oxide should be investigated.
- The simulation of the HPSR process is essential to design, development, analysis, and optimization of the HPSR process, which has not been conducted. The model can be validated concerning the results of experiments carried out using the laboratory scale and testing plant of HPSR.

- The design of the reactor crucible, refractory lining and the selection of refractory material are the key knowledge to industrialize this process.
- In the present study, the reduction behavior of iron ore within the continuous feeding was studied. However, it should be further investigated to find out the optimal process parameters such as grain size of fines, feeding rate, composition and flow rate of gas, gas velocity through the HGE, etc.

7 Publications published within this PhD thesis

During the preparation of this thesis, several publications were established. In all publications, the author of this thesis wrote 100% of the original draft. The complete contribution of the author is given in Table VIII. All peer-reviewed journal articles are attached with the permission of the publishing companies. Additionally, all conference papers, published in the frame of this thesis are listed in Chapter 7.6. In all conference papers, 100% of the original draft was written by the author of this thesis.

7.1 Contribution of the author to the papers

Table 7-1: Contribution of the author to the appended publication in percent

Publication	Conception and planning	Experiments	Analysis and interpretation	Project administration	Manuscript preparation	Review and editing
1	100%	100%	90%	70%	100%	50%
2	100%	100%	90%	70%	100%	50%
3	100%	100%	90%	70%	100%	50%
4	100%	100%	90%	70%	100%	50%

7.2 Publication 1: Slag Formation during Reduction of Iron Oxide Using Hydrogen Plasma Smelting Reduction

Masab Naseri Seftejani, Johannes Schenk, Daniel Spreitzer, and Michael Andreas Zarl

Materials 2020, 13(4), 935; https://doi.org/10.3390/ma13040935

Workload

Masab Naseri Seftejani: Conceptualization, methodology, project administration, validation, formal analysis, investigation, visualization, writing and original draft preparation (100%), review and editing, supervision.

Johannes Schenk: Project administration, validation, writing and original draft preparation (100%), review and editing, supervision, writing - review and editing.

Daniel Spreitzer: Validation, writing - review and editing.

Michael Andreas Zarl: Validation, writing - review and editing.

7.3 Publication 2: Reduction of Hematite Using Hydrogen Thermal Plasma

Masab Naseri Seftejani, Johannes Schenk, and Michael Andreas Zarl

Materials 2019, 12(10), 1608; https://doi.org/10.3390/ma12101608

Workload

Masab Naseri Seftejani: Conceptualization, methodology, project administration, validation, formal analysis, investigation, visualization, writing and original draft preparation (100%), review and editing, supervision.

Johannes Schenk: Project administration, validation, writing and original draft preparation (100%), review and editing, supervision, writing - review and editing.

Michael Andreas Zarl: Validation, writing - review and editing.

7.4 Publication 3: Thermodynamic of Liquid Iron Ore Reduction by Hydrogen Thermal Plasma

Masab Naseri Seftejani, Johannes Schenk, and Michael Andreas Zarl

Metals 2018, 8(12), 1051; https://doi.org/10.3390/met8121051

Workload

Masab Naseri Seftejani: Conceptualization, methodology, project administration, validation, formal analysis, investigation, visualization, writing and original draft preparation (100%), review and editing, supervision.

Johannes Schenk: Project administration, validation, writing and original draft preparation (100%), review and editing, supervision, writing - review and editing.

Michael Andreas Zarl: Validation, writing - review and editing.

7.5 Publication 4: Kinetics of molten iron oxides reduction using hydrogen

**Masab Naseri Seftejani, Johannes Schenk,
and Michael Andreas Zarl**

La Metallurgia Italiana 2018, Volume 7/8, 5–14.

Workload

Masab Naseri Seftejani: Conceptualization, methodology, project administration, validation, formal analysis, investigation, visualization, writing and original draft preparation (100%), review and editing, supervision.

Johannes Schenk: Project administration, validation, writing and original draft preparation (100%), review and editing, supervision, writing - review and editing.

Michael Andreas Zarl: Validation, writing - review and editing.

7.6 Conference proceedings (not attached to this thesis)

1. **M. Naseri Seftejani** (Writing – original draft: 100%), J. Schenk, Thermodynamic aspects of hydrogen plasma smelting reduction of iron oxides. Paper presented at the 8th International Congress on Science and Technology of Ironmaking 2018 (ICSTI 2018). Vienna, Austria.
2. **M. Naseri Seftejani** (Writing – original draft: 100%), J. Schenk, M.A. Zarl, Transport properties of HPSR gases. Paper presented at the 1st China Symposium on Sustainable Steelmaking Technology (CSST 2018). Chinese Society for Metals; 2018
3. Sormann, J. Schenk, **M. Naseri Seftejani** (Review and editing), M. A. Zarl, Spreitzer D, Hydrogen - The way to a carbon free steelmaking. Paper presented at Multidisciplinary International Conference Advances in Metallurgical Processes and Materials; 2018 (AdMet 2018). Lviv, Ukraine
4. **M. Naseri Seftejani** (Writing – original draft: 100%), J. Schenk, Fundamentals of hydrogen plasma smelting reduction (HPSR) of iron oxides, a new generation of steelmaking processes. Paper presented at AsiaSteel 2018. Iron and steel Society. Bhubaneshwar, India
5. **M. Naseri Seftejani** (Writing – original draft: 100%), J. Schenk, Kinetics of hydrogen plasma smelting reduction of iron oxides. Paper presented at the 7th International Congress on Science and Technology of Steelmaking, 2018 (ICS2018). Venice, Italy

8 List of literatures

[1] Ushio, M., Arc discharge and electrode phenomena, Pure and Applied Chemistry, (1988) 60, 5. doi:10.1351/pac198860050809.

[2] Badr, K; E. Bäck; W. Krieger, Reduction of iron ore by a mixture of Ar-H2 with CO and CO2 under plasma application, (2007) Kyoto University, Japan.

[3] Badr, K., Smelting of iron oxides using hydrogen based plasmas, Doctoral Dissertation, Leoben, Austria, 2007.

[4] IEA clean coal centre, http://www.iea-coal.org.uk/site/2010/home, Abgerufen am: 22.01.2016.

[5] Hasanbeigi, A., Infographic: The Iron and Steel Industry's Energy Use and Emissions. Global Efficiency Intelligence, LLC., https://www.globalefficiencyintel.com/new-blog/2017/nfographic-steel-industry-energy-emissions, (2017).

[6] Hasanbeigi, A; M. Arens; J. C. R. Cardenas; L. Price; R. Triolo, Comparison of carbon dioxide emissions intensity of steel production in China, Germany, Mexico, and the United States, Resources, Conservation and Recycling, (2016) 113, 127–139. doi:10.1016/j.resconrec.2016.06.008.

[7] Lisienko, V.G; A. V. Lapteva; Y. N. Chesnokov; V. V. Lugovkin, Greenhouse-gas (CO2) emissions in the steel industry, Steel Transl., (2015) 45, 9, 623–626. doi:10.3103/S0967091215090107.

[8] Kopfle, J.T., J.M. McClelland and G.E. Metius, Green steelmaking with the MIDREX® direct reduction process. Midrex Technologies, Inc., http://www.spongeironindia.in/midrex.pdf, (2008).

[9] Zhang, W; J. Zhang; Z. Xue, Exergy analyses of the oxygen blast furnace with top gas recycling process, Energy, (2017) 121, 135–146. doi:10.1016/j.energy.2016.12.125.

[10] Wang, K; C. Wang; X. Lu; J. Chen, Scenario analysis on CO2 emissions reduction potential in China's iron and steel industry, Energy Policy, (2007) 35, 4, 2320–2335. doi:10.1016/j.enpol.2006.08.007.

[11] Babich, A; D. Senk, Coal use in iron and steel metallurgy, in: The Coal Handbook: Towards Cleaner Production, Elsevier, 2013, pp. 267–311.

[12] Dayal, A.R; D. R. Sadedin, Application of pulsed traveling hydrogen arcs for metal oxide reduction, Plasma Chemistry and Plasma Processing, (2003) 23, 4, 627–649. doi:10.1023/A:1025506326697.

[13] Kirschen, M; K. Badr; H. Pfeifer, Influence of direct reduced iron on the energy balance of

the electric arc furnace in steel industry, Energy, (2011) 36, 10, 6146–6155. doi:10.1016/j.energy.2011.07.050.

[14] Brecelj, F; M. Mozetic, Reduction of metal oxide thin layers by hydrogen plasma, Vacuum, (1990) 40, 1-2, 177–181. doi:10.1016/0042-207X(90)90149-S.

[15] Bullard, D.E; D. C. Lynch, Reduction of titanium dioxide in a nonequilibrium hydrogen plasma, Metall and Materi Trans B, (1997) 28, 6, 1069–1080. doi:10.1007/s11663-997-0061-z.

[16] Major, S; S. Kumar; M. Bhatnag; K. L. Chopra, Effect of hydrogen plasma treatment on transparent conducting oxides, Appl. Phys. Lett., (1986) 49, 7, 394. doi:10.1063/1.97598.

[17] Murphy, A.B., Transport coefficients of hydrogen and argon–hydrogen plasmas, Plasma Chemistry and Plasma Processing, (2000) 20, 3, 279–297. doi:10.1023/A:1007099926249.

[18] Sabat, K.C; R. K. Paramguru; S. Pradhan; B. K. Mishra, Reduction of cobalt oxide (Co3O4) by low temperature hydrogen plasma, Plasma Chem Plasma Process, (2015) 35, 2, 387–399. doi:10.1007/s11090-014-9602-9.

[19] Weigel, A; M. Lemperle; W. Lyhs; H. Wilhelmi, Experiments on the reduction of iron ores with an argon hydrogen plasma, ISPC-7 Eindhoven, (1985), 1214–1219.

[20] Gold, R.G; W. R. Sandall; P. G. Cheplick; D. R. MacRae, Plasma reduction of iron oxide with hydrogen and natural gas at 100 kW and 1 MW, Ironmaking & Steelmaking, (1977) 4, 10–14.

[21] Hiebler, H; J. F. Plaul, Hydrogen plasma- smelting reduction- an option for steel making in the future, METABK, (2004), Abgerufen am: 20.01.2016 43, 0543-5846, 155–162.

[22] Plaul, J.F., Schmelzreduktion von hämatitischen Feinerzen im Wasserstoff-Argon-Plasma, Doktoral Dissertation, Leoben, Austria, 2005.

[23] Sormann, A., Untersuchungen zur Schmelzreduktion von Eisenoxiden mit Wasserstoff als Reduktionsmittel, Doktoral Dissertation, Leoben, Austria, 1992.

[24] Bäck, E., Schmelzreduktion von Eisenoxiden mit Argon-Wasserstoff- Plasma, Doctoral Dissertation, Leoben, Austria, 1998.

[25] Fridman, A.A., Plasma chemistry. 0511546076, Cambridge University Press, Cambridge University Press, Cambridge, New York, 2008.

[26] Lichtenberg, A.J. and M.A. Lieberman, Principles of plasma discharges and materials processing. 0471720011, Wiley-Interscience, 2nd ed., Wiley-Interscience, Hoboken, N.J., Chichester, 2005.

[27] Feinman, J., Plasma technology in metallurgical processing. 09328971216, Iron and steel Society, Iron and steel Society, USA, 1987.

[28] Mills, R., Spectral emission of fractional quantum energy levels of atomic hydrogen from a helium–hydrogen plasma and the implications for dark matter, International Journal of Hydrogen Energy, (2002) 27, 3, 301–322. doi:10.1016/S0360-3199(01)00116-1.

[29] Piel, A., Plasma physics: An introduction to laboratory, space, and fusion plasmas / Alexander Piel. 9783642104916, Springer, Springer, Heidelberg, 2010.

[30] Zhang, Y; W. Ding; S. Guo; K. Xu, Reduction of metal oxide in nonequilibrium hydrogen plasma, China Nonferrous Met, (2004) 14, 317–321.

[31] Keidar, M. and I. Beilis, Plasma Engineering: Applications from aerospace to bio and nanotechnology. 0123859786, Elsevier Science, Elsevier Science, San Diego, 2013.

[32] Janev, R.K., D. Reiter and U. Samm, Collision processes in low-temperature hydrogen plasmas. 0944-2952, 1Institut f¨ur Plasmaphysik, Forschungszentrum J¨ulich GmbH, EURATOM Association, Trilateral, 1Institut f¨ur Plasmaphysik, Forschungszentrum J¨ulich GmbH, EURATOM Association, Trilateral, D-52425 Jülich - Bundesrepublik Deutschland, 2003.

[33] Trelles, J.P; E. Pfender; J. V.R. Heberlein, Non-Equilibrium Modeling of Arc Plasma

Torches, (2007), Abgerufen am: 23.05.2018 40, 5937–5952. doi:10.1088/0022-3727/40/19/024.

[34] Bentley, R.E., A departure from local thermodynamic equilibrium within a freely burning arc and asymmetrical Thomson electron features, J. Phys. D: Appl. Phys., (1997) 30, 20, 2880–2886. doi:10.1088/0022-3727/30/20/015.

[35] Kramida, A. and Y. Ralchenko, NIST Atomic Spectra Database, NIST Standard Reference Database 78, National Institute of Standards and Technology, National Institute of Standards and Technology, 1999. doi:10.18434/T4W30F.

[36] Boulos, M.I., P. Fauchais and E. Pfender, Thermal plasmas: Fundamentals and applications / Maher I. Boulos, Pierre Fauchais, and Emil Pfender. Vol.1. 0306446073, Plenum Press, Plenum Press, New York, London, 1994.

[37] Goldston, R.J. and P.H. Rutherford, Introduction to plasma physics. 0750303255, Institute of Physics Pub, Institute of Physics Pub, Bristol, 1995 (2000 [printing]).

[38] Kanhe, N.S; A. K. Tak; S. V. Bhoraskar; V. L. Mathe; A. K. Das, Transport properties of Ar-Al plasma at 1 atmosphere, SRM University, Kattankulathur, Tamilnadu, India, (2012), pp. 1025–1026.

[39] Lisal, M; W. Smith; M. Bures; V. Vacek; J. Navratil, REMC computer simulations of the thermodynamic properties of argon and air plasmas, Molecular Physics, (2002) 100, 15, 2487–2497. doi:10.1080/00268970210130227.

[40] Naseri Seftejani, M, and J. Schenk, Kinetics of hydrogen plasma smelting reduction of iron oxides, La Metall. Ital. 2018, n. 7/8 2018, 5–14.

[41] Naseri Seftejani, M, and J. Schenk, Thermodynamic aspects of hydrogen plasma smelting reduction of iron oxides, 8 th International Congress on Science and Technology of Ironmaking, (ICSTI 2018), Vienna, Austria, 2018.

[42] Murphy, A.B., Transport coefficients of plasmas in mixtures of nitrogen and hydrogen, Chemical Physics, (2012) 398, 64–72. doi:10.1016/j.chemphys.2011.06.017.

[43] Tanaka, M; S. Tashiro; T. Satoh; A. B. Murphy; J. J. Lowke, Influence of shielding gas composition on arc properties in TIG welding, Science and Technology of Welding and Joining, (2013) 13, 3, 225–231. doi:10.1179/174329308X283929.

[44] Kamiya, K; N. Kitahara; I. Morinaka; K. Sakuraya; M. Ozawa et al., Reduction of molten iron oxide and FeO bearing slags by H2-Ar plasma, ISIJ Int., (1984) 24, 1, 7–16. doi:10.2355/isijinternational1966.24.7.

[45] Naseri Seftejani, M; J. Schenk; M. A. Zarl, Reduction of Haematite Using Hydrogen Thermal Plasma, Materials 2019, 12 (10), 1608. doi:10.20944/preprints201904.0261.v1.

[46] Semenyshyn, R.V; A. N. Veklich; I. L. Babich; V. F. Boretskij, Spectroscopy peculiarities of thermal plasma of electric arc discharge between electrodes with Zn admixtures, Advances in Space Research, (2014) 54, 7, 1235–1241. doi:10.1016/j.asr.2013.11.042.

[47] Mašláni, A; V. Sember; T. Stehrer; H. Pauser, Measurement of Temperature in the Steam Arcjet During Plasma Arc Cutting, Plasma Chem Plasma Process, (2013) 33, 3, 593–604. doi:10.1007/s11090-013-9443-y.

[48] Dzierżęga, K; Ł. Bratasz; S. Pellerin; B. Pokrzywka; K. Musioł, Stark Width and Shift Measurements for the 696.543 nm ArI Line using Degenerate Four-Wave Mixing (DFWM) Spectroscopy, J. Phys. D: Appl. Phys., (2003) 67, 1, 52–58. doi:10.1238/Physica.Regular.067a00052.

[49] Jenista, J., Numerical Modeling of Hybrid Stabilized Electric Arc With Uniform Mixing of Gases, IEEE Trans. Plasma Sci., (2004) 32, 2, 464–472. doi:10.1109/TPS.2004.826143.

[50] Javidi Shirvan, A; I. Choquet; H. Nilsson; H. Jasak, Coupling boundary condition for high-intensity electric arc attached on a non-homogeneous refractory cathode, Computer Physics Communications, (2018) 222, 31–45. doi:10.1016/j.cpc.2017.09.010.

[51] Pauna, H; T. Willms; M. Aula; T. Echterhof; M. Huttula et al., Pilot-scale AC electric arc

furnace plasma characterization, J. Phys. D: Appl. Phys., (2019) 1, 3, 35007. doi:10.1088/2516-1067/ab30dd.

[52] Zhang, N; F. Sun; L. Zhu; M. P. Planche; H. Liao et al., Electron Temperature and Density of the Plasma Measured by Optical Emission Spectroscopy in VLPPS Conditions, J Therm Spray Tech, (2011) 20, 6, 1321–1327. doi:10.1007/s11666-011-9681-6.

[53] Zhang, N; F. Sun; L. Zhu; C. Verdy; M. P. Planche et al., Characteristics of Cu Film Deposited Using VLPPS, J Therm Spray Tech, (2011) 20, 1-2, 351–357. doi:10.1007/s11666-010-9538-4.

[54] Cui, J; Z. Xu; J. Zhang; Q. Nie; G. Xu et al., Online diagnosis of electron excitation temperature in CH4+H2 discharge plasma at atmospheric pressure by optical emission spectra, Sci. China Ser. G-Phys. Mech. Astron., (2008) 51, 12, 1892–1896. doi:10.1007/s11433-008-0175-6.

[55] Mirapeix, J; A. Cobo; S. Fernandez; R. Cardoso; J. M. Lopez-Higuera, Spectroscopic analysis of the plasma continuum radiation for on-line arc-welding defect detection, J. Phys. D: Appl. Phys., (2008) 41, 13, 135202. doi:10.1088/0022-3727/41/13/135202.

[56] Mirapeix, J; A. Cobo; J. Fuentes; M. Davila; J. M. Etayo et al., Use of the Plasma Spectrum RMS Signal for Arc-Welding Diagnostics, Sensors (Basel, Switzerland), (2009) 9, 7, 5263–5276. doi:10.3390/s90705263.

[57] Semenov, S; B. Cetegen, Spectroscopic Temperature Measurements in Direct Current Arc Plasma Jets Used in Thermal Spray Processing of Materials, J Therm Spray Tech, (2001) 10, 2, 326–336. doi:10.1361/105996301770349411.

[58] Aula, M; A. Leppänen; J. Roininen; E.-P. Heikkinen; K. Vallo et al., Characterization of Process Conditions in Industrial Stainless Steelmaking Electric Arc Furnace Using Optical Emission Spectrum Measurements, Metall and Materi Trans B, (2014) 45, 3, 839–849. doi:10.1007/s11663-014-0032-0.

[59] Aula, M; A. Mäkinen; T. Fabritius, Analysis of arc emission spectra of stainless steel electric arc furnace slag affected by fluctuating arc voltage, Applied spectroscopy, (2014) 68, 1, 26–32. doi:10.1366/13-07079.

[60] Gilles, H.L; C. W. Clump, Reduction of iron ore with hydrogen in a direct current plasma jet, Ind. Eng. Chem. Proc. Des. Dev., (1970) 9, 2, 194–207. doi:10.1021/i260034a007.

[61] Rajput, P; B. Bhoi; S. Sahoo; R. K. Paramguru; B. K. Mishra, Preliminary investigation into direct reduction of iron in low temperature hydrogen plasma, Ironmaking & Steelmaking, (2013) 40, 1, 61–68. doi:10.1179/1743281212Y.0000000023.

[62] MacRae Sandall, C. D. Thompson and P. G. Cheplick, D.R., R.G. Gold, W.R. Sandal, C.D. Thompson and P.G. Cheplick, Method of reducing ores(US 4002466 A).

[63] Nakamura, Y; M. Ito; H. Ishikawa, Reduction and dephosphorization of molten iron oxide with hydrogen-argon plasma, Plasma Chem Plasma Process, (1981) 1, 2, 149–160. doi:10.1007/BF00564577.

[64] Kitamura, T; K. Shibata; K. Takeda, In-flight reduction of Fe2O3, Cr2O3, TiO2 and Al2O3 by Ar-H2 and Ar-CH4 plasma, ISIJ International, (1993) 33, 11, 1150–1158. doi:10.2355/isijinternational.33.1150.

[65] Nagasaka, T; M. Hino; S. Ban-ya, Interfacial kinetics of hydrogen with liquid slag containing iron oxide, Metall and Materi Trans B, (2000) 31, 5, 945–955. doi:10.1007/s11663-000-0071-6.

[66] Nagasaka, T; Y. Iguchi; S. Ban-ya, Effect of additives on the rate of reduction of liquid iron oxide with CO, tetsu-to-hagane, (1989) 75, 1, 74–81.

[67] Gudenau, H. W., D. Senk, S. Wang, K. D. M. Martins and C. Stephany, Research in the Reduction of Iron Ore Agglomerates Including Coal and C-containing Dust, ISIJ Int., (2005) 45, 4, 603–608. doi:10.2355/isijinternational.45.603.

[68] Uchikoshi, M., J. Imaizumi, H. Shibuya, T. Kékesi, K. Mimura and M. Isshiki, Production of

semiconductor grade high-purity iron, Thin Solid Films, (2004) 461, 1, 94–98. doi:10.1016/j.tsf.2004.02.076.

[69] Naseri Seftejani, M; J. Schenk; D. Spreitzer; M. A. Zarl, Slag Formation during Reduction of Iron Oxide Using Hydrogen Plasma Smelting Reduction, Materials 2020, 13, 4, 935. https://doi.org/10.3390/ma13040935

[70] Sabat, K.C; P. Rajput; R. K. Paramguru; B. Bhoi; B. K. Mishra, Reduction of oxide minerals by hydrogen plasma: An Overview, Plasma Chem Plasma Process, (2014) 34, 1, 1–23. doi:10.1007/s11090-013-9484-2.

[71] Robino, C.V., Representation of mixed reactive gases on free energy (Ellingharn-Richardson) diagrams, Metall and Materi Trans B, (1996) 27, 1, 65–69. doi:10.1007/BF02915078.

[72] Dembovsky, V., How the polarity of a surface reacting with a low temperature plasma affects the thermodynamic variables in metallurgical reactions, Achta Physic Slovenia, (1984) 34, 1, 11–18.

[73] Allen, J.E., The plasma–sheath boundary: Its history and Langmuir's definition of the sheath edge, Plasma Sources Sci. Technol., (2009) 18, 1, 14004. doi:10.1088/0963-0252/18/1/014004.

[74] Ban-ya, S; Y. Ighuchi; T. Nagasaka, Rate of reduction of liquid wustite with hydrogen, tetsu-to-hagane, (1984) 70, 1689–1696. doi:10.2355/tetsutohagane1955.70.14_1689.

[75] Hayashi, S; Y. Iguchi, Hydrogen reduction of liquid iron oxide fines in gas-conveyed systems, ISIJ International, (1994) 34, 7, 555–561. doi:10.2355/isijinternational.34.555.

[76] Katayama, H., S. Taguchi, and N. Tsuchiya, H; s. Taguchi; N. Tsuchiya, Reduction of iron oxide in molten slag with H2 gas, ISIJ Int., (1982), Abgerufen am: 20.01.2016 68, 2279–2286.

[77] Gabriel, O, W.E.N. van Harskamp, J.J.A. van den Dungen, D.C. Schram,, R. Engeln (Eds.), Gas phase kinetics and surface interaction in a hydrogen plasma jet, ispc-conference.org, Bochum, Germany, 2009.

[78] Mankelevich, Y.A; M. N. R. Ashfold; J. Ma, Plasma-chemical processes in microwave plasma-enhanced chemical vapor deposition reactors operating with C/H/Ar gas mixtures, J. Appl. Phys., (2008) 104, 11, 113304. doi:10.1063/1.3035850.

[79] Nagasaka,, T; Y. Iguchi; S. Ban-ya, Rate of reduction of liquid wustite with CO, ISIJ Int., (1985) 71, 2, 204–211.

[80] Tsukihashi, F; M. Amatatsu; T. Soma, Reduction of molten iron ore with carbon, ISIJ Int., (1982), Abgerufen am: 21.01.2016 22, 688–695.

[81] Soma, T., Smelting reduction of iron ore, Bulletin of the Japan Institute of Metals, (1982) 21, 8, 620–625. doi:10.2320/materia1962.21.620.

[82] Kato, K; Y. Saskai; T. Soma, Reduction of Molten Iron Oxide with CO Gas, ISIJ Int., (1977) 17, 9, 532–533. doi:10.2355/isijinternational1966.17.532.

[83] Takahashi, K; M. Amatatsu; T. Soma, Reduction of Molten Iron Ore with Solid Carbon, tetsu-to-hagane, (1975), Abgerufen am: 21.01.2016 61, 2525–2530.

[84] Sasaki, Y; Y. Okamoto; T. Soma, Kinetics of Reaction between Iron Oxide Slags and Solid Carbon, ISIJ International, (1978) 64, 3, 367–375.

[85] Sato, A; G. Aragane; K. Kamihira; S. Yoshimatsu, Reduction Rate of Molten Iron Oxide by the Solid Carbon or the Carbon in Molten Iron, tetsu-to-hagane, (1987), Abgerufen am: 21.01.2016 73, 812–819.

[86] Levenspiel, O. and B. Levien, The chemical reactor omnibook. 9781300991847, Lulu.com, Lulu.com, [Raleigh, N.C.], op. 2013.

[87] Bleakney, W., The Ionization Potential of Molecular Hydrogen, Phys. Rev., (1932) 40, 4, 496–501. doi:10.1103/PhysRev.40.496.

[88] Herzberg, G., Dissociation Energy and Ionization Potential of Molecular Hydrogen, Phys. Rev. Lett., (1969) 23, 19, 1081–1083. doi:10.1103/PhysRevLett.23.1081.

[89] Bowman, B. and K. Krüger, Arc furnace physics. 3514007683, Verlag Stahleisen GmbH, Verlag Stahleisen GmbH, Düsseldorf, op. 2009.

1 Attachment A: Publications

Publication 1:

Slag Formation During Reduction of Iron Oxide Using Hydrogen Plasma Smelting Reduction

Publication 2:

Reduction of Hematite Using Hydrogen Thermal Plasma

Publication 3:

Thermodynamic of Liquid Iron Ore Reduction by Hydrogen Thermal Plasma

Publication 4:

Kinetics of Molten Iron Oxides Reduction Using Hydrogen